

THE UNIVERSITY OF HULL

The Design, Synthesis and Properties of Dimeric Molecules Exhibiting  
Nematic-Nematic Transitions

being a Thesis submitted for the Degree of Doctor of Philosophy

at the University of Hull

by

Ziauddin Ahmed, BSc

November, 2014

## **ACKNOWLEDGMENTS**

I would like to thank my supervisor Professor Georg Mehl for giving me the opportunity to carry out this research project and for all his support, guidance and patience during the course of this PhD. I would also like to thank Dr. Mike Hird for guidance regarding synthetic strategy and his chemistry anecdotes.

I would like to thank Professor Oriano Francescangeli for his in depth discussion of correlation lengths and their derivation. I would like to thank Prof. G. Ungar and Dr. X. Zeng for allowing me to accompany them and experience Diamond Light Source and learn so much about conducting experiments at the synchrotron. I would also like to thank Prof. E. Gorecka and Ms. A. Zep for collaborating and performing AFM measurements.

I would like to thank Dr. Rob Lewis for teaching me all about NMR, Dr. Rob McDonald for teaching me the use of HPLC and DSC instruments. I would like to thank Dr. M. G. Tamba and Dr. A. J. T. Ferreira for teaching me all I know about XRD. Special thanks to Dr. Chris Welch for constant discussion from day one about synthetic techniques, characterisation, cricket and formula one. Thanks to Mr. P. Gawne and Mr. A. Forster for synthesis during their undergraduate project.

I would also like to thank all my colleagues past and present for always helping out and making this experience so much more enjoyable. Special thanks to my Hull family, Sumera, Raluca, Ben and especially David Allan for being my partner in crime.

Thanks to my brothers Vasseh (party money) and Salu (DotA) and all the friends and family around the world for their support and happy thoughts.

I owe most thanks to Mum and Dad for their unwavering support and for letting me pursue this adventure and making it easier for me every step of the way, Love you both!

**Dedicated to the memory of**

**Umair Abdullah**

## **ABSTRACT**

Several hydrocarbon linked mesogenic dimers are known to exhibit an additional nematic phase ( $N_{TB}$ ) below a conventional uniaxial nematic phase (N). The correlation between molecular structure and the nematic - nematic phase transitions (N- $N_{TB}$ ) is not yet well understood. Nematic-nematic transitions are in thermotropic liquid crystals associated in most cases with the formation of a columnar structure in the low temperature nematic phase or the onset of cluster formation or with folding processes of polymer chains, there is evidence too for the formation of twist-bend structures as well as the formation of domain assemblies.

The synthesis of a range of such dimeric materials, symmetric as well non-symmetric systems with both positive and negative dielectric anisotropy, containing linear and bent structures in the aromatic core systems is described in this thesis. The characterisation of these systems by the use of differential scanning calorimetry (DSC), optical polarizing microscopy (OPM) and X-ray diffraction (XRD) studies is described in detail and the results for these systems are compared and structure properties relationships and the impact on the formation of nematic-nematic transitions are discussed.

## Contents

Introduction.....	1
Liquid crystals .....	1
History .....	1
Classification .....	2
Mesophases.....	5
Nematic phases.....	5
Smectic phases <sup>2</sup> .....	18
Bent core <sup>33</sup> .....	19
Characterisation.....	20
Optical polarising microscopy.....	20
Differential scanning calorimetry .....	21
X-ray diffraction .....	22
Dimers .....	24
Aims.....	25
Results and Discussion .....	26
Synthetic strategy .....	26
Synthetic Schemes .....	26
Name reactions.....	31
Liquid Crystal Properties .....	37
Symmetric Dimers.....	37
Asymmetric Dimers .....	58
Conclusion and Outlook .....	84
Experimental.....	85
Synthesis of bis(4'-cyano-[1,1'-biphenyl]-4-yl) nonanedioate (1) .....	87
Synthesis of bis(4'-cyano-[1,1'-biphenyl]-4-yl) heptanedioate (2) .....	88
Synthesis of bis(4'-cyano-[1,1'-biphenyl]-4-yl) undecanedioate (3) .....	89

Synthesis of bis(4'-cyano-[1,1'-biphenyl]-4-yl) tridecanedioate (4) .....	90
Synthesis of bis(4'-cyano-[1,1'-biphenyl]-4-yl) octanedioate (5) .....	91
Synthesis of bis(4'-cyano-[1,1'-biphenyl]-4-yl) decanedioate (6).....	92
Synthesis of bis(4-bromophenyl) undecanedioate (7).....	93
Synthesis of bis(4-bromophenyl) heptanedioate (8).....	94
Synthesis of bis (2',3'-difluoro-4''-pentyl-[1,1':4',1''-terphenyl]-4-yl) undecanedioate (9) .....	95
Synthesis of bis (2',3'-difluoro-4''-pentyl-[1,1':4',1''-terphenyl]-4-yl) heptanedioate (10) .....	96
Synthesis of bis(4-iodophenyl) nonanedioate (11).....	97
Synthesis of 1,9-bis(4'-(trifluoromethyl)-[1,1'-biphenyl]-4-yl)nonane (12) .....	98
Synthesis of bis(2',3'-difluoro-4''-pentyl-[1,1':4',1''-terphenyl]-4-yl) nonanedioate (13) .....	99
Synthesis of 1,11-bis(4-bromophenoxy)undecane (14).....	100
Synthesis of 1,11-bis((2',3'-difluoro-4''-pentyl-[1,1':4',1''-terphenyl]-4-yl)oxy)undecane (15).....	101
Synthesis of 1,7-bis(4-bromophenoxy)heptane (16) .....	102
Synthesis of 1,7-bis((2',3'-difluoro-4''-pentyl-[1,1':4',1''-terphenyl]-4-yl)oxy)heptane (17) .....	103
Synthesis of 4',4''-nonanedioylbis([1,1'-biphenyl]-4-carbonitrile) (18) .....	104
Synthesis of 1,9-bis(4-bromophenyl)nonane-1,9-dione (19) .....	105
Synthesis of 1,9-bis(4-bromophenyl)nonane (20) .....	106
Synthesis of 4'-(9-(4-bromophenyl)nonyl)-[1,1'-biphenyl]-4-carbonitrile (21) ....	107
Synthesis of 5-(4-(9-(4'-cyano-[1,1'-biphenyl]-4-yl)nonyl)phenyl)thiophene-2-carbonitrile (22) .....	108
Synthesis of 4'-(9-(2',3'-difluoro-4'-pentyl-[1,1'-biphenyl]-4-yl)nonyl)-[1,1'-biphenyl]-4-carbonitrile (23) .....	109

Synthesis of 4'-(4'-pentyl-[1,1'-biphenyl]-4-yl)nonyl)-[1,1'-biphenyl]-4-carbonitrile (24) .....	110
Synthesis of 4-(9-(4-bromophenyl)nonyl)-2',3'-difluoro-4''-pentyl-1,1':4',1''-terphenyl (25) .....	111
Synthesis of 4'-(9-(4'-butoxy-2',3'-difluoro-[1,1'-biphenyl]-4-yl)nonyl)-[1,1'-biphenyl]-4-carbonitrile (26) .....	112
Synthesis of 4-(9-(2',3'-difluoro-4'-pentyl-[1,1'-biphenyl]-4-yl)nonyl)-2',3'-difluoro-4''-pentyl-1,1':4',1''-terphenyl (27) .....	113
Synthesis of 5-(4-(9-(2',3'-difluoro-4''-pentyl-[1,1':4',1''-terphenyl]-4-yl)nonyl)phenyl)thiophene-2-carbonitrile (28).....	114
Synthesis of 4-(9-(2',3'-difluoro-4'-butyloxy-[1,1'-biphenyl]-4-yl)nonyl)-2',3'-difluoro-4''-pentylterphenyl (29) .....	115
Synthesis of 2',3'-difluoro-4-pentyl-4''-(9-(4'-pentyl-[1,1'-biphenyl]-4-yl)nonyl)-1,1':4',1''-terphenyl (30) .....	116
Synthesis of 1,9-bis(2',3'-difluoro-4'-pentyl-[1,1'-biphenyl]-4-yl)nonane (31) ....	117
Synthesis of 4-((trimethylsilyl)ethynyl)benzonitrile (32) .....	118
Synthesis of 4-ethynylbenzonitrile (33) .....	119
Synthesis of 4'-(9-(4-((4-cyanophenyl)ethynyl)phenyl)nonyl)-[1,1'-biphenyl]-4-carbonitrile (34) .....	120
Synthesis of 1,9-bis(2',3'-difluoro-4''-pentyl-[1,1':4',1''-terphenyl]-4-yl)nonane-1,9-dione (35).....	121

Figure 1: 4-Cyano-4'-pentylbiphenyl .....	3
Figure 2: 2,3,6,7,10,11-hexakis(hexyloxy)triphenylene.....	3
Figure 3: 1,3-phenylene bis(4-((E)-(4-ethoxyphenyl)diazenyl)benzoate).....	4
Figure 4: Schematic representation of molecular order in the nematic phase in calamitic (left) and discotic (right) systems .....	5
Figure 5 : Schematic representation of the chiral nematic phase. ....	6
Figure 6 : Schematic representation of biaxial nematic phase. ....	6
Figure 7 : Schematic representation of the random fluctuations leading to smectic arrangements within a nematic phase. ....	7
Figure 8: twist-bend and Splay-bend structures proposed by Dozov .....	8
Figure 9 : Sepelj's dimer showing lower temperature nematic phase.....	8
Figure 10 : Schematic representation of the $N_{TB}$ phase in comparison with a N and $N^*$ phase.....	10
Figure 11 : Example of texture exhibited by a conventional nematic phase (left) and a $N_{TB}$ phase (right). ....	11
Figure 12 : Example of texture exhibited by a conventional nematic phase (left) and a $N_{TB}$ phase (right). ....	11
Figure 13 : Example of $N_{TB}$ textures. ....	12
Figure 14 : Polygonal fish scale texture of $N_{TB}$ . ....	12
Figure 15 : Narrow focal conic texture of $N_{TB}$ . ....	13
Figure 16 : 2 examples of shearing experiment of $N_{TB}$ before (left) and after shearing (right).....	13
Figure 17: Diffractogram for CB-C9-CB at N (top) and $N_{TB}$ (bottom) phase. Images on the right have isotropic scattering subtracted. ....	15
Figure 18 : Another example of the differences observed in XRD measurements <sup>42</sup> . ....	16
Figure 19 : Graphical representation of XRD data theta scans (left) and chi scans (right). ....	16
Figure 20 : FFTEM images of CB7CB fractured parallel to the helix axis .....	17
Figure 21: FFTEM images of CB7CB oblique fractured .....	17
Figure 22: Direct cryo-TEM observation of CB7CB pure (left) and with right-handed limonene.....	18
Figure 23: Schematic representation of molecular order in smectic A and smectic C phase respectively. ....	19

Figure 24: A typical optical polarising microscope showing its working components...	20
Figure 25: A schematic representation of the interaction of light with liquid crystals between crossed polarisers.....	21
Figure 26: Micrographs of nematic phase, (left) schlieren texture, (centre) marble texture, (right) thread-like texture. ....	21
Figure 27: Schematic representation of a differential scanning calorimeter. ....	22
Figure 28: Schematic representation of Bragg's law. ....	22
Figure 29: Schematic representation of powder diffraction. ....	23
Figure 30: Schematic representation of XRD patterns and molecular arrangements. ...	23
Figure 31: Griffin's dimer .....	24
Figure 32: Schematic representation of odd-even effect in simple dimers .....	24
Figure 33 : Compound 2 at 188 °C (left) and compound 3 151 °C (right) between cross polarisers on untreated and unrubbed slides. ....	38
Figure 34 : DSC curves of compound 1 (left) and compound 4 (right). ....	39
Figure 35: XRD images of scattering experiments aligned under magnetic field. Compound 1 at 160 °C (top left), Compound 2 at 168 °C (top right), Compound 3 at 150 °C (bottom left), Compound 4 at 150 °C (bottom left). ....	40
Figure 36 : Plot of 2 theta against intensity for compounds 1, 3 and 4.....	41
Figure 37: 2theta against intensity plot of compound 3 with mathematical function fit to peak.....	42
Figure 38: Micrographs of compound 5 at 210 °C (left) and 220 °C (right) under crossed polarizers and untreated slides. ....	43
Figure 39: Micrographs of compound 9 at 177 °C (left) and 205 °C (right) under crossed polarizers and untreated slides. ....	44
Figure 40: XRD scattering data for compound 9 at 140 °C aligned under magnetic field. ....	45
Figure 41: Plot of $\chi$ against intensity for compound 9 at 140 °C in the small angle.....	45
Figure 42: 2theta against intensity plot of compound 9 with mathematical function fit to peak.....	46
Figure 43: Micrographs of compound 10 at 195 °C (left) and 200 °C (right) under crossed polarizers and untreated slides. ....	46
Figure 44: Micrograph of compound 10 at 144 °C upon cooling under crossed polarizers and on untreated slides. ....	47

Figure 45: XRD scattering data for compound 10 at 200 °C (left) and 150 °C (right) aligned under magnetic field.....	47
Figure 46: 2θ against intensity plot of compound 10 at several temperatures. ....	48
Figure 47: Molecular packing in compound 10. ....	49
Figure 48: Wide angle plot of X scans against intensity for compound 10. ....	49
Figure 49: Micrographs of compound 15 at 150 °C on first heating (left) and on first cooling (right) under crossed polarizers and on untreated slides.....	50
Figure 50: Differential calorimetric scans for compound 35 (left) and expansion of first transition on heating (right). ....	51
Figure 51: Micrographs of compound 35 at 195 °C at 100x (left) and 200X (right) magnification between crossed polarizers and on untreated slides. ....	51
Figure 52: XRD scattering data for compound 35 and 192 °C.....	52
Figure 53: Micrographs of compound 35 at 184 °C (left) and 160 °C (right) under crossed polarizers and on untreated slides. ....	52
Figure 54: XRD scattering data of compound 35 at 184 °C and 144 °C. ....	53
Figure 55: Expansion of small angle scattering for compound 35 at 184 °C and 144 °C. ....	53
Figure 56: 2θ against intensity plot of compound 35 at all mesophases. ....	54
Figure 57: Possible molecular arrangement of molecules in low temperature mesophase. ....	55
Figure 58: Micrographs of compound 35 cooling from 185 °C every 0.5 °C.....	56
Figure 59: Micrographs of the growth of B6 reported by Sadashiva et al (left) and Achard et al (right). ....	57
Figure 60: Micrographs of compound 15 at 201 °C and compound 17 at 204 °C under crossed polarizers and on untreated slides. ....	57
Figure 61: Micrograph of intermediate 21 at 20 °C under crossed polarizers and on untreated slide.....	59
Figure 62: Calorimetric data of compound 22. ....	60
Figure 63: Micrographs of compound 22 at 91 °C (left) and 88 °C (right) under crossed polarizers and on untreated slides. ....	60
Figure 64: Calorimetric data for compound 23. ....	61

Figure 65: Micrographs of compound 23 at 41°C (top left), 36 °C (top right), upon sheering and at 33 °C after sheering. All micrographs were recorded on cooling under crossed polarizers and on untreated slides. ....	62
Figure 66: XRD scattering data for compound 23 at 41 °C (left) and 36 °C (right).....	62
Figure 67: 2θ against intensity plot of compound 23.....	63
Figure 68: Calorimetric data for compound 24.....	64
Figure 69 : Nematic phase of compound 24 shown by OPM and XRD at 82 °C.....	64
Figure 70: Calorimetric data of compound 26. ....	66
Figure 71: Micrographs of compound 26 at 56 °C (left) and 53 °C (right) under crossed polarizers and on untreated slides. ....	66
Figure 72: XRD scattering data of compound 26 at 58 °C (left) and 52 °C (right) on cooling from isotropic. ....	67
Figure 73: 2θ against intensity plot of compound 26 in the nematic and N <sub>TB</sub> phase....	67
Figure 74: Micrographs of compound 34 at 108 °C (left) and 95 °C (right) under crossed polarizers and on untreated slides. ....	68
Figure 75: XRD scattering data of compound 34 at 115 °C (left) and 95 °C right. ....	69
Figure 76 : Plot of the 2θ against intensity of compound 34 in the nematic phase at 115°C and nematic twist bend phase at 95 °C. ....	70
Figure 77: Plot of χ against intensity of compound 34 at 95 °C of the wide angle. ....	70
Figure 78: XRD scattering data of compound 34 at 115 °C (left) and 95 °C (right) with isotropic scattering subtracted.....	71
Figure 79: Calorimetric data for intermediate 25. ....	72
Figure 80: Micrographs of intermediate 25 at 77 °C (left) and 60 °C (right) under crossed polarizers and on untreated slides. ....	72
Figure 81: Micrograph and XRD scattering data of compound 27 at 50 °C.....	73
Figure 82: Calorimetric data for compound 28.....	74
Figure 83: Micrographs of compound 28 at 90 °C (left) and 78 °C (right) under crossed polarizers and on untreated slides. ....	74
Figure 84: XRD scattering data of compound 28 at 100 °C and 80 °C.....	75
Figure 85: Plot of 2θ against intensity of compound 28 in both nematic phases.....	75
Figure 86: Calorimetric data for compound 29.....	76

Figure 87: Micrographs of compound 29 at 100 °C (top left), 84 °C (top right), 81 °C (bottom left) and 78 °C (bottom right) under crossed polarizers and on untreated slides.....	77
Figure 88: XRD scattering data for compound 29 at 90 °C and 70 °C.....	78
Figure 89: Plot of $2\theta$ against intensity for compound 29 at various temperatures.....	78
Figure 90: Calorimetric data for compound 30 .....	80
Figure 91: Micrographs of compound 30 at 101 °C (left) and 85 °C (right) under crossed polarizers and on untreated slides. ....	80
Figure 92: Micrograph of compound 30 at 75 °C. ....	81
Figure 93: XRD scattering data for compound 30 at 103 °C (left) and 83 °C (right).....	81

## **Introduction**

### **Liquid crystals**

The liquid crystal state is an intermediate state of matter between conventional liquids and crystalline solids. Liquid crystals tend to flow like liquids and possess orientational crystal like structure. This intermediate state is known as a liquid crystalline mesophase. The mesophase exists due to anisotropy within the phase; not all molecular directions are equivalent, as opposed to a conventional liquid where an isotropic distribution is observed. Molecular order within a crystal is typically both positional and orientational, while in contrast an isotropic liquid is devoid of molecular order, with random diffusion throughout the sample<sup>1</sup>.

### **History**

In 1888 Friederich Reinitzer, a botanist of the Institute for Plant Physiology of the University of Prague, described his observations of the coloured phenomena occurring in melts of cholesteryl acetate and cholesteryl benzoate. Most prominently, Reinitzer observed that cholesteryl benzoate appeared to have two melting points; at 145.5 °C; the crystalline solid melted to an opaque liquid, which at 178.5 °C became transparent. The phenomenon was also observed to be reversible, and that dramatic colours were apparent near the transition temperatures<sup>2</sup>.

Reinitzer knew of the work of the physicist Professor Otto Lehmann, in designing and developing polarizing microscopes, and recognized that Lehmann could advise on the optical behaviour of his cholesteryl esters. Reinitzer and Lehmann agreed on the homogenous nature of the cholesteryl ester system<sup>3,4</sup>.

In 1903, Daniel Vorländer, at the University of Halle began intense research which would propel him to the forefront of the field for the next 30 years. Vorländer determined that liquid crystalline behaviour was a result of molecular shape, with the

liquid crystal phase primarily formed by molecules with a *rod-like* structure. His work also showed that if the major axis of a molecule were long enough, protrusions could be tolerated without sacrifice of the liquid crystal properties His research culminated in the discovery of hundreds of materials with liquid crystalline properties<sup>2</sup>.

In 1922 G. Friedel published in “Annales de Physique, a paper entitled ‘Les Etats Méomorphes de la Mathé<sup>5</sup>. In addition to containing a wealth of information on microscopic techniques and materials, Friedel’s article represented the first classification of liquid crystals, i.e., nematic, smectic and cholesteric.

The twisted nematic (TN) effect was discovered by Charles-Victor Mauguin<sup>6</sup>. Pioneering work by George Gray and co-workers at the University of Hull led to the discovery of the cyanobiphenyl class of nematic liquid crystals, which exhibited electrochemically stable nematic phases at ambient temperatures.<sup>7</sup> This enabled the successful implementation of a new type of liquid crystal display and offered significant advantages over other display technologies of the time, including low power consumption and small size, making them ideal for battery operated, hand-held devices. This has culminated in the global LCD market to reportedly be surpassing the \$165 billion mark in 2017<sup>8</sup>.

## **Classification**

Liquid crystals can broadly be divided into two distinct classes, thermotropic and lyotropic. In thermotropic liquid crystals the mesophases are temperature dependant and on the other hand in lyotropic systems the mesophases are dependent on a combination of solvent concentration and temperature. For low molar mass LC these two types can further be classified according to their molecular architecture into calamitic, discotic, and bent-core.

Calamitic systems are rod like shaped molecules where one of the molecular axis is much longer than the other two. It is this shape that allows these molecules to align along that long direction. Perhaps the most known and investigated liquid crystal, **5CB** is an example of calamitic type liquid crystalline molecule.

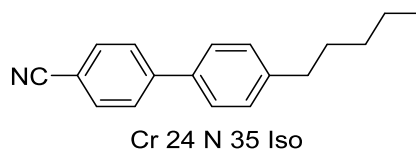


Figure 1: 4-Cyano-4'-pentylbiphenyl<sup>9</sup>

Discotic systems as the name suggests are disk like molecules that usually consist of flat aromatic cores with flexible chains on the peripheries. Due to their architecture the mesophases exhibited by these molecules involves the formation of stacks to form higher ordered columnar assemblies. Triphenylene based systems are an example of widely studied discotics<sup>10</sup>.

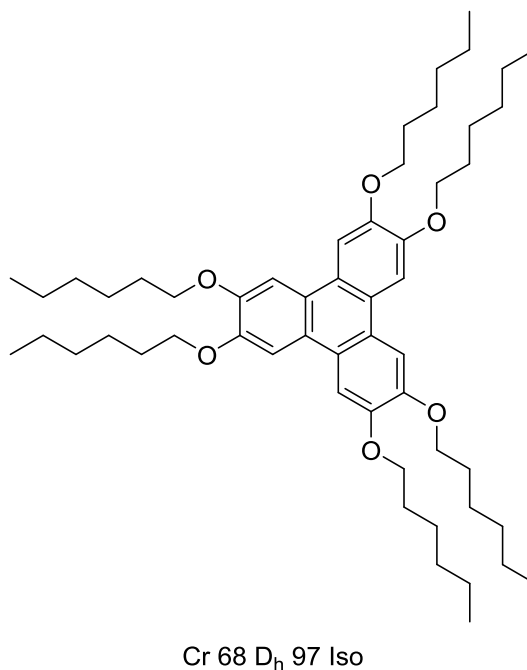
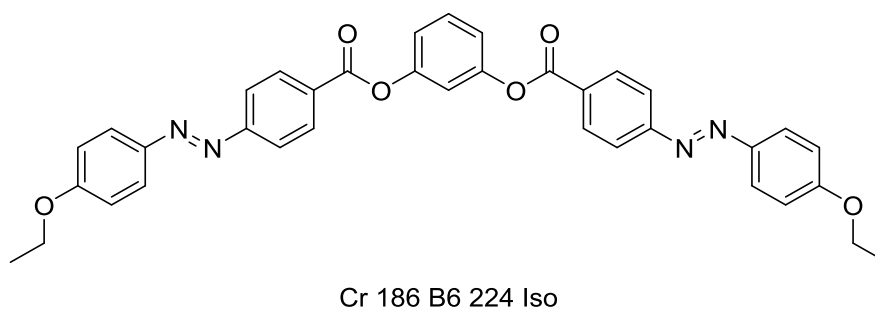


Figure 2: 2,3,6,7,10,11-hexakis(hexyloxy)triphenylene

Bent core systems, also known as banana molecules, can be described as having a V-shaped structure first described by Niori<sup>11</sup>. Vorlander<sup>12</sup> in 1929 synthesized the first bent core systems but it wasn't until 2001 when Pelzl<sup>13</sup> found the bent core shown in Figure 3 to exhibit the B6 phase. These systems form polar smectic phases from achiral molecules and stirred up a considerable amount of interest in the ferroelectric liquid crystal community. These systems were also considered as candidates for exhibiting the biaxial nematic phase.



**Figure 3: 1,3-phenylene bis(4-(4-ethoxyphenyl)diazenyl)benzoate)**

High molar mass LC systems such as dendritic and polymeric are a combination of one of the above mentioned classes, and are branched or polymerised to form LC phases. As these systems will not be featured in this thesis, nothing further will be mentioned regarding these systems.

## Mesophases

### Nematic phases

The liquid crystal nematic phase (N) is the simplest and least ordered of all the mesophases. In this phase the molecules have no short range positional order like in an isotropic liquid but unlike an isotropic liquid they tend to orientate along their long axis. This direction is known as the nematic director as shown in Figure 4.

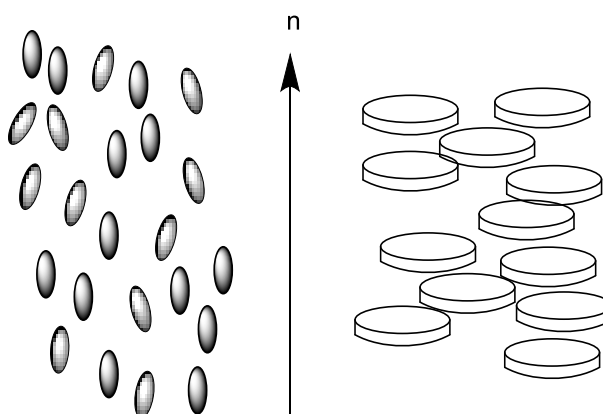


Figure 4: Schematic representation of molecular order in the nematic phase in calamitic (left) and discotic (right) systems

Although rare, a similar picture is true for discotic systems as first predicted by Vorlander<sup>14</sup> 90 years ago. The first nematic discotic was discovered in 1979 by Nguyen<sup>15</sup>. In 1999 only 0.7% of known nematics were discotic nematic<sup>16</sup>.

The chiral nematic phase ( $N^*$ ) is also known as the cholesteric phase as it was first observed in the derivatives of cholesterol<sup>3,4</sup>. It is essentially a nematic phase but due to the molecular asymmetry the molecules form helical superstructures. The  $360^\circ$  rotation of the director is known as one pitch length.

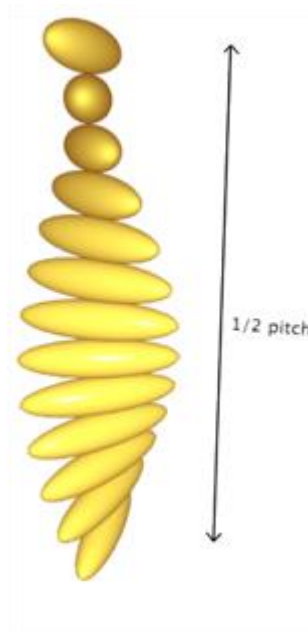


Figure 5 : Schematic representation of the chiral nematic phase<sup>17</sup>.

Apart from the above mentioned uniaxial nematic phases the existence of biaxial systems is also known. Biaxial nematics are best described as board shaped molecules that have two axes of rotation.

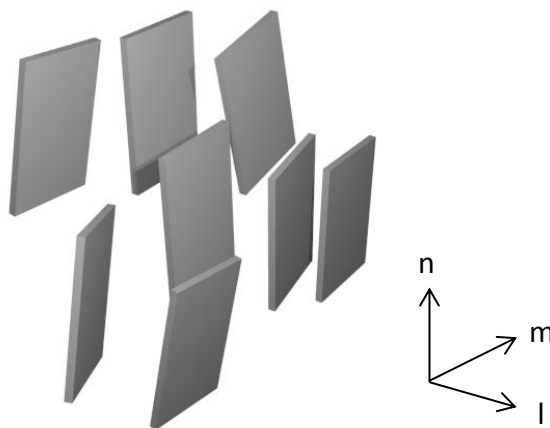


Figure 6 : Schematic representation of the biaxial nematic phase.

Freiser<sup>18</sup> theoretically proposed the existence of a biaxial nematic phase but it was not until a decade later that Saupe<sup>19</sup> reported conoscopic observation and deuterium NMR of a biaxial nematic phase in lyotropic mixtures of potassium laurate and decanol. Biaxial nematic phases have also been observed for particles under external

forces<sup>20,21,22</sup>, and polymeric systems<sup>23,24,25,26</sup> but low molecular weight systems have been more elusive. After an enormous amount of effort, a bent core based on an oxadiazole core<sup>27</sup>, a hybrid bent core dimer<sup>28</sup> and systems based on tetrapodes<sup>29</sup> were found to show stable biaxial nematic phases.

Due to the random nature of orientation of molecules within a nematic phase the presence of smectic cybotactic clustering is known. First proposed in 1970<sup>30</sup> these clusters may exist as a pre-transitional feature of Sm-N transitions or be present through the entire nematic range<sup>31</sup>. Examples of cybotactic clusters have been found in bent core mesogens<sup>32</sup>, liquid crystal polymeric systems<sup>33</sup>, supramolecular inorganic-organic assemblies<sup>31</sup> and disc shaped dimers<sup>34</sup>.

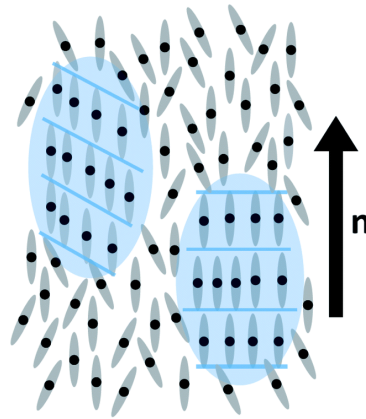


Figure 7 : Schematic representation of the random fluctuations leading to smectic arrangements within a nematic phase<sup>35</sup>.

Since the discovery of the conventional uniaxial nematic phase almost 125 years ago it has remained as the simplest example of LC phases. This has recently been disrupted with the discovery of new nematic phases. Meyer *et al* (1973)<sup>36</sup> and Dozov *et al* (2001)<sup>37</sup> proposed a model shown in Figure 8, where the shape of the molecule induces a local bending of the nematic director and predicted that this spontaneous periodic distortion leads to the formation of a combination of splay-bend or a twist bend helix.

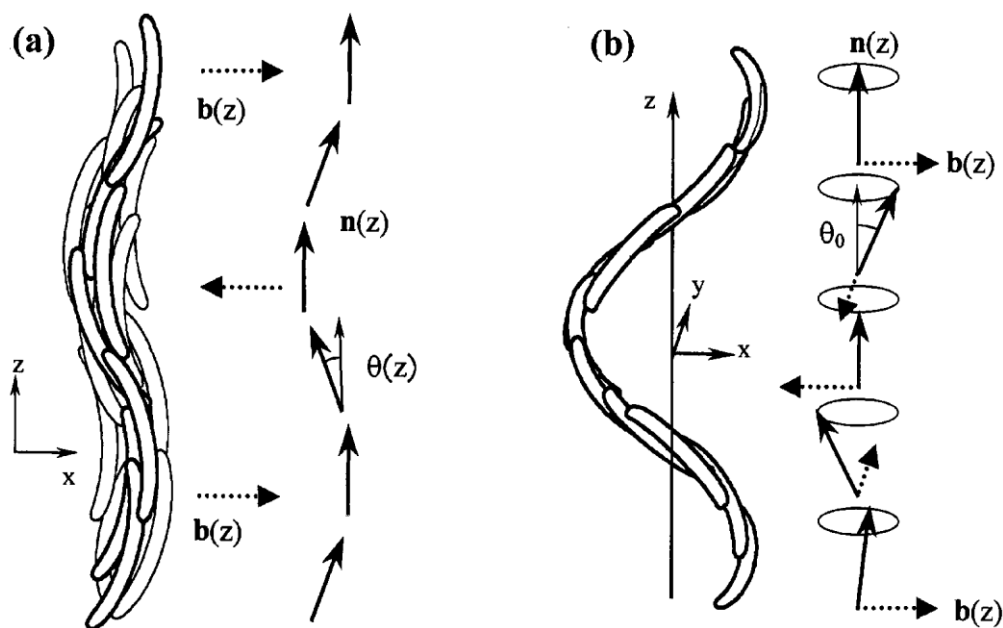


Figure 8: Twist-bend and splay-bend structures proposed by Dozov

Ungar<sup>38</sup> *et al* in 1992 reported sharp transitions on differential scanning calorimetry (DSC) between nematic phases in polymeric systems and then linked it to the folding of the alkyl chains. Schroeder<sup>39</sup> *et al* in 2003 synthesized hockey shaped asymmetric bent core molecules with two nematic phases above the columnar phase. It was concluded not to be smectic due to the absence of short range order on X-ray diffraction (XRD) studies. The proposed model was a columnar nematic which was regarded as a precursor to the formation of the higher order B<sub>1</sub> phase.

Sepelj<sup>40</sup> *et al* synthesized symmetric dimers based on salicylaldimine connected to alkylene spacers via imino groups. For short chain odd numbered spacers of five and seven a second monotropic nematic phase was observed and was again attributed to a columnar nematic phase, but in these examples there was not a higher order columnar phase at lower temperatures.

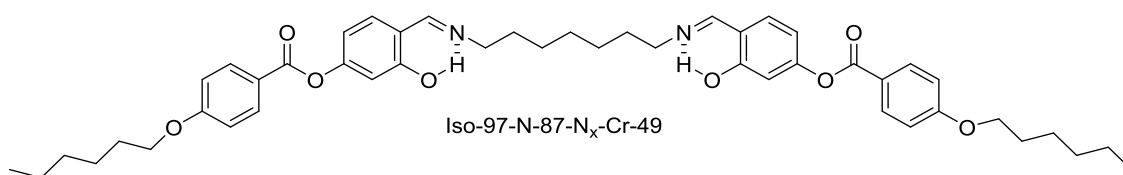


Figure 9 : Sepelj's dimer showing lower temperature nematic phase.

Panov<sup>41</sup> *et al* in 2010 reported two nematic mesogens linked *via* a methylene spacer. The compounds exhibited a secondary nematic phase and distinct stripes were observed along the rubbing direction under optical polarising microscopy (OPM). XRD studies showed there was no short range order present and hence it was called an  $N_x$  phase. This became the first reported experimental example of Meyer's predicted model.

Asymmetric chiral ester dimers with cholesterol and methylethanaminecyanobiphenyl mesogens were investigated<sup>42</sup> and systems of odd numbers from lengths varying between three and fifteen showed multiple nematic phases. In the case of the longest dimer with a fifteen carbon chain, high resolution differential scanning calorimetry showed up an additional five mesophases between a conventional chiral nematic and  $N_{TB}$ .

Although the structure of the phase is still under debate, the discussion seems to have been narrowed down to two hypotheses. Borsch<sup>43</sup> *et al* and Clark<sup>44</sup> *et al* in 2013 performed detailed freeze-fracture tunnelling electron microscopy (FFTEM) on the cyanobiphenyl (CB) dimeric compounds and found striped periodicity in the lower temperature nematic phase and attributed it to the short twist-bend helix of a 3-4 molecule long pitch. FFTEM involves heating the sample to the mesophase followed by rapid quenching in a cryogenic mixture of liquid ethane and liquid nitrogen to freeze the mesophase. The sample is then fractured open and the topology of the exposed surface is replicated by deposition of heavy metal at an angle. This creates shadows of the topography which is studied with the aid of a contrast agent. If during quenching some crystallization occurs then the fracture will occur along the crystal front as it will be the most prone to fracturing. Hori<sup>45</sup> *et al* investigated the crystal structure of the CB dimers and found the dimensions of the crystal lattice to be almost identical to the periodicity reported from the FFTEM measurements. Gorecka<sup>46</sup> *et al* performed Atomic force microscopy studies on the CB dimers and found that the 3-4 molecule long periodicity of the twist-bend helix is in fact related to the crystalline structure of the solid state. The proposed twist-bend model is schematically represented below<sup>20</sup>.

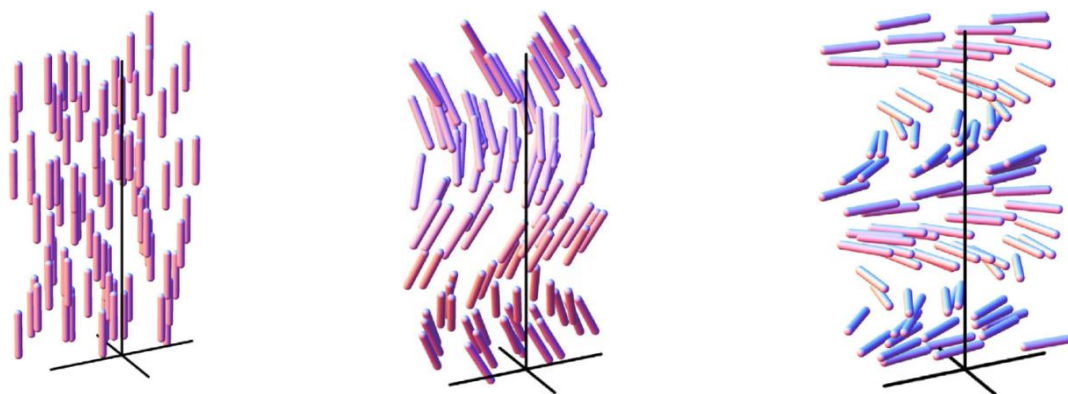


Figure 10 : Schematic representation of the  $N_{TB}$  phase in comparison with a N and  $N^*$  phase

N

$N_{TB}$

$N^*$

The other proposed hypothesis on the structural details of the  $N_x$  phase was made by Hoffmann<sup>47</sup> et al. They proposed that the lower temperature phase experiences a chiral environment and are ordered about a unique direction. Using NMR experiments they reported the absence of a spontaneously modulated director and showed that behaviour on switching the magnetic field from parallel to perpendicular was that of a single director either throughout the sample or more likely in smaller domains of opposite handedness.

The major argument against this model is the presence of a strong magnetic field ( $B_0 = 11.7$  T) required to carry out these NMR experiments is strong enough to unwind the twist-bend helix. If the helix is unwound all the measurements fit the proposed model. There is more uncertainty as it is possible that in the absence of a magnetic field the chiral domains under particular anchoring effects can spontaneously form large length scale helices *via* soft-assembly.

Identification of the  $N_{TB}$  phase is not entirely straight forward by OPM as some of the exhibited textures are very similar to those exhibited by smectic phases. This is the reason the existence of this phase was originally identified incorrectly as a smectic phase when the cyanobiphenyl dimers were first investigated<sup>48</sup> in 1984 and even as recently as 2001<sup>49</sup> in odd numbered dimers based on methylethaniminecyanobiphenyl.

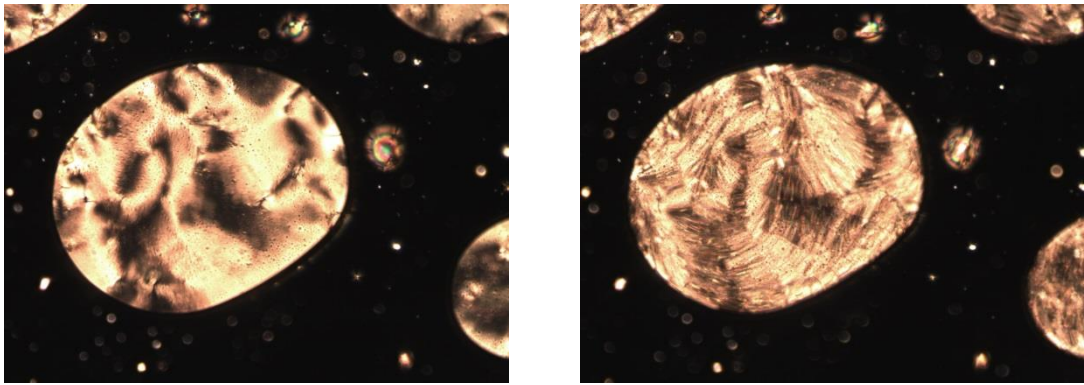


**Figure 11** : Example of texture exhibited by a conventional nematic phase (left) and a  $N_{TB}$  phase (right).

Shown above is an example of the difference in texture between the two nematic phases shown from this work. On the left you can observe conventional nematic texture with a few disclinations. On the right is the same region at a lower temperature in the  $N_{TB}$  phase and the change in texture is striking, additional features appear that can be described as having a plated like texture.

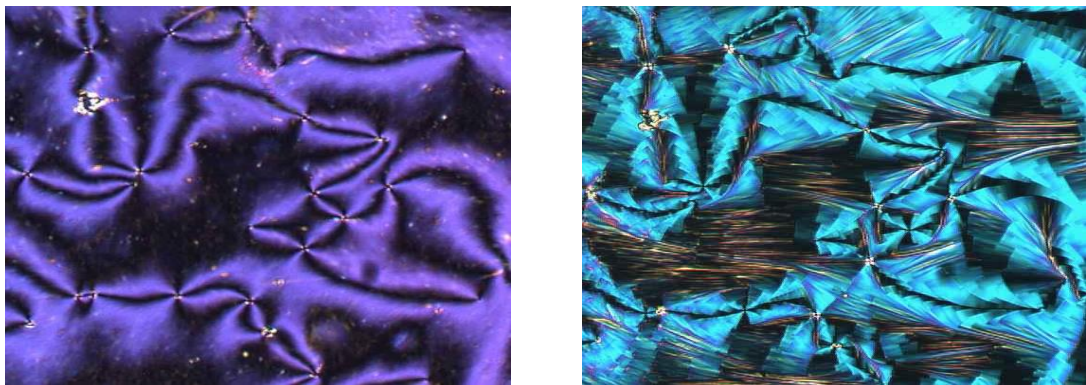


**Figure 12** : Example of texture exhibited by a conventional nematic phase (left) and a  $N_{TB}$  phase (right).

As seen in the above images there are variations within this plated texture, possibly depending on how the microscope slide is prepared. The micrograph on the left shows thread like nematic texture with 2 and 4 point brush defects whereas the micrograph on the right shows plated texture with broader more defined plates. It is interesting to note on the micrograph on the right that disclinations lines are still present, meaning the bulk of the molecules still contain these defects. Also, the regions around the middle of the micrograph with homeotropic alignment, seen as dark regions in the nematic phase, show streaky ribbon like texture.

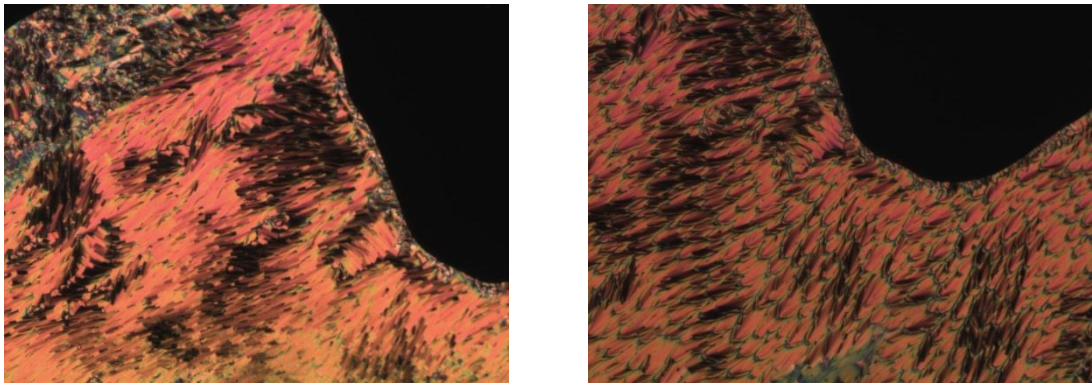


**Figure 13 : Example of  $N_{TB}$  textures.**

Shown in the above micrograph is the same region of a  $N_{TB}$  sample, the only difference is the micrograph on the right is at a temperature 2 °C lower. As observed the plated texture goes into the polygonal fish scale texture. It is important to note that this texture change does not register a thermal event on calorimetric studies. As both types of textures are kinetically stable at constant temperatures it is likely the plated texture retains some characteristics of the preceding conventional nematic phase. If that is the case the true texture of the  $N_{TB}$  phase would be the polygonal fish scale texture. Shown below is this texture at double the magnification.

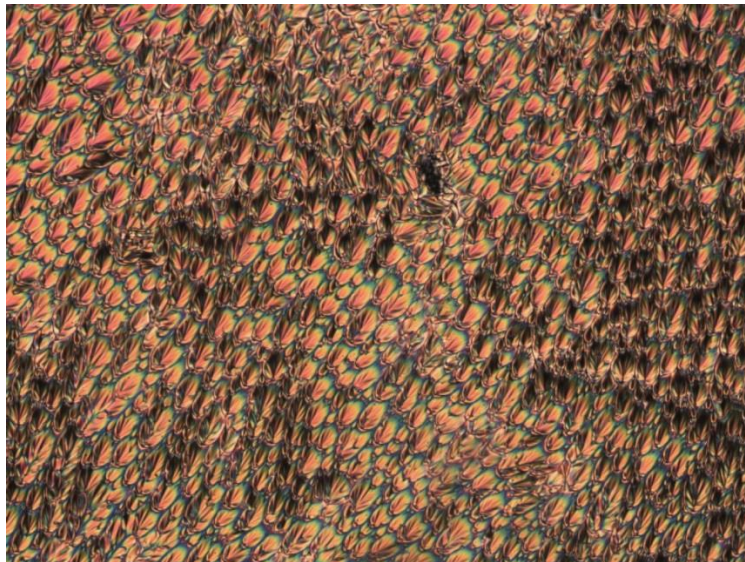


**Figure 14 : Polygonal fish scale texture of  $N_{TB}$ .**

Another example of the variety of  $N_{TB}$  texture is shown below. This texture can be described similar to focal conic textures usually observed for the smectic A mesophase. The observed focal conics are much narrower than normally observed.

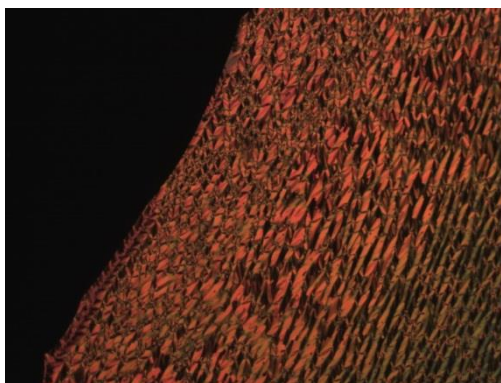


Figure 15 : Narrow focal conic texture of  $N_{TB}$ .

A characteristic observation for the nematic mesophase is its homeotropic alignment under shearing. This is also true for the  $N_{TB}$  phase as shown in the below micrographs.

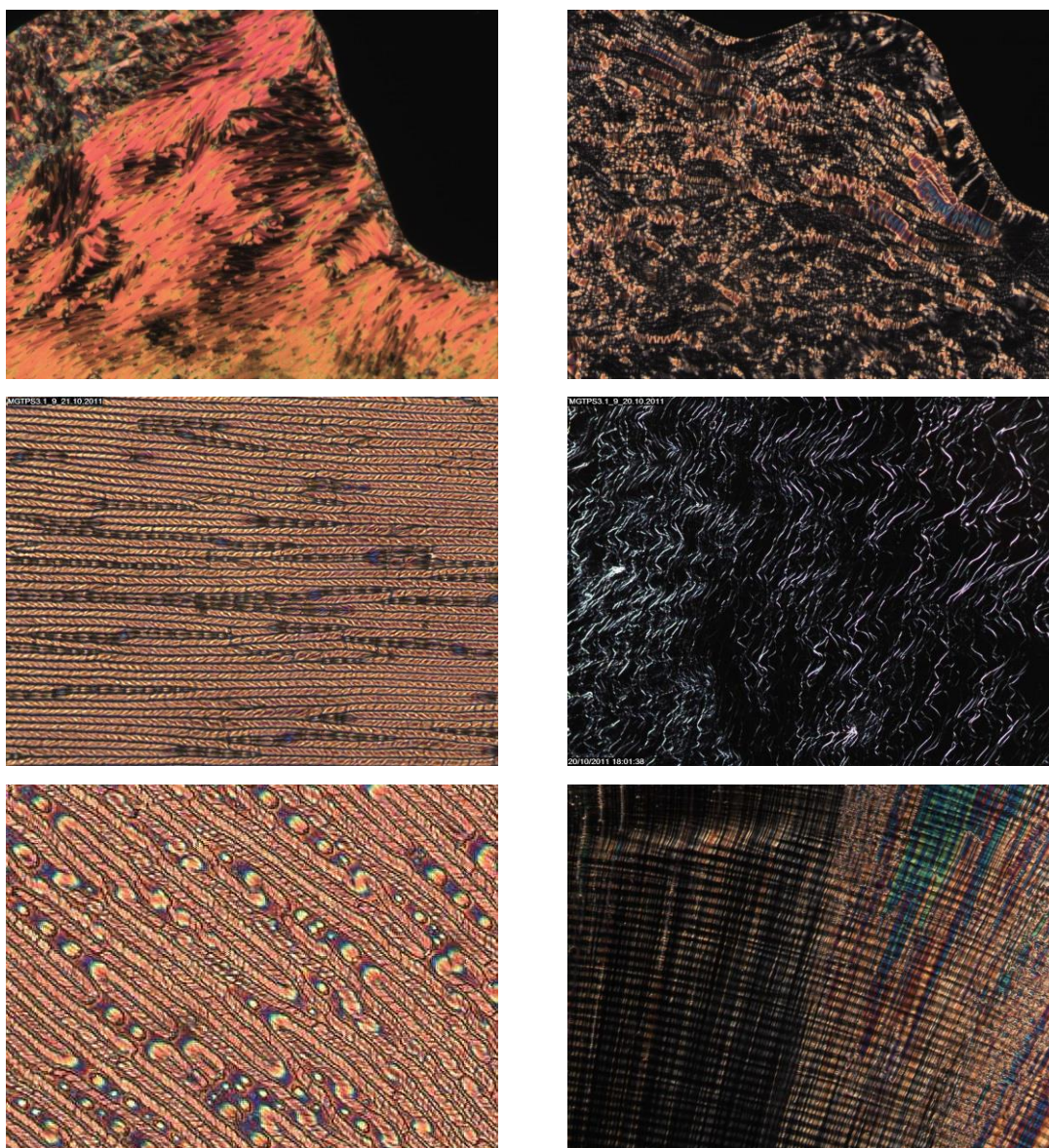


Figure 16 : 2 examples of shearing experiment of  $N_{TB}$  before (left) and after shearing (right).

The first sets of micrographs were prepared on untreated glass slides. The second set of micrographs, were prepared on a lightly rubbed slide, with a horizontal rubbing direction. The third sets of micrographs were prepared with planar coated 6  $\mu\text{m}$  cells. As observed in the second set, the polygonal fish scale like texture now aligns along the rubbing direction, this in turn is also a good example to show the origin of the characteristic rope like texture which is always observed in planar cells.

As the transition to the  $N_{\text{TB}}$  phase is a first order transition it is observable on differential scanning calorimetry with smaller transition enthalpies than conventional nematic systems. Of the systems currently known in literature this value has been observed from  $1/2 - 1/5$  of the enthalpy of nematic isotropic transition on cooling and heating. As the formation of the  $N_{\text{TB}}$  phase is not completely understood its possible a number of combinations of splay, twist and bend phases are present below the conventional nematic phase that have been generalized as the  $N_{\text{TB}}$  phase in the reported systems which might be the reason for the varying enthalpies.

So far the only reliable way of identifying the  $N_{\text{TB}}$  phase has been using X-ray diffraction, as the  $N_{\text{TB}}$  phase, similar to the nematic phase has no short range order, they can easily be differentiated from smectic phases.

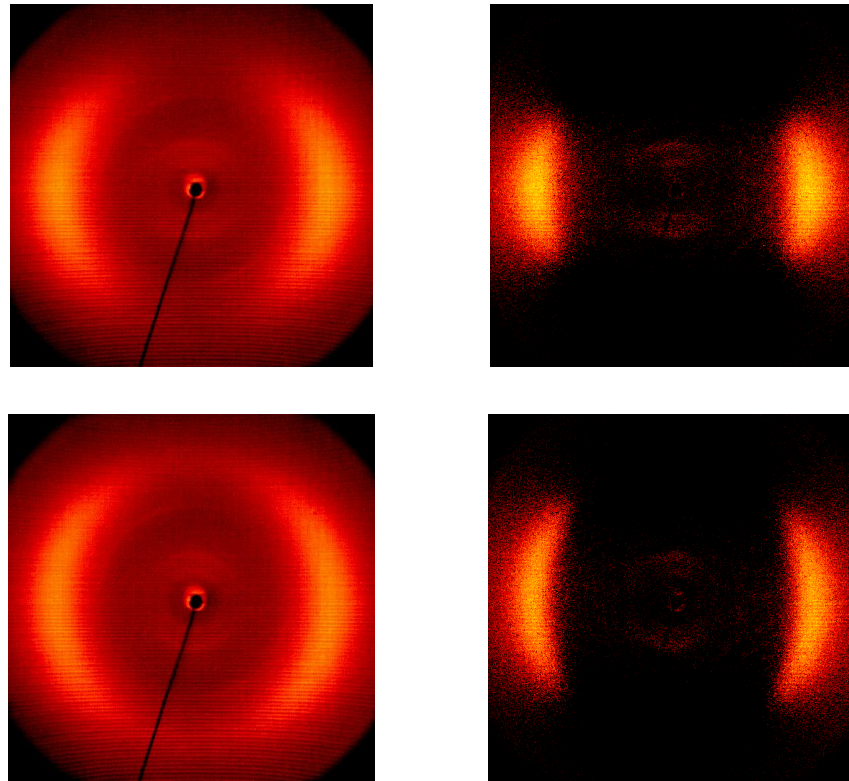


Figure 17: Diffraction pattern for CB-C9-CB at N (top) and  $N_{TB}$  (bottom) phase. Images on the right have isotropic scattering subtracted.

Although the two sets of diffraction patterns by themselves are indicative of only the presence of a nematic phase, placed together it is easy to tell the  $N_{TB}$  phase apart. Very weak scattering in the small angle region is characteristic of nematic behaviour but the important thing to note is the change in the wide angle scattering. The diffused halos in the wide angle still have a maxima at 4.6 which is normal for calamitic systems but the distribution of the signal in the  $N_{TB}$  phase is much narrower, indicating increased macroscopic order. Another important thing to note which is sometimes also observed is the 10-20 ° tilt observed in the wide angle scattering.

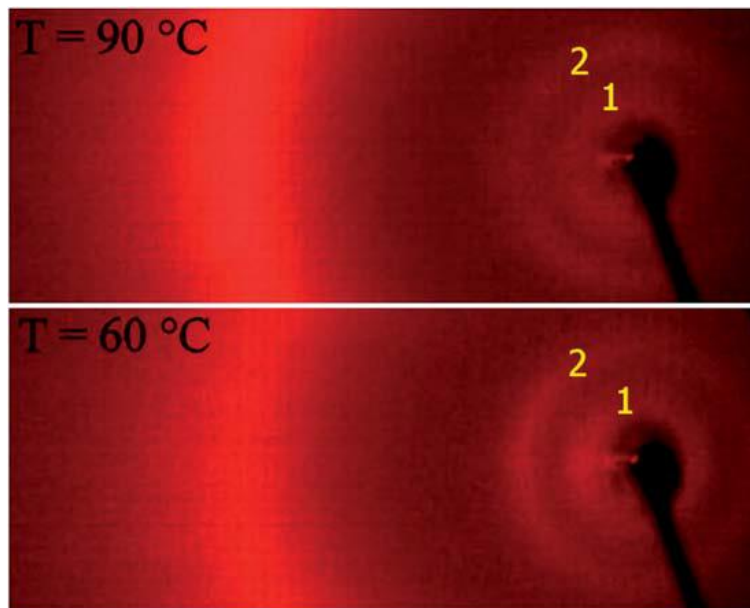


Figure 18 : Another example of the differences observed in XRD measurements<sup>42</sup>.

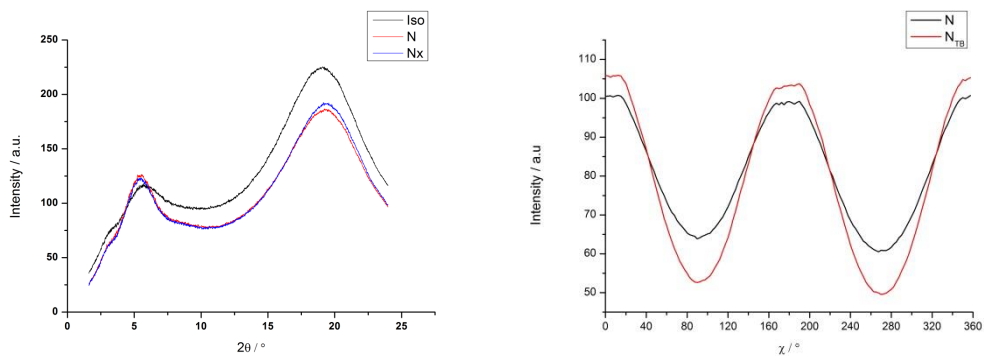
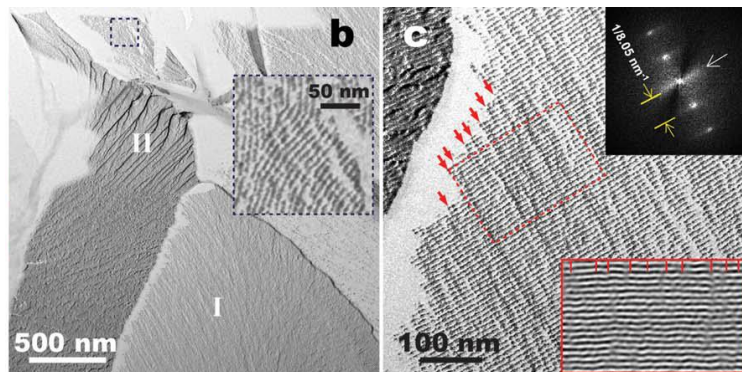


Figure 19 : Graphical representation of XRD data theta scans (left) and chi scans (right).

If the XRD data is shown in suitable graphs it becomes easier to observe the subtle differences between the two phases. From the 2theta against intensity plot it can be seen that the d-spacings remain unchanged and the only difference is the slight change in intensity with the  $N_{TB}$  higher. In the chi against intensity plot, in this example there is no evidence of a tilt but the slight increase in intensity can be rationalised. As the scattering from the sample should remain uniform between the two phases, the narrowing of the peak leads to higher intensities.

Recently the structural features of the  $N_{TB}$  have been investigated by the use FFTEM. Direct observation has not been possible<sup>50</sup> until recently and only replica studies have

been carried out. The process of replicating has been described earlier. The observed topography directly depends on the angle at which the sample is fractured.



**Figure 20** : FFTEM images of **CB7CB** fractured parallel to the helix axis<sup>43</sup>

Shown in Figure 20 is an example of the topography of the sample observed if the fracture is parallel to the helix axis. This fracture reveals clean layer structure and subsequent layers provide information on the helical pitch.

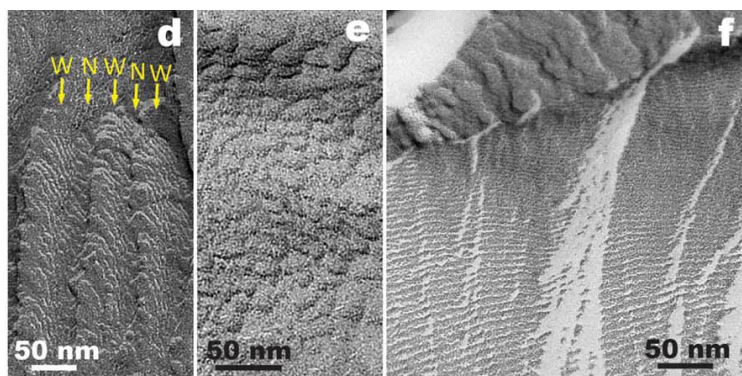


**Figure 21**: FFTEM images of **CB7CB** oblique fractured<sup>43</sup>

Shown in Figure 20 is an example of the topography of the sample observed if the fracture is at an angle to the helix axis. Fracture reveals steps and some layer structuring. Bouligand<sup>51</sup> arches are formed for  $N_{TB}$  and help differentiate from helixes observed for a chiral nematic phase. A system of wide and narrow Bouligand arches and a system of periodic incomplete arches can be seen in sections labelled **d** and **e**. In a chiral nematic a  $180^\circ$  twist of the director should result in a complete arch.

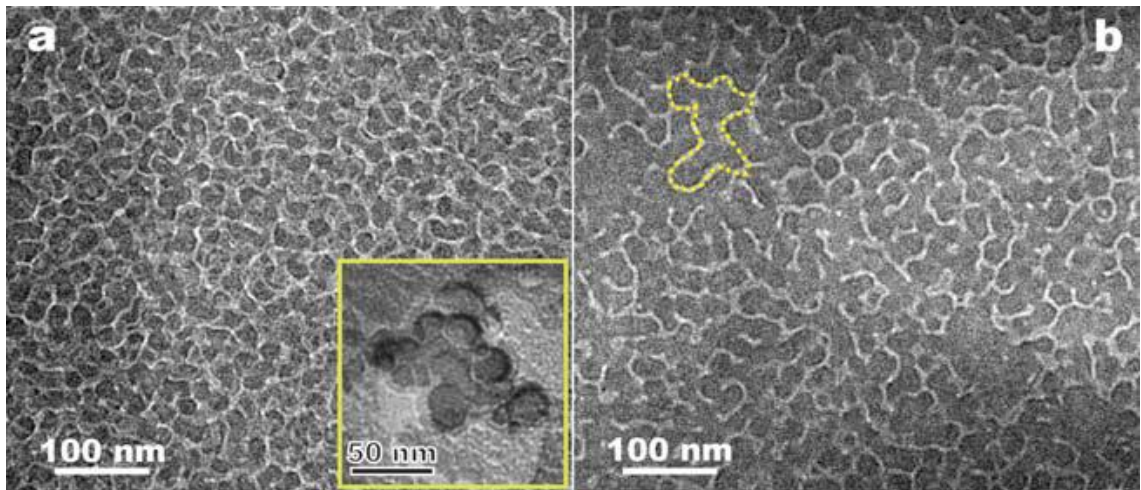


**Figure 22:** Direct cryo-TEM observation of **CB7CB** pure (left) and with right-handed limonene.

Figure 22 shows the column like structure observed on direct observation by cryo-TEM of **CB7CB**. This observation is also predicted if in FFTEM, the fracture can be made perpendicular to the helix axis. It is interesting to note the domains are separated by narrow areas of low density areas. Upon addition of right-handed limonene the number of domains observed roughly halves and the column sizes increases. This is a similar observation to that observed in NMR experiments by Hoffmann<sup>47</sup>.

### **Smectic phases<sup>2</sup>**

The smectic phase is one in which molecules align along the long axis and within layers. If there is no positional order within each layer and if the layers are perpendicular on average to the long axis, the director, then is characterised as a smectic A phase (shown in Figure 23 left). If the layers propagate at any other angle the mesophase is characterised as a smectic C phase (shown in Figure 23 right).

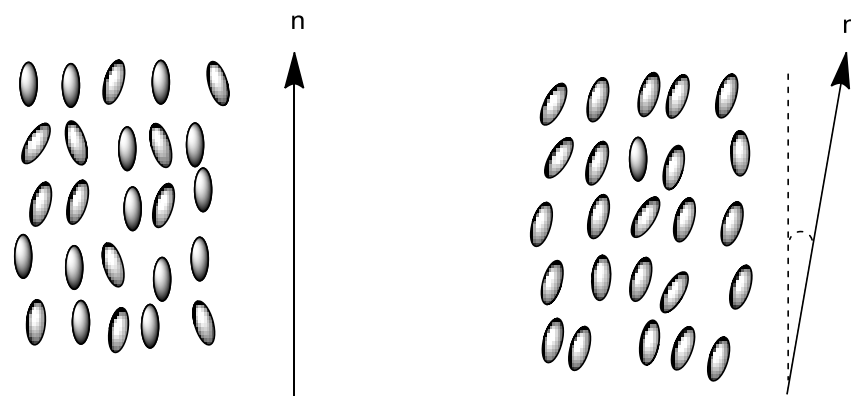


Figure 23: Schematic representation of molecular order in smectic A and smectic C phase respectively.

### Bent core<sup>52,33</sup>

Bent core or banana phases as the name suggests are found in molecules with a bent architecture. As these mesophases do exhibit some similarities with conventional calamitic phases, The presence of many complicated sub phases<sup>53</sup> led to  $B_n$  type nomenclature.  $B_1$  phase is similar to a columnar rectangular phase<sup>54</sup>. The  $B_2$  is a tilted smectic phase with polar order<sup>55</sup>.  $B_3$  is tilted lamellar crystalline phase<sup>56</sup>.  $B_4$  has only very recently been characterised as the helical nano-filament phase only due to the advent of FFTEM<sup>57</sup>. This phase is discussed as comprising of bundles of rope like helical nano-filaments that pack together with opposite handedness. The  $B_5$  is often observed below the  $B_2$  phase and shows similar polar order<sup>58</sup>. The  $B_6$  is an intercalated smectic C type phase and is proposed to have formed from the collapse of a  $B_2$  phase<sup>59</sup>. The  $B_7$  phase is a smectic phase with polar ordering similar to the  $B_2$  phase<sup>60</sup>. Unlike in the  $B_2$  the macroscopic polarisation is reduced due to the spontaneous splay of the polar directions and this leads to interesting optical textures. The  $B_8$  phase has a bilayer structure with the molecules organised in a double tilt arrangement<sup>33</sup>.

## Characterisation

To investigate the nature of liquid crystal mesophases three main techniques are used. These are optical polarising microscopy (OPM), differential scanning calorimetry (DSC) and X-ray diffraction (XRD). Using a combination of these techniques it is possible to investigate the mesophase and its structure in detail.

### Optical polarising microscopy

Liquid crystals are optically anisotropic materials, when light propagates through a liquid crystal it is split into two rays, ordinary and extraordinary. This phenomenon occurs due to the material showing different refractive indices in different directions and hence the light propagates through the material at different speeds<sup>61</sup>. This property is also known as birefringence and can be calculated using the following formula;

$$\Delta n = n_e - n_o$$

Where  $\Delta n$  is birefringence,  $n_e$  is extraordinary refractive index ray and  $n_o$  is the ordinary refractive index ray. Shown below in Figure 24 is a schematic representation of a polarising optical microscope. The sample is viewed between two polarisers perpendicular with respect to each other labelled here polariser and analyser.

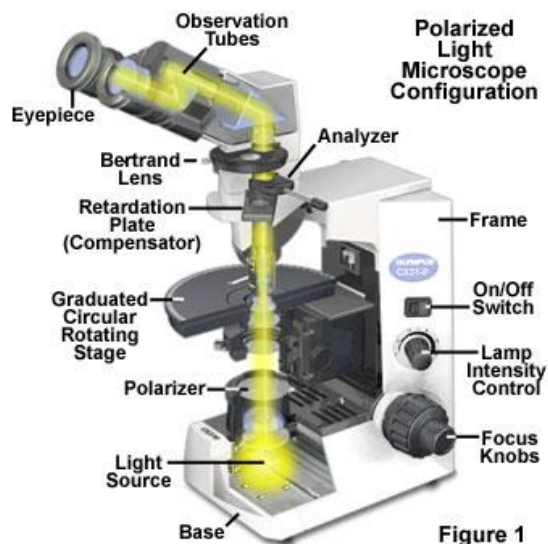


Figure 24: A typical optical polarising microscope showing its working components<sup>62</sup>.

As the light passes the first polariser it is polarised in that particular direction, it then passes through the liquid crystal sample and is split into two rays that will travel at

different speeds and out of phase, where now the light has a component that will be parallel to the analyser. The component parallel to the analyser passes through and it is viewed as coloured. This concept is represented schematically below.

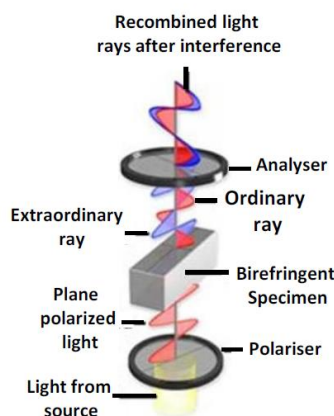


Figure 25: A schematic representation of the interaction of light with liquid crystals between crossed polarisers<sup>63</sup>.

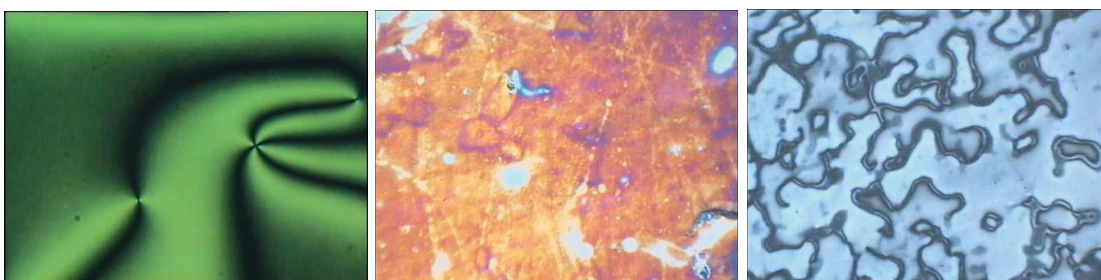


Figure 26: Micrographs of nematic phase, (left) Schlieren texture, (centre) marble texture, (right) thread-like texture.

### Differential scanning calorimetry

Differential scanning calorimetry (DSC) is a technique applied to accurately investigate the thermal behaviour of liquid crystalline samples. The technique provides vital information such as accurate transition temperatures and transition enthalpies. The technique involves an enthalpic measurement of a liquid crystal against a reference material, usually gold, within a closed system. Energy is supplied to both the reference and sample at a constant rate, at a transition, for example melting, the sample will require extra energy to maintain a uniform rate, and this extra input of energy is measured and amplified as the output and plotted as the change in enthalpy against time. The reverse is true for exothermic processes such as crystallization. These

measurements are performed under inert atmosphere to avoid any changes due to other chemical process such as oxidation. The components of a DSC are shown below in Figure 27<sup>64</sup>.

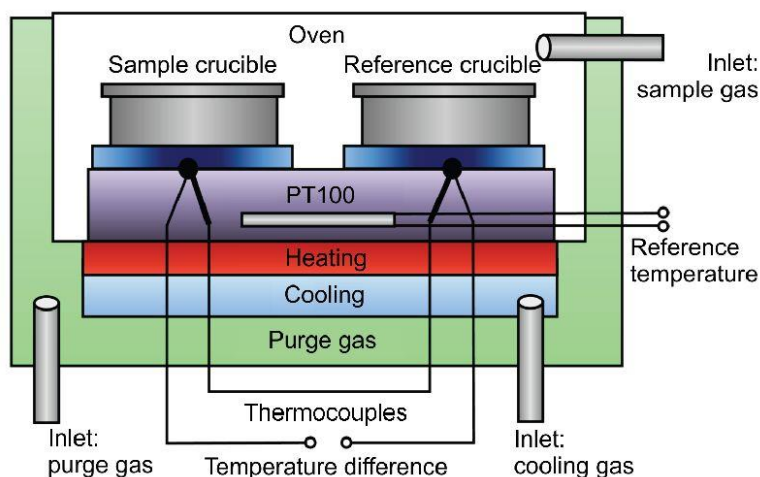


Figure 27: Schematic representation of a differential scanning calorimeter.

### X-ray diffraction

X-ray diffraction (XRD) is an experimental technique utilised to study the structure of a mesophase. It works on the principle of Bragg's law<sup>65</sup>, as x-rays interact with the atoms in planes, the interaction between planes is constructive when the path difference is an integer multiple of the wavelength. This relationship can be mathematically represented as the Bragg equation is shown schematically below in Figure 28<sup>66</sup>.

$$n\lambda = 2 d \sin\theta$$

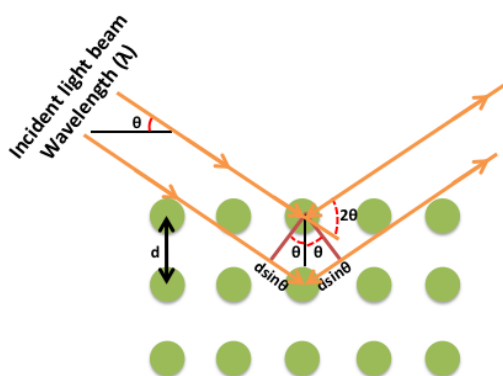


Figure 28: Schematic representation of Bragg's law.

It is also possible to study powder samples as they will consist of several micro domains and there will be a number of them that will satisfy Bragg's law. As there are many micro domains present, each spot will be averaged out as rings shown below in Figure 29<sup>67</sup>.

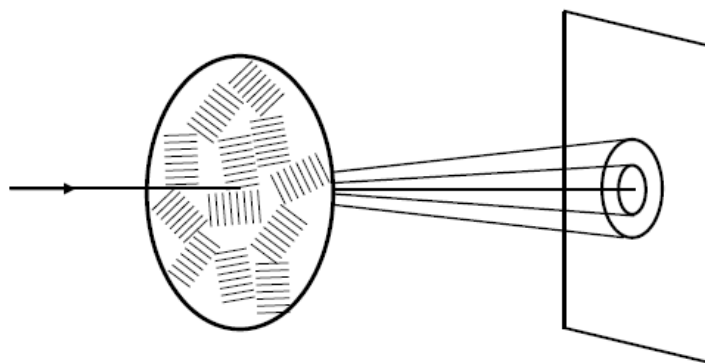


Figure 29: Schematic representation of powder diffraction.

The diffraction patterns of liquid crystalline samples are quite different to those observed for crystalline samples. Liquid crystals tend to show more diffused scattering rather than strong reflections depending on the mesophase.

Shown below in Figure 30 are typical XRD patterns and alongside them the molecular arrangements that lead to such scattering.

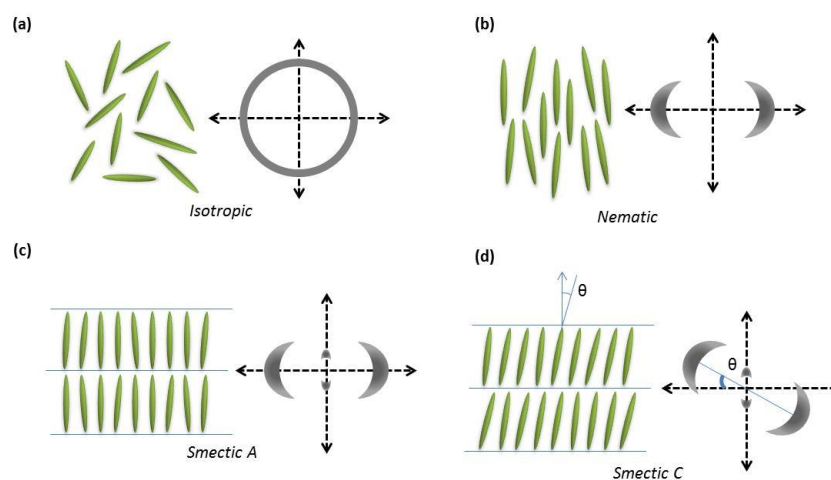


Figure 30: Schematic representation of XRD patterns and molecular arrangements.

## Dimers

In this thesis liquid crystal dimers are molecules that comprise of two mesogens connected via a flexible spacer. These compounds are also known as bimesogens, Siamese and twin mesogens. The initial interest arose in dimeric systems due to semi-flexible main chain liquid crystal polymers<sup>68</sup>. These polymeric systems showed unusual liquid crystalline behaviour<sup>16</sup> and in order to gain better understanding dimers were synthesized as simple oligomeric intermediates between polymers and monomers. Historically Vorlander<sup>69</sup> in 1927 is credited with synthesising the first dimer, Griffin *et al*<sup>70</sup> in 1981 with their alkoxybenzoate dimeric system shown in Figure, were historically most impactful.

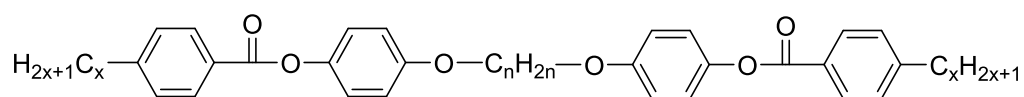


Figure 31: Griffin's dimer

Griffin and Britt investigated the effects of varying the spacer length and terminal chain length, they were also first to observe the odd-even effect of spacer length in dimeric systems. More recently dimers of all geometries have been studied in detail, these include linear<sup>71</sup>, H-shaped<sup>72, 73</sup> and T-shaped dimers<sup>74,75</sup>. For linear dimers the number of carbons in the spacer leads to the odd-even effect. Even number spacers tend to form linear zig-zig geometry which is more conventionally shaped than the odd numbered spacer where both mesogens are inclined to each other.

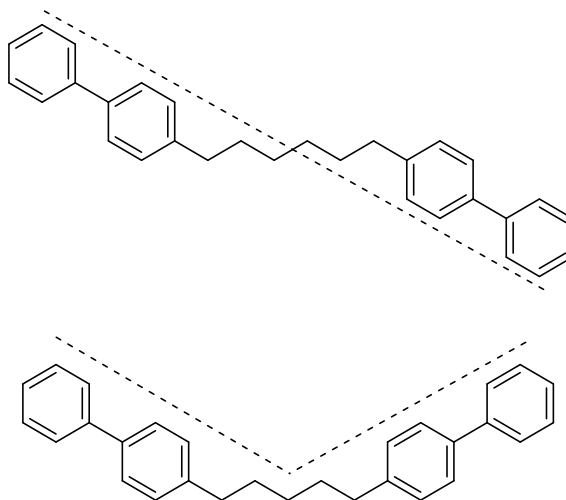


Figure 32: Schematic representation of the odd-even effect in simple dimers

## **Aims**

The overall aim of the project was to increase the understanding of the molecular features which are responsible for the formation of the  $N_{TB}$  phase. The recent discovery of the  $N_{TB}$  phase has refocused research on the fundamentals of nematic phase behaviour, which is structurally the simplest and technologically currently the most important of all the thermotropic liquid crystal phases.

The structural requirements for the formation of the  $N_{TB}$  phase are not well understood and hence a systematic investigation was to be undertaken where spacer lengths, connecting groups and a range of mesogenic were investigated. This involved the synthesis of a number of symmetric and non-symmetric molecular systems, their full chemical characterisation and the investigation of the liquid crystalline phase behaviour by optical polarizing microscopy, differential scanning calorimetry and systemic X-ray diffraction studies.

Based on this understanding it was the target to design and investigate systems which show  $N_{TB}$  phase behaviour at room temperature.

## Results and Discussion

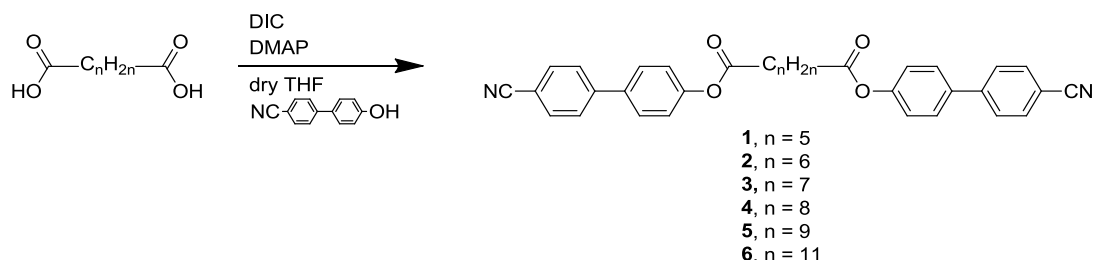
### Synthetic strategy

In this section the synthesis of the compounds will be rationalised and discussed as shown in schemes and a general literature review of the reactions will be reported.

### Synthetic Schemes

#### Scheme 1;

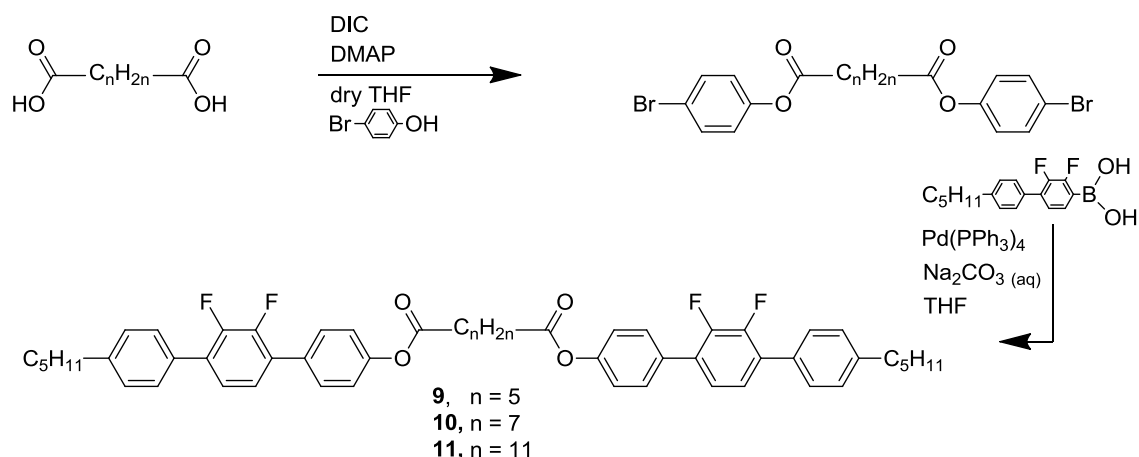
The synthesis of final compounds **1**, **2**, **3**, **4**, **5** and **6** were carried out *via* Steglich esterification<sup>76</sup> in the presence of N, N- diisopropylaminecarbodiimide(DIC) and 4-dimethylaminopyridine. DIC was preferred to N, N-dicyclohexylcarbodiimide(DCC) to ease the handling due to the highly sensitizing nature of these carbodiimides. The yields of this reaction were from 25-71% and were directly proportional to the length of the diacid chain, with the pimelaic acid (C5) with the lowest and tridecaneedioic acid (C11) with the highest.



#### Scheme 2;

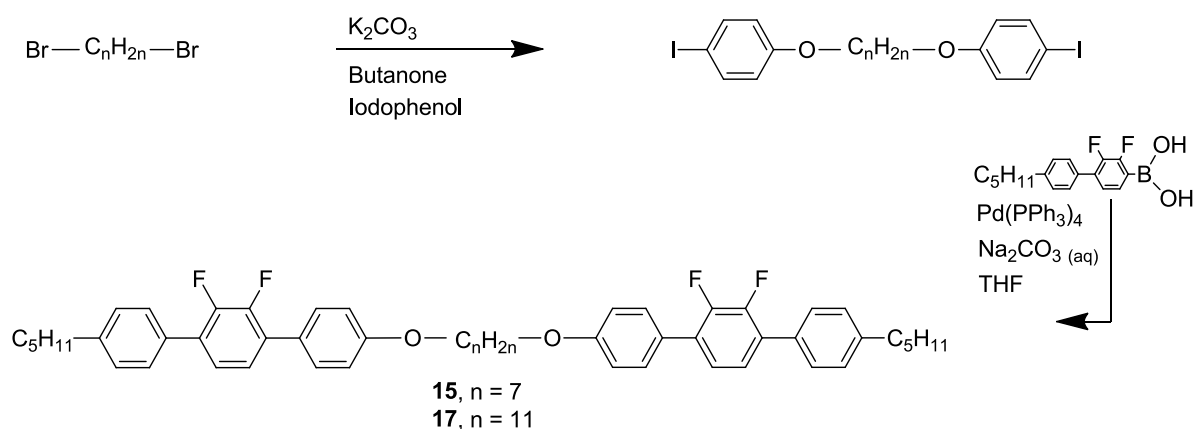
The synthesis of final compounds **9**, **10**, and **13** were carried out in 2 steps. Steglich esterification was used to synthesize the appropriate spacer with a phenylbromide or iodide followed by a Suzuki coupling<sup>77</sup> in the presence of a palladium catalyst with commercially available boronic acid. The yields were found to be 23, 21 and 74% respectively to the length of the chain. The low yield of the shorter length spacers can

possibly be explained due to the lack of solubility of the final compound during chromatography.



### Scheme 3;

Final compounds **15** and **17** were synthesized in two steps. A Williamson etherification<sup>78</sup> was carried out with dibromoalkanes to synthesize appropriate phenyliodide spacers followed by Suzuki coupling. The yields were found to be 68 % and 77%.

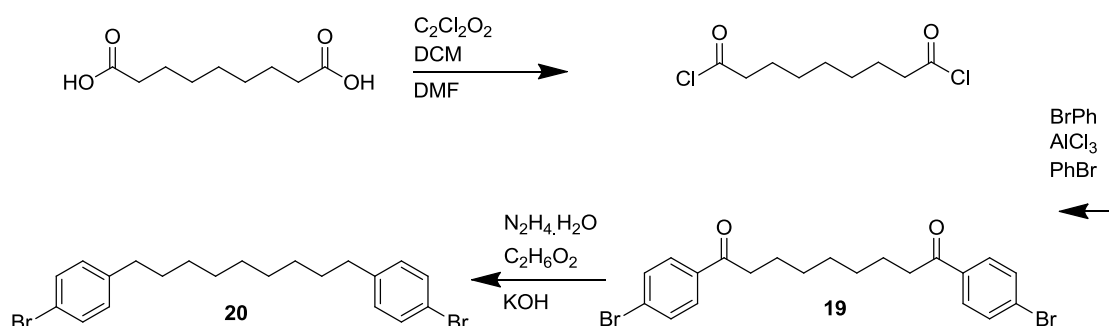


### Scheme 4;

The intermediate diketone spacer **19** was prepared by carrying out a Friedel Craft's acylation after converting the appropriate diacid to diacidchloride *via* oxalyl chloride. Thionyl chloride reacted significantly poorly and resulted in partially unreacted diacid, using the same conditions oxalyl chloride gave full conversion. This is thought to be due to the lack of solubility of the diacid in dichloromethane In the case of the oxalyl

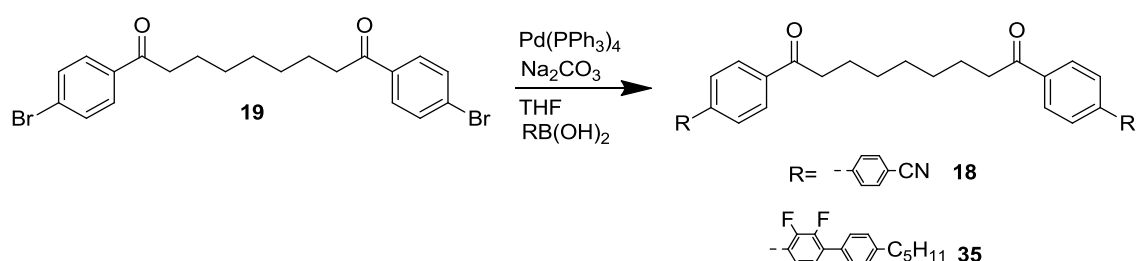
chloride, upon addition the reaction progresses and the sample gradually dissolves and subsequently reacts. The Friedel Craft's reaction was undertaken with relative ease, the scale of the reaction meant the work up had to be carried out in batches, the solubility of the diketone was similar to the diacid and a larger portion of the lost yield can be put down the amount of solvent required to carry out the extraction.

The intermediate methylene spacer **20** was prepared by reducing the diketone via a Wolff Kishner reaction<sup>79,80</sup>. Reduction of similar systems was tried with triethylsilane in trifluoroacetic acid but these experiments yielded as low as 30%. The work up required chromatography, although straightforward some batches with partially reduced ketone co-eluted meant a series of long repeats followed by multiple recrystallizations.



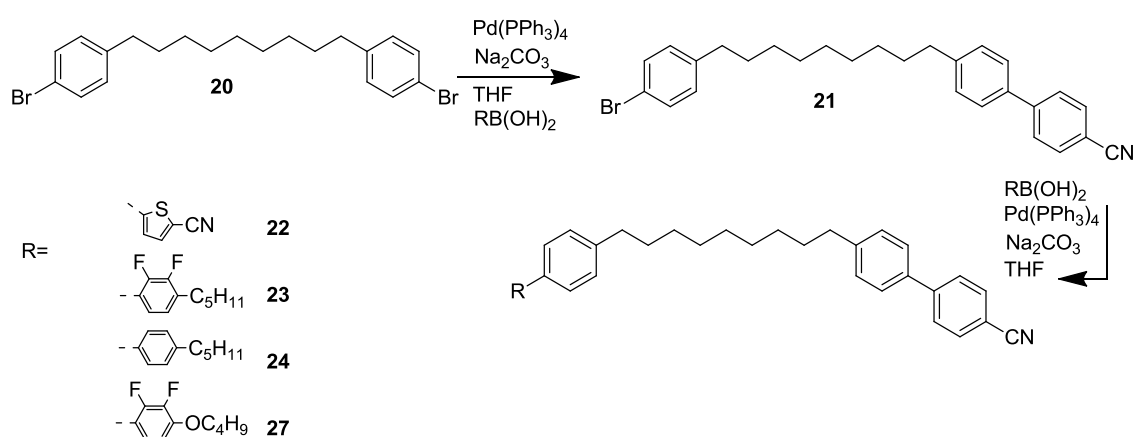
### Scheme 5;

Final compounds **18** and **35** were synthesized via a Suzuki coupling of commercially available boronic acids with diketone intermediate spacer **19** in the presence of a palladium catalyst.



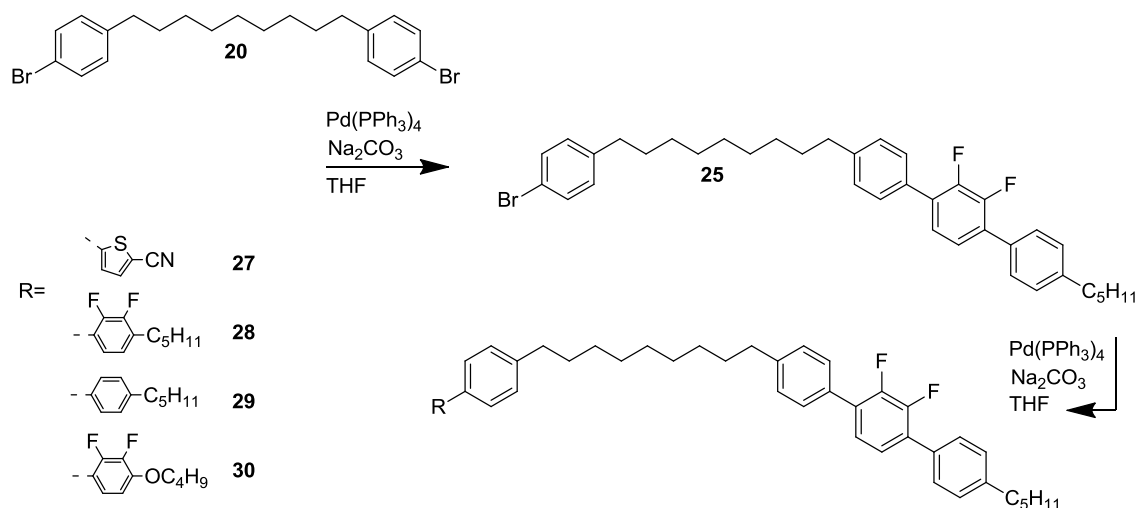
### Scheme 6;

The asymmetric final compounds **22**, **23**, **24** and **27** were prepared by two successive Suzuki coupling reactions. The first reaction was carried out with cyanophenyl boronic acid with a large excess of the spacer **20** (4x). The mono substituted compound is the major product with the conditions mentioned in the procedure, a 10 times dilution was also tried but no significant difference was observed. The unreacted spacer is easily isolated by chromatography and is reused. The yield was observed to be 65%. The second reaction is carried out with the appropriate boronic acid in excess this time to achieve complete conversion. The yields were found to be between 42-71% with the lowest yielding reaction containing cyanothiophene boronic acid. This is possibly due to the deboronation of the boronic acid. Strongly electron withdrawing groups promote deboronation in basic conditions<sup>81</sup>.



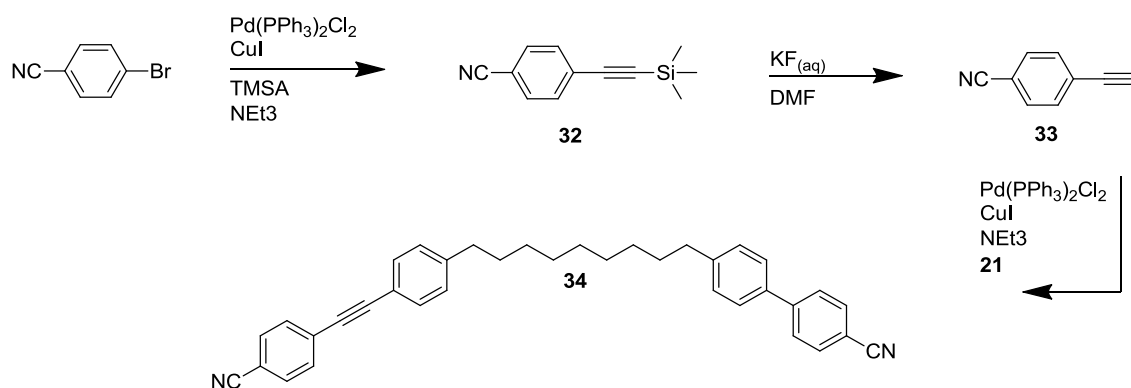
### Scheme 7;

Asymmetric final compounds **27**, **28**, **29** and **30** were prepared by two successive Suzuki coupling reactions. The first reaction was carried out with difluorobiphenylpentyl boronic acid with a large excess of the spacer **20** (4x). The unreacted spacer is isolated by chromatography and is reused. The yield was 65%. The second reaction is carried out with the appropriate boronic acid in excess this time to get completely conversion. The yields were found to be between 44-77% with the lowest yielding reaction again containing cyanothiophene boronic acid.



### Scheme 8;

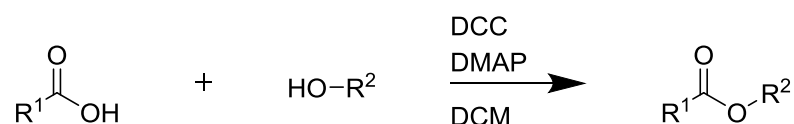
The asymmetric final compound **34** was prepared by palladium catalysed Sonogashira coupling reaction. The acetylenic section of the mesogen is prepared by reacting the aromatic halide with trimethylsilylacetylene with palladium catalyst and copper iodide co-catalyst. This reaction carried out in sealed conditions is clean and high yielding. The acetylene is then deprotected in the presence of potassium fluoride. The terminal acetylene is reacted with dimer intermediate **21** prepared as mentioned in scheme 6 to give final compound **34**. Using the same conditions for the Sonogashira reaction as before gives significantly lower yields for this final reaction. This is believed to be due to the insolubility of the asymmetric starting material **21** in triethylamine. As the reaction does not proceed with the desired reagents a considerable amount of acetylene homo-couples to form butadiynes. It is suggested to use a more polar solvent like *N,N*-dimethylformamide along with triethylamine to improve yields.



## Name reactions

### Steglich Coupling

Steglich coupling or Steglich esterification is a dimethylaminopyridine (DMAP) catalysed reaction used for ester, amide and peptide formation. The reaction is particularly useful as it uses mild conditions and modifications make working up clean and efficient. Below is the general scheme of the reaction.



DIC was preferred to DCC mainly for ease of handling as DCC is a waxy solid at room temperature. This makes it difficult to weigh out carefully and safely. Carbodiimides are highly sensitizing and extra caution needs to be taken while working with these reagents. The urea of DIC is also more soluble than its cyclohexyl variant which makes working up simpler. Tetrahydrofuran (THF) was preferred to dichloromethane (DCM) due to solubility of the diacid starting materials.

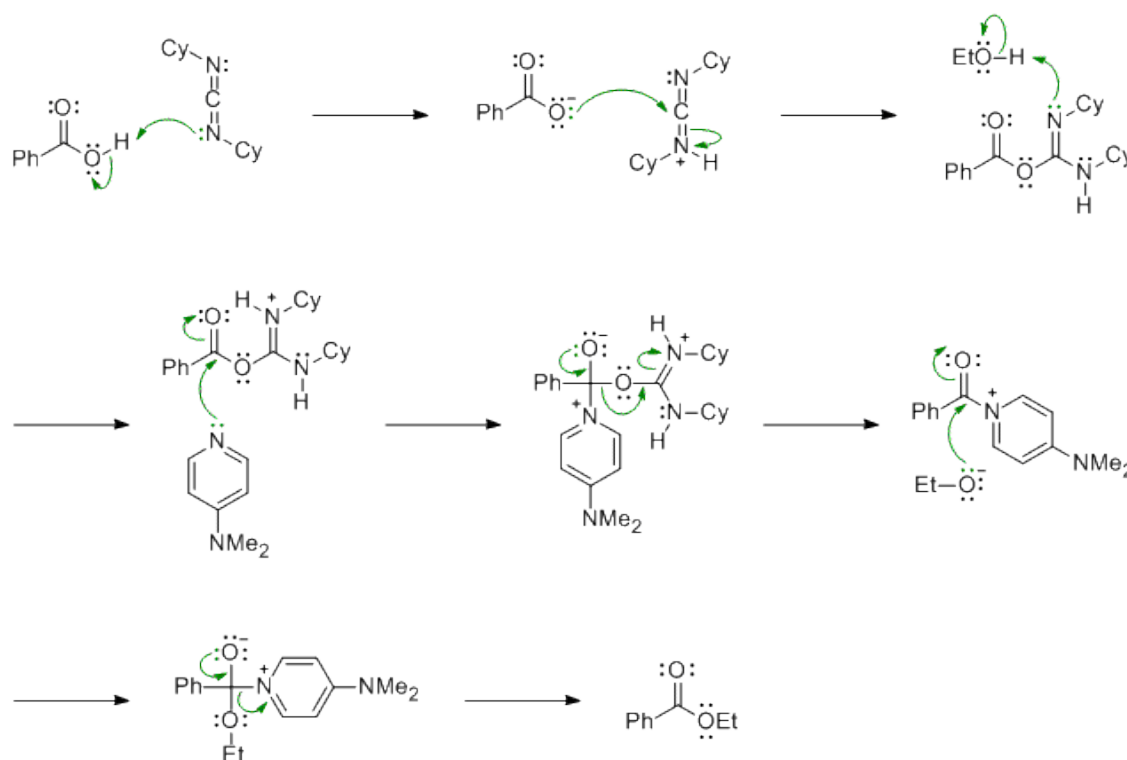
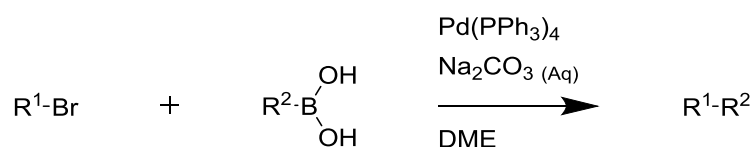


Figure 33 : Mechanism of Steglich esterification.

Shown above is an example of the reaction mechanism<sup>76</sup> of the esterification of benzoic acid and ethanol. DCC and the benzoic acid react to form an O-acylisourea intermediate. DMAP being a strong nucleophile rapidly reacts with this intermediate preventing side reactions and forming an active ester which can then be attacked by the alcohol to form dicyclohexyl urea and the required ester.

### Suzuki Coupling

Arguably the most important reaction for the formation of C-C bonds, since its discovery in 1979<sup>77</sup> has developed into a very versatile and reliable reaction. Suzuki coupling is a palladium catalysed reaction between a halide or pseudohalide and an organoborane compound. Carried out under basic conditions the reaction is stable to a wide variety of bases and solvents<sup>82,83</sup>. Shown below is a general scheme for the reaction.



A wide variety of palladium based catalysts can be used for the reaction. The preferred catalyst was tetrakis(triphenylphosphine) palladium(0) due to its relative stability to air. THF was used instead of dimethoxyethane (DME) as the solubility of the substrates observed was already known in THF and the yields were comparable to reactions carried out in DME.

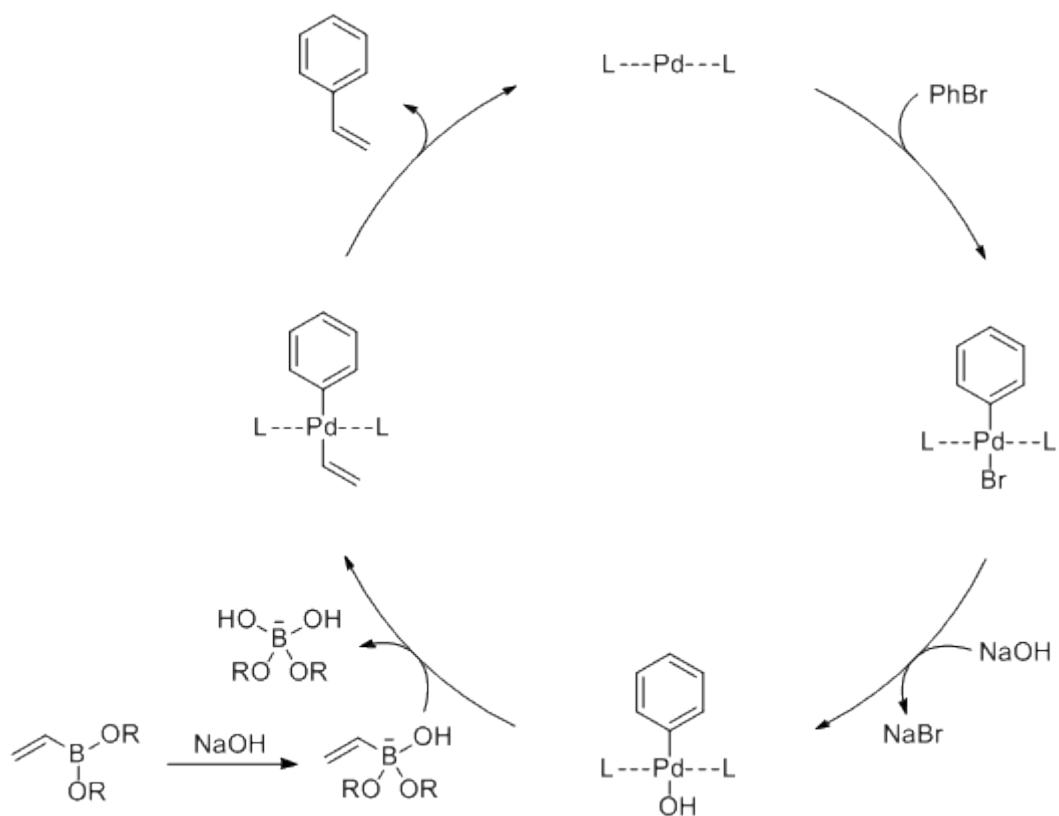
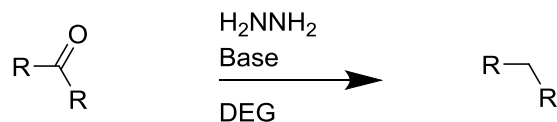


**Figure 34: Mechanism of Suzuki coupling reaction.**

Shown above is an example of the reaction mechanism<sup>83</sup> of coupling between vinylboronic ester and bromobenzene. The palladium catalyst undergoes oxidative addition with bromobenzene to form palladium (II) species. This then undergoes transmetalation and the base replaces the halide. The base also activates the boronic ester creating a four coordinate negatively charged borate species. This then undergoes transmetalation followed by reductive elimination. The palladium (0) is regenerated as the product is reduced off the catalyst.

## Wolff Kishner Reduction

Wolff Kishner reduction is used to reduce a carbonyl to a methylene group. This reaction progresses by the formation of a hydrazone from hydrazine and is released eventually as nitrogen. Shown below is a general scheme for Wolff Kishner reduction.



A number of modifications are known for this century old reaction. The Huang Minlon modification<sup>84</sup> which utilizes potassium hydroxide instead of elemental sodium as a base and the procedure distills off excess hydrazine and water after the formation of hydrazone to greatly increase yield and reduce reaction times by shifting the reaction equilibrium.

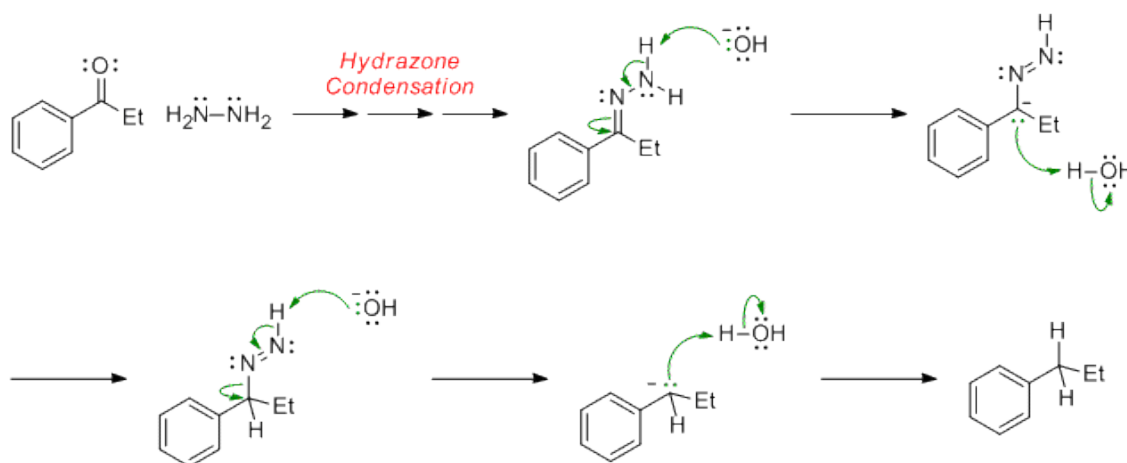
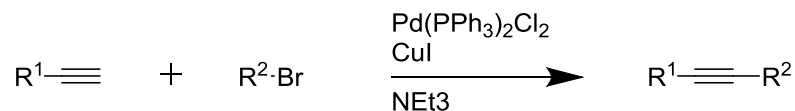


Figure 35: Mechanism of Wolff Kishner reduction.

Shown above is the reaction mechanism of Wolff Kishner reduction. The hydrazine and ketone form hydrazone via condensation. This is reduced by the base to form diimide species which leaves as nitrogen and the charge is taken up to regenerate the base and produce the reduced product.

## Sonogashira reaction

The Sonogashira reaction is a palladium catalysed reaction used to form carbon-carbon bonds between a terminal alkyne and a halide<sup>85</sup>.



Sonogashira provides a reliable route to synthesize asymmetric acetylenes in reasonable yields. The copper cycle plays a crucial role in this reaction as it activates the acetylene, the presence of air disrupts the reaction at this stage promoting oxidative Hay<sup>86</sup> or Glaser<sup>87</sup> coupling. These side reactions make the purification of the product quite complicated. It is essential to thoroughly deoxygenate all the solvents and reagents before the reaction is started.

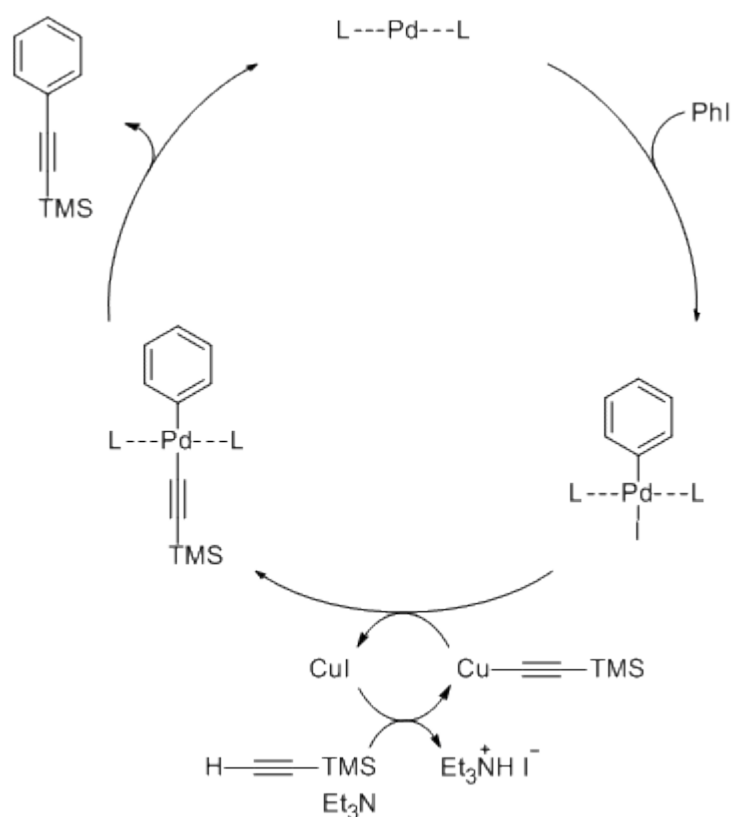


Figure 36: Mechanism of Sonogashira coupling reaction

The catalyst undergoes reduction in situ to form palladium (0) species. This is followed by fast oxidative addition of the aromatic halide to the active catalyst.

Transmetalation between the copper acetylide occurs followed by reductive elimination regenerating the catalyst and forming the cross coupled product. The

copper cycle is less well understood, It is proposed that the base takes up the acetylenic proton. The strength of amine bases are usually inadequate to form an anion instead a copper complex is formed<sup>88</sup>. This complex makes the proton more acidic. The copper acetylide then undergoes transmetallation. It has also been suggested the copper cycle is involved in the formation of the palladium (0) species<sup>89</sup>.

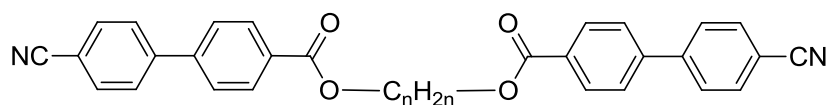
## Liquid Crystal Properties

This section will be divided into two subsections, symmetric systems and asymmetric systems. Mesophases will be described by OPM and DSC and where appropriate the molecular organisation of the structure will be described by XRD.

### Symmetric Dimers

The phase behaviour of symmetric systems, with the same mesogens on both sides of the spacer will further be sectioned according to the group connecting the spacer and mesogen. The connecting group can greatly affect the properties of the system as these connections contribute to the overall bend of the molecule. The overall bend of the system takes into account the bending of the spacer and the connecting moiety. The connecting bond is the first bond between the spacer and the *para* axis of the mesogen. The methylene spacer is calculated to have 113 ° bend whereas the ether spacer systems are reported to have 126 °<sup>90</sup>. These values have been calculated using molecular simulations. No comment will be made regarding the values of the diketone or diester spaced systems as simulations for these compounds have yet to be simulated. Just from the behaviour of the systems we think the diketone systems have closer angles to that of the methylene systems whereas the diester systems are believed to be higher than the diether systems.

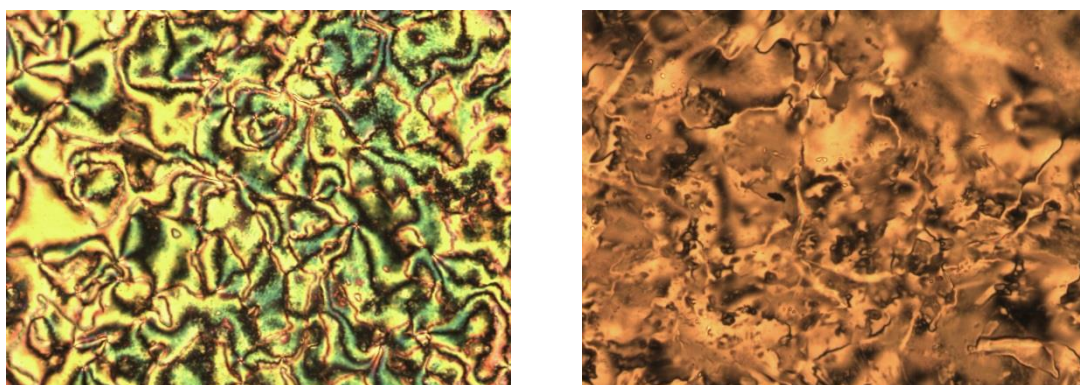
### Cyanobiphenyl ester dimers



- 1, n = 5
- 2, n = 6
- 3, n = 7
- 4, n = 8
- 5, n = 9
- 6, n = 11

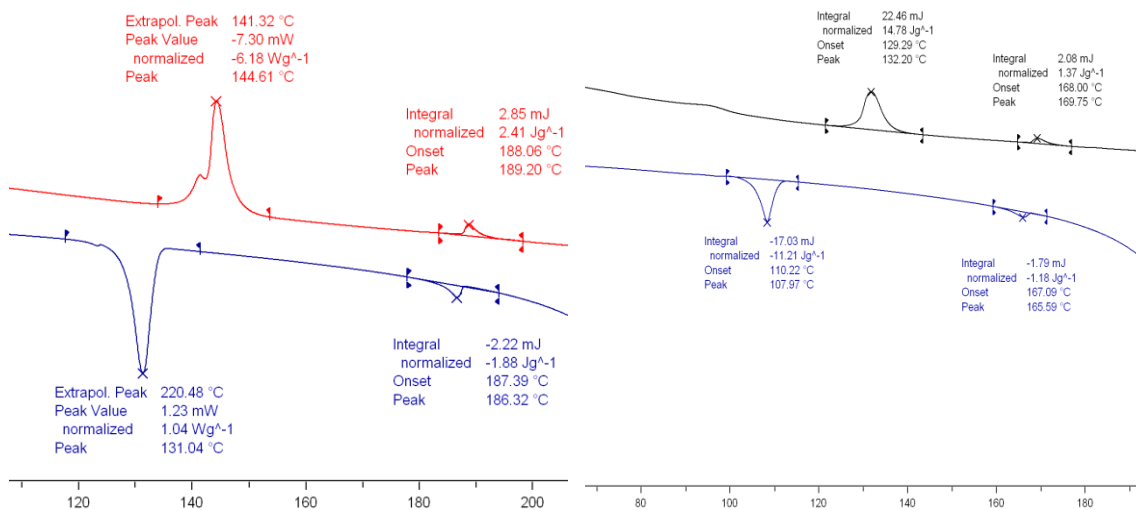
Compounds **1**, **2**, **3** and **4** were all found to show broad nematic phases. These odd numbered dimers showed very similar transitions. All the phases were identified as a conventional nematic phase with 55-37 °C wide phases. The lowest Cr-N transition temperature of 122 °C along with the largest phase width of 55 °C wide was observed

in **3** with spacer being nine methylene units long. A trend can be observed in the further two **1** and **4** with seven and eleven methylene units long spacers having 45 and 37 °C wide phases respectively. From the trend it can be deduced that nematic behaviour is promoted with increasing the length of the spacer until spacer length reaches nine methylene units long and then it is destabilised. This can be rationalised by increasing nano-segregation between the spacer and mesogen ends. The behaviour of the eleven methylene groups long spacer is possibly due to the molecule being long enough to fold on itself. The shortest spacer only five methylene units long only showed a monotropic nematic phase. This observation also follows the trend that longer spacers stabilize the nematic phase up till a certain length.



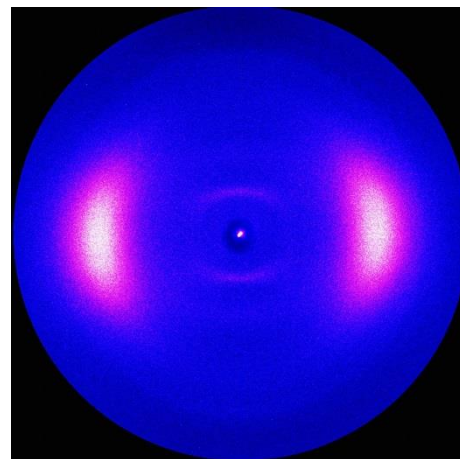
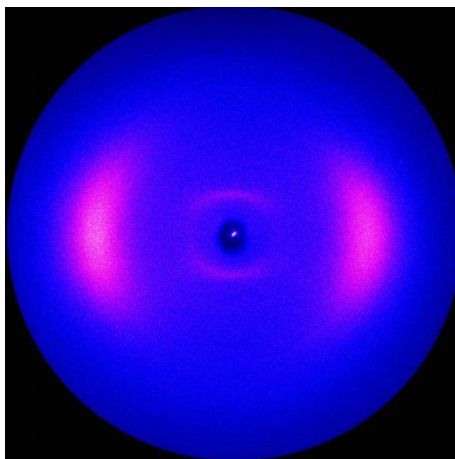
**Figure 37** : Compound **2** at 188 °C (left) and compound **3** 151 °C (right) between cross polarisers on untreated and unrubbed slides.

As shown above the two micrographs represent nematic textures. Compound **2** shows Schlieren texture with very defined two and four brush disclinations whereas compound **3** shows a marbled texture. Both the above mentioned examples are distinctive textures observed for nematic phases.



**Figure 38** : DSC curves of compound **1** (left) and compound **4** (right).

Shown above are the DSC curves for compound **1** and **4**. Two transitions are observed, these are Cr-N and N-I, an additional crystal-crystal transition can be observed in compound **1** (left) just before the Cr-N transition. The data agrees with the observations reported earlier, the enthalpic change for both compounds is 2.41 and 1.37 J g<sup>-1</sup> respectively. These values are considered to be within the range observed for conventional nematic compounds.



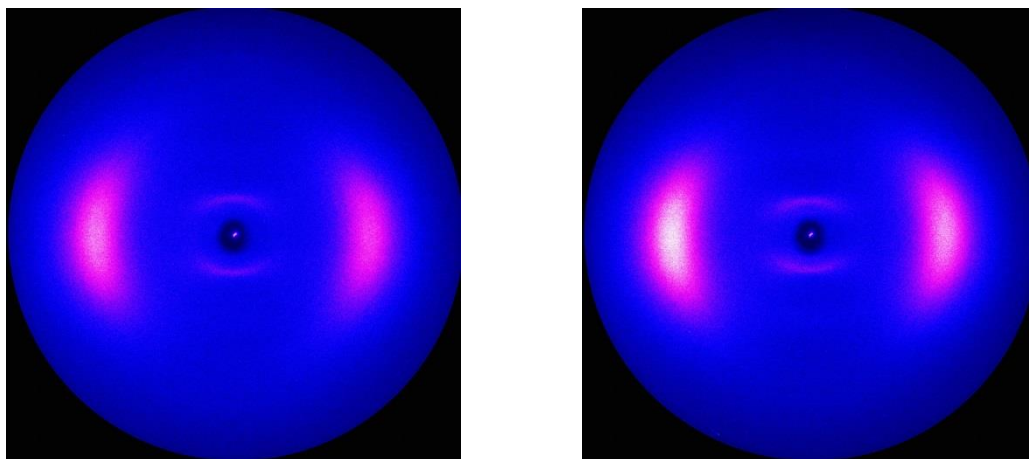


**Figure 39:** XRD images of scattering experiments aligned under magnetic field. Compound **1** at 160 °C (top left), Compound **2** at 168 °C (top right), Compound **3** at 150 °C (bottom left), Compound **4** at 150 °C (bottom left).

With X-ray diffraction experiments it was confirmed that the mesophase is in fact nematic as no strong intensities indicative of layer ordering can be observed in the small angle scattering. The  $2\theta$  against intensity plots shown in Figure 40 allows the visualisation of the subtly changing small angle region. As the length of the molecule increases the peak in the small angle shifts to the left, showing an increase in the d-spacing. These d-spacings are given below;

Compound	Temperature / °C	$2\theta$ / °	d-spacing / Å
<b>2</b>	168	6.5	13.6
<b>1</b>	160	6.0	14.7
<b>3</b>	150	5.5	16.1
<b>4</b>	150	5.1	17.3

The wide angle scattering was observed to be at 19.2 ° and equals to 4.6 Å which is characteristic for conventional calamitic mesogens.

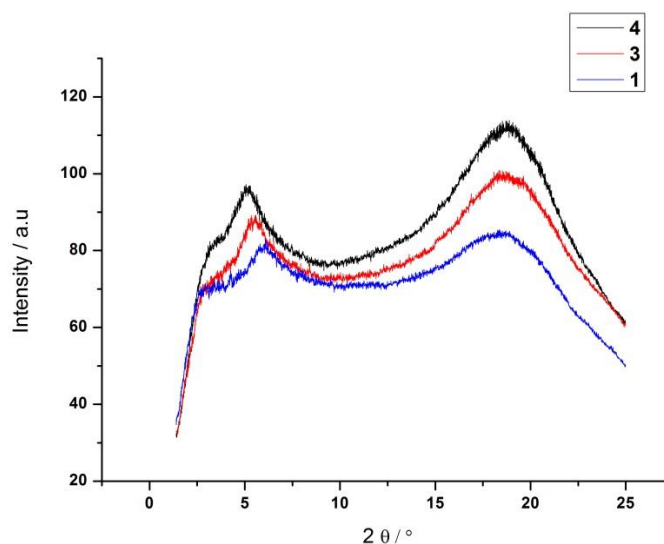


**Figure 40** : Plot of 2 theta against intensity for compounds **1**, **3** and **4**.

Another observation easily seen from the plots is the increasing intensity as the spacer length is increased. This is due to the difference in electron density modulation. Compound **2** was omitted from this plot as the exposure time of that experiment was not consistent with the other three experiments, but if repeated with same conditions the trend as explained above would be expected.

The d-spacings calculated for all four systems vary by 1.1 – 1.4 Å, this is consistent with addition of an extra methylene group. As all the systems are odd numbered and the increase is 2 carbons per compounds this hints to a 50 % overlap being observed in the XRD data. This in fact is the case as the d-spacings are also about half the molecular length.

Correlation lengths, derived originally from the Scherrer<sup>91</sup> equation, can be calculated from scattering data and is a value indicative of length scale over which particle-particle positional correlations are lost. Although not precise it can assist in cases where textures and scattering pattern is inconclusive.

$$\xi = \frac{c}{\Delta q}$$

Where  $\xi$  is correlation length,  $c$  is number of the order of unity used to describe the model used to calculate full width at half maximum and  $\Delta q$  is the full width at half maximum (FWHM) of the diffraction peak.

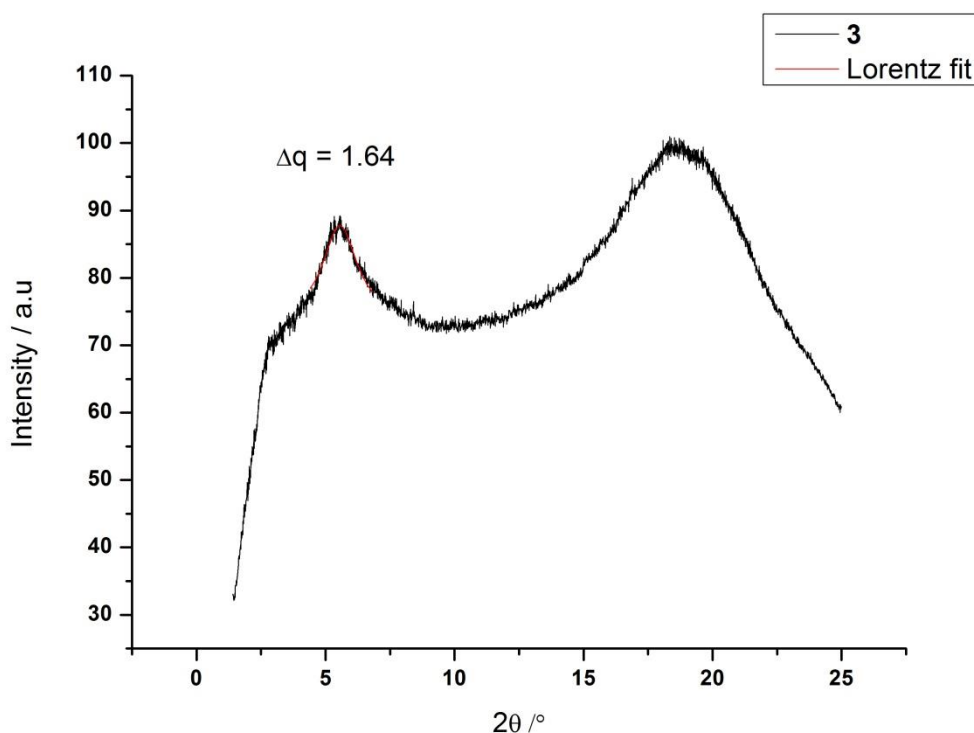


**Figure 41:** 2theta against intensity plot of compound **3** with mathematical function fit to peak.

Using Lorentzian function the FWHM of the small angle peak is 1.64 theta. This is converted wave vector ( $q$ ) by the following formula;

$$q = \frac{4 \pi \sin \theta}{\lambda}$$

Using this conversion and applying to the correlation length formula mentioned earlier with  $c=2$  for Lorentzian decay, the longitudinal correlation length parallel to the director  $\xi = 8.5 \text{ \AA}$ . This value is almost a quarter of the molecular length which implies that correlation is lost between one molecule to the next, this in fact is the case for nematic systems as molecules are not influenced by the position of the molecules immediately around them instead just point to a general direction of the nematic director.

Even spaced compounds **5** and **6** with six methylene groups and eight methylene groups spacer respectively behaved entirely different compared to the odd spacer systems. Compound **5** with just six methylene groups spacer showed a nematic phase at 205 °C which is almost 70 °C higher than the odd numbered spacer of similar

lengths. The phase has a width of 21 °C which is also almost half the width of odd members of the series with similar lengths. Compound **6** did not have a mesophase and melted at 151 °C.

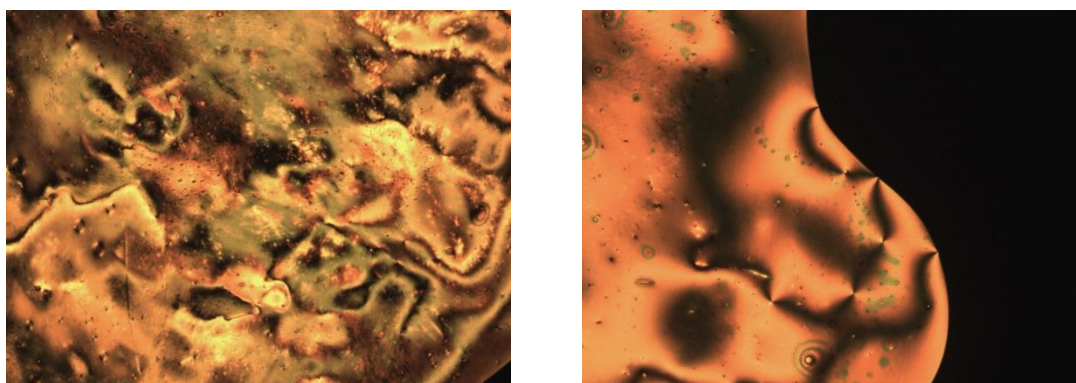
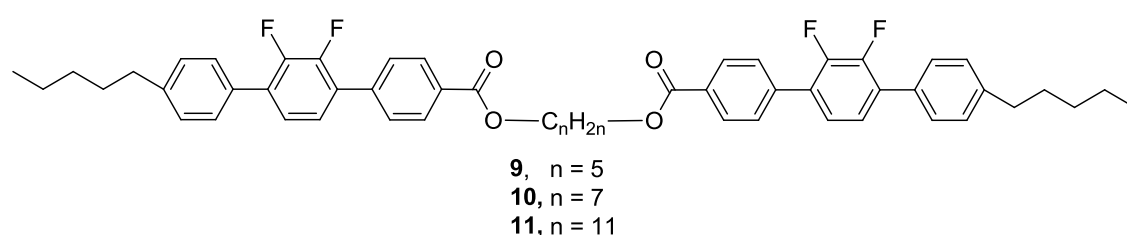


**Figure 42:** Micrographs of compound **5** at 210 °C (left) and 220 °C (right) under crossed polarizers and untreated slides.

Shown above in Figure 42 are two micrographs of compound **5** in the nematic phase. At the lower temperature a grainy marble texture can be seen whereas closer to clearing temperature a schlieren texture with brush disclinations can be observed. The lower temperature micrograph's grainy appearance can be rationalised by the low viscosity, at these higher temperature Brownian motion is easily noticeable. Regions of varying orientation can also be observed as green and reddish regions. As the slide nears clearing temperature (right), it is observed that the sample looks more uniform.

### Difluoroterphenyl ester dimers



Compounds **9**, **10** and **13** showed very different behaviour when compared to the previously discussed symmetric systems based on cyanobiphenyl. Of the three systems studied a trend was observed and the mesophase behaviour is rationalized. Compound **9** with nine methylene units long ester spacer showed an 86 °C broad nematic phase from 136 °C. Pentyl difluoroterphenyl (DTC) mesogens are known to be stronger nematogens than cyanobiphenyls. If we compare the free mesogens without spacers, i.e. **5CB** and **MCT5** (dipentyl difluoroterphenyl), **5CB** shows a 17 °C wide nematic phase

from 18 °C whereas **MCT5** shows a 60 °C wide phase from 61 °C. Using this information it was expected to see wider nematic phases in the diester.

Compound **10** with five methylene units long spacer also showed an even broader phase of 92 °C from 147 °C. This suggested that this mesogen possibly interdigitates and a more stabilized phase is observed for a length similar to that of the chain on the periphery. On cooling a very narrow monotropic SmA phase is also observed.

Compound **13** with seven methylene long spacers varied a bit from the other two compounds in the series as it did not exhibit a mesophase. The clearing point of this compound was lower than the five and nine methylene units long spacers. This seems to suggest a more stable molecular arrangement within the crystal phase is achieved. This could be the reason why no mesophases are observed.

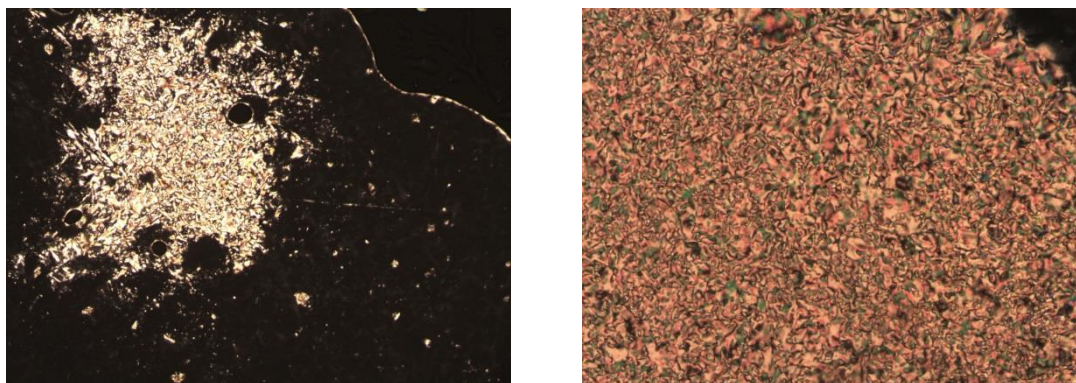


**Figure 43:** Micrographs of compound **9** at 177 °C (left) and 205 °C (right) under crossed polarizers and untreated slides.

Shown above in Figure 43 are two micrographs of compound **9**, as seen in the micrograph at lower temperature the molecules spontaneously align homeotropically and as the temperature is increased the molecules align perpendicular to the substrate and a defect texture can be observed. At 205 °C the bulk of the sample is now aligned planar and a marbled texture characteristic of a nematic phase can be observed. In both micrographs the defects present are making identification difficult.

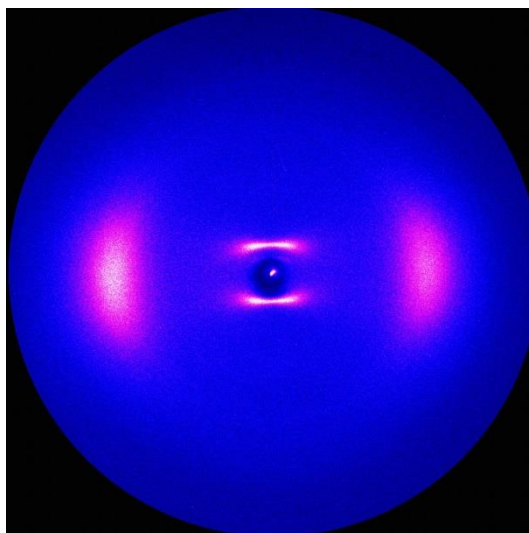


**Figure 44:** XRD scattering data for compound **9** at 140 °C aligned under magnetic field.

The scattering data confirms the nematic nature of the mesophase. Another observation is the presence of cybotactic clusters seen offset at 45 ° in the small angle region shown in Figure 45. The origin of these clusters<sup>92</sup> is due to the random fluctuations with in the nematic phase leading to regions where molecules appear to be in layers. The small angle peak at 3.9 a value of 23 Å, this is exactly half the molecular length of 46 Å. End to spacer stacking, where the alkyl chain at the periphery stack with the spacer could explain this diffraction data. The wide angle peak at 4.6 Å is characteristic in calamitic systems and is attributed to average end to end and side to side interactions of the molecules.

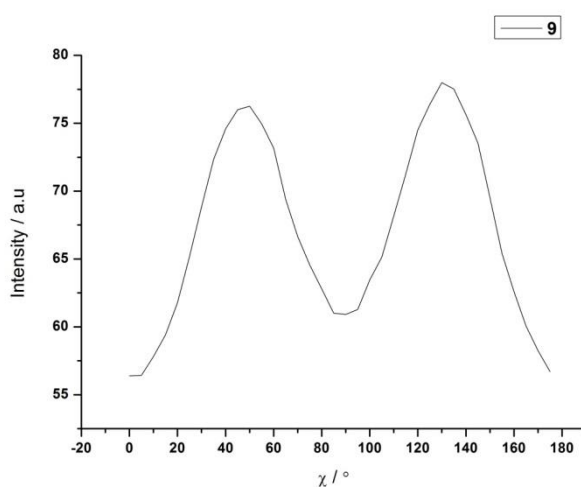


**Figure 45:** Plot of  $\chi$  against intensity for compound **9** at 140 °C in the small angle.

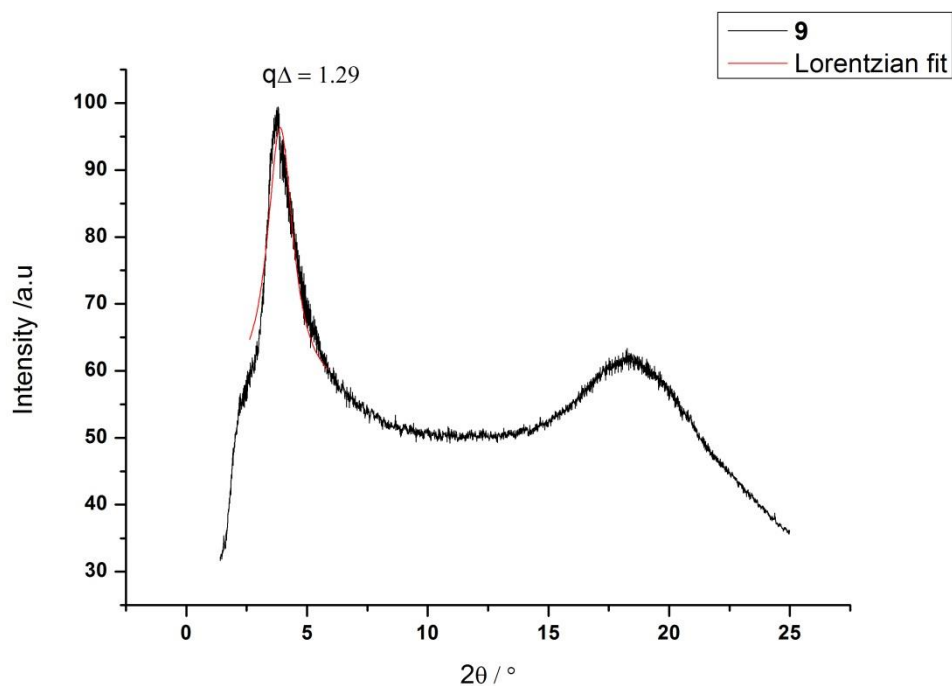


**Figure 46:** 2theta against intensity plot of compound **9** with mathematical function fit to peak.

From the scattering data and the  $2\theta$  plot it can be observed that the small angle peak is twice as intense as the wide angle peak. Fitted to Lorentzian shape the longitudinal correlation length was calculated to 10.9 Å. This is roughly a quarter of the molecular length confirming that correlations between one molecule and the next are lost and the mesophase is in fact nematic.

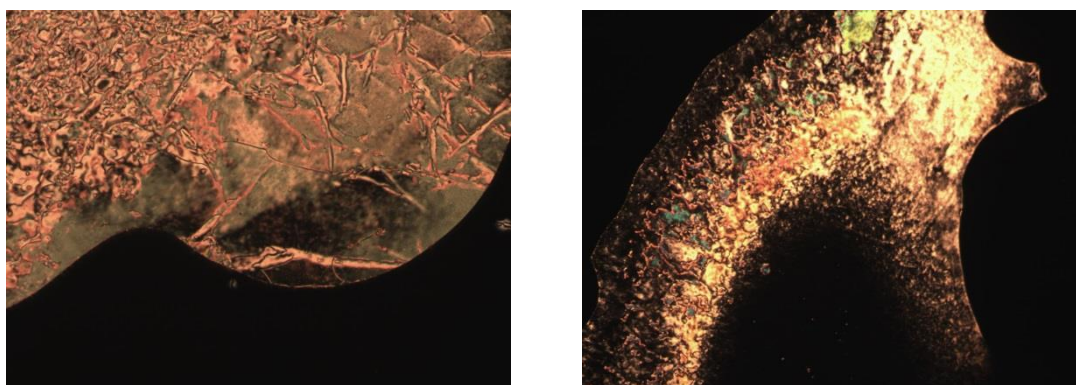


**Figure 47:** Micrographs of compound **10** at 195 °C (left) and 200 °C (right) under crossed polarizers and untreated slides.

Shown above in Figure 47 are two micrographs of compound **10** at two temperatures. The micrograph at 195 °C on heating appears to have marbled texture with very small defects. The micrograph at 200 °C is shown from a cooling run after clearing the

sample, the bulk of the sample is homeotropically aligned along with the thin sections near the edge of the sample towards the top. This is similar to the nine methylene spacer analogue.



**Figure 48:** Micrograph of compound **10** at 144 °C upon cooling under crossed polarizers and on untreated slides.

Cooling the sample further it can be seen that it develops fan shaped, focal conic texture, seen for smectic A phases. Two separate domains can also be identified in dark and light.

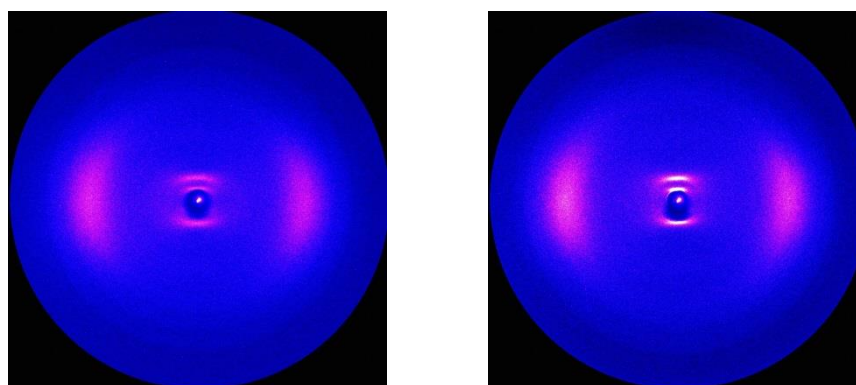


**Figure 49:** XRD scattering data for compound **10** at 200 °C (left) and 150 °C (right) aligned under magnetic field.

Shown above in Figure 49 are the diffraction scattering images for compound **10** in the nematic and smectic phase. The southern hemisphere appears to be missing a signal, this is due to the shadow cast by the lead beam stop. Signals are symmetric and all measurements were performed on the northern hemisphere of the plate. The two peaks in the small angle are 45.7 Å and 22.5 Å and the wide angle maxima at 4.6 Å. It is evident structurally the transition from nematic to smectic does not vary the d-spacings noticeably, however there is a very obvious increase in the intensity between

the two phases.

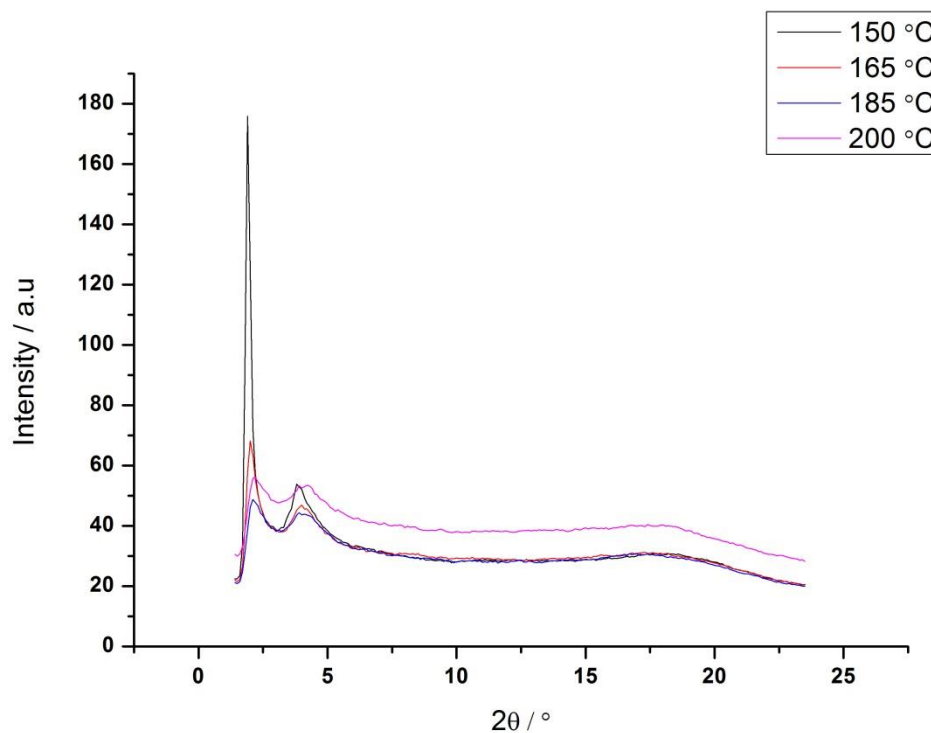


**Figure 50:**  $2\theta$  against intensity plot of compound **10** at several temperatures.

As can be seen in Figure 50 the intensity of the small angle peaks within the nematic phase is low at higher temperatures, as the phase approaches the nematic – smectic transition the intensity increases fivefold. The correlation length in the smectic phase is about eight times higher than that of the nematic phase. In terms of molecular length scale there is longitudinal correlation between at least two molecular lengths. This gives a picture of a mono layered smectic phase and explains the small angle peak at 45.7 Å which is roughly one molecular length. The 22.5 Å peak suggests a possible incommensurate smectic phase which indicates molecules within the smectic layers shown below in Figure 51

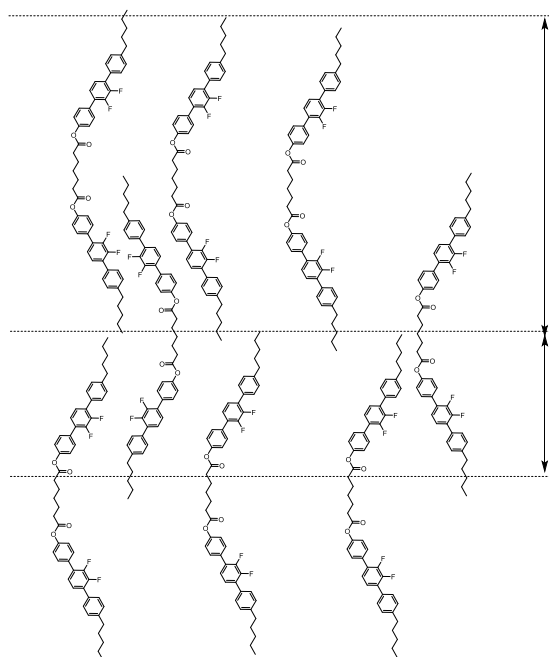


**Figure 51:** Molecular packing in compound **10**.

The smectic nature of the lower temperature mesophase has been discussed in terms of its layered nature. To further assign the phase we can observe the lack of tilt in Figure 49. This can be better view by plotting  $\chi$  scans against intensity shown below in Figure 52. The maxima of the peaks can be observed at 0 and 180 ° showing the absence of tilt. This can also be plotted for the small angle and the maxima observed at 90 and 270 °. With no tilt in the XRD data we can assign the smectic phase as Smectic A.

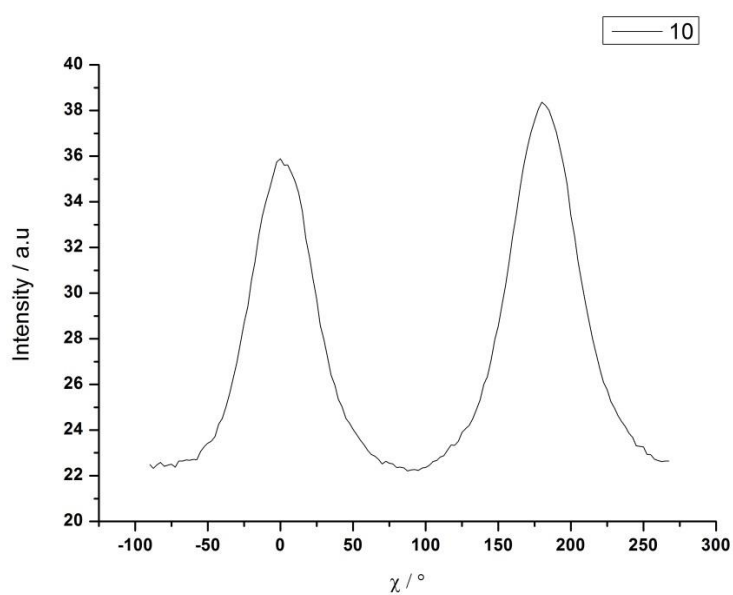
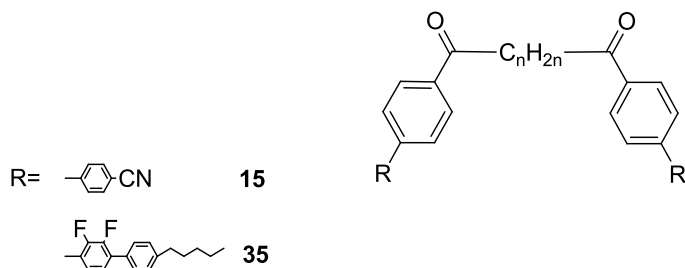


**Figure 52:** Wide angle plot of X scans against intensity for compound **10**.

## Diketone dimers



Two compounds based on a diketone spacer with seven methylene groups were investigated. Compound **15** based on the cyanobiphenyl mesogen and compound **35** based on difluoroterphenyl mesogen.

Compound **15** was found to exhibit a 19 °C wide nematic phase from 167 to 186 °C.

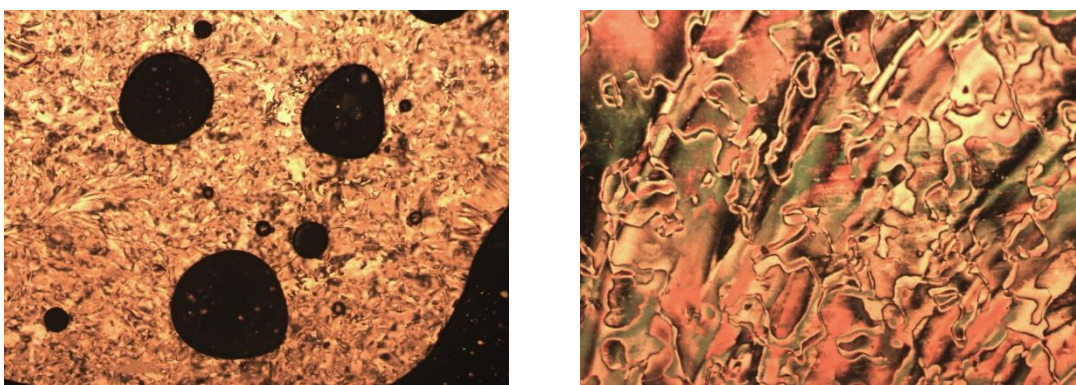


**Figure 53:** Micrographs of compound **15** at 150 °C on first heating (left) and on first cooling (right) under crossed polarizers and on untreated slides.

The two micrographs shown above in Figure 53 at 150 °C of compound **15** show two different textures for the nematic phase. On heating an uneven texture with very small defects and a lot of graining can be observed. After going past the clearing point and cooling back down to the same temperature a more recognisable marbled like texture with some disclinations can be observed. This is considered to be due to the even thickness of the sample after clearing.

Compound **35** was found to exhibit multiple mesophases.

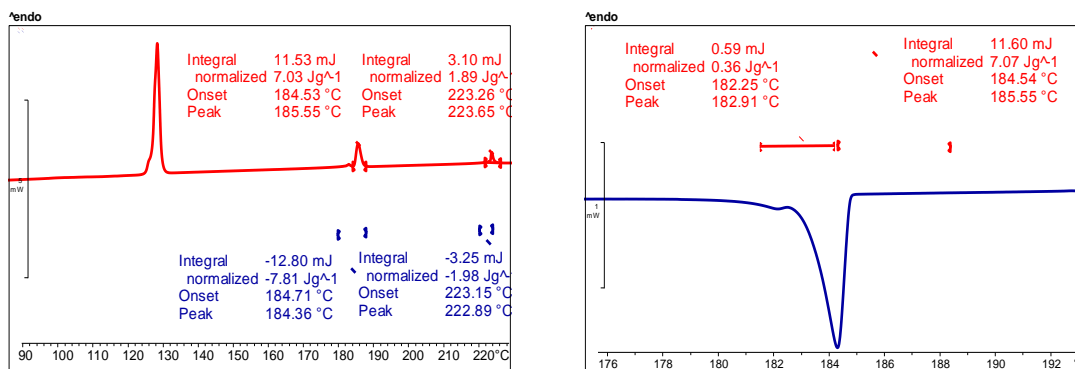


**Figure 54:** Differential calorimetric scans for compound **35** (left) and expansion of first transition on heating (right).

As shown above in the calorimetric data there are three mesophases observed on heating.

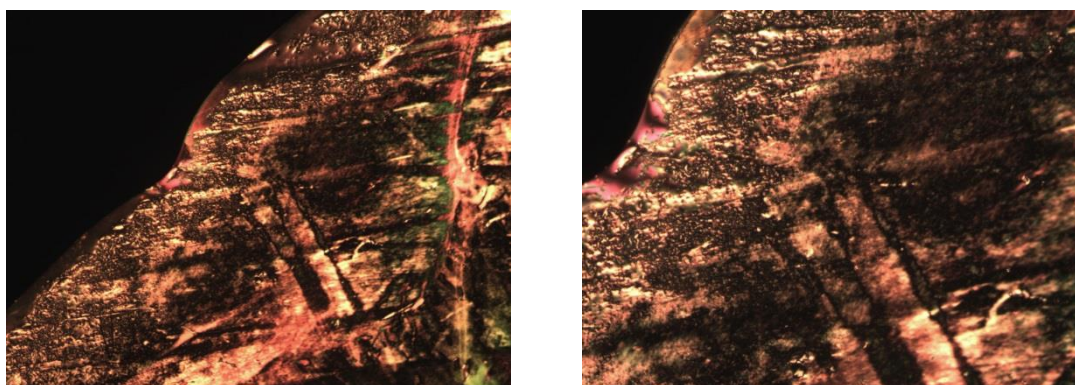


**Figure 55:** Micrographs of compound **35** at 195 °C at 100x (left) and 200X (right) magnification between crossed polarizers and on untreated slides.

From the calorimetric data it was expected that the high temperature phase would be nematic due to the enthalpy of the transition being 1.89 J g<sup>-1</sup>. The micrographs shown at 2 magnifications in this high temperature phase looked inconclusive. Features from previous phases seemed to persist within phases, making the identification of the phase complicated. The highly viscous nature of the sample did not allow shearing experiments to give any additional insight into classifying the phase.

XRD experiments at 192 °C shown below in Figure 55 show a characteristic nematic scattering pattern. Weak small angle scattering and diffused scattering at the equator can be observed. The peak in the small angle at 4.0 2θ equals to 22Å. This is roughly the size of the difluoroterphenyl mesogen. This suggests substantial molecular overlap in the mesophase.

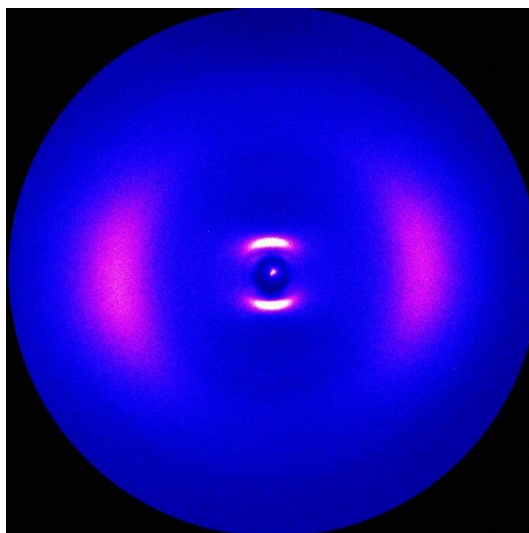


**Figure 56:** XRD scattering data for compound **35** and 192 °C.

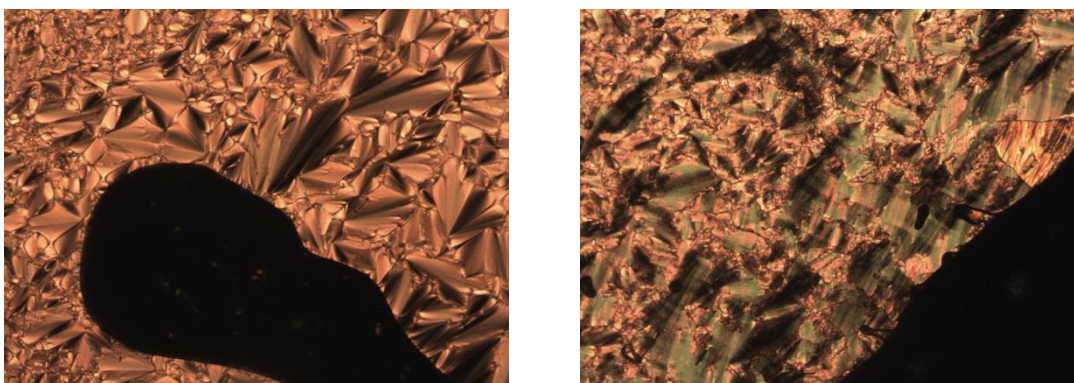


**Figure 57:** Micrographs of compound **35** at 184 °C (left) and 160 °C (right) under crossed polarizers and on untreated slides.

Based on calorimetric data a narrow LC phase between 185 and 183 °C is observed. This phase is shown Figure 57. The polygonal texture shown in the micrograph can be attributed to a smectic A phase. The micrograph at 160 °C shows a striated texture with lots of defects and very high viscosity. This texture points almost to a soft crystalline or pseudo crystalline phase.

Figure 58 shows the XRD scattering data for the two phases described above. The data at 184 °C shows no tilt and agrees with the smectic A polygonal textures observed in the micrographs. The scattering data for the lower temperature shows diffuse halo which confirms the non-crystalline nature of the phase.

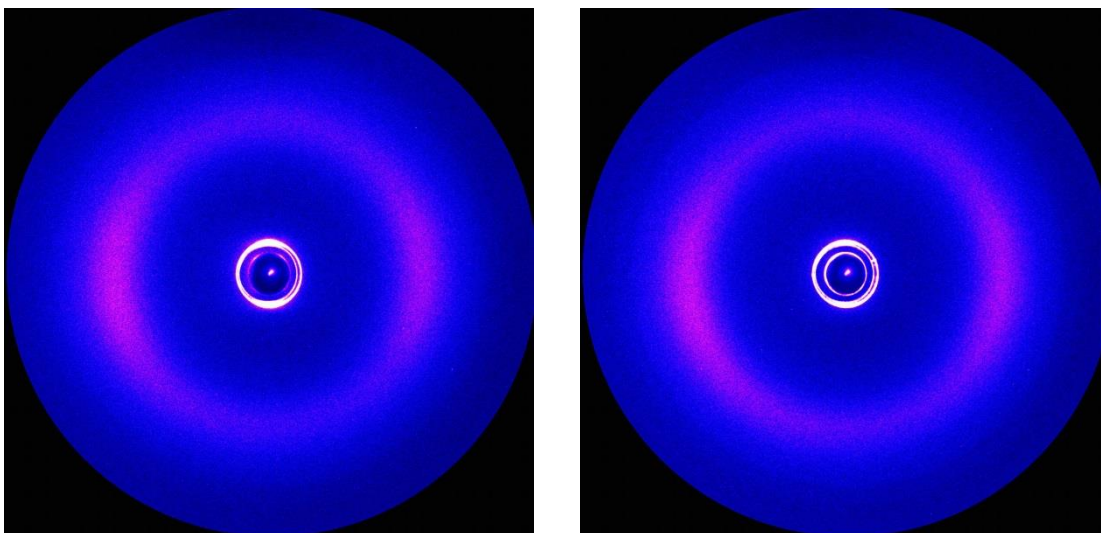


**Figure 58:** XRD scattering data of compound **35** at 184 °C and 144 °C.

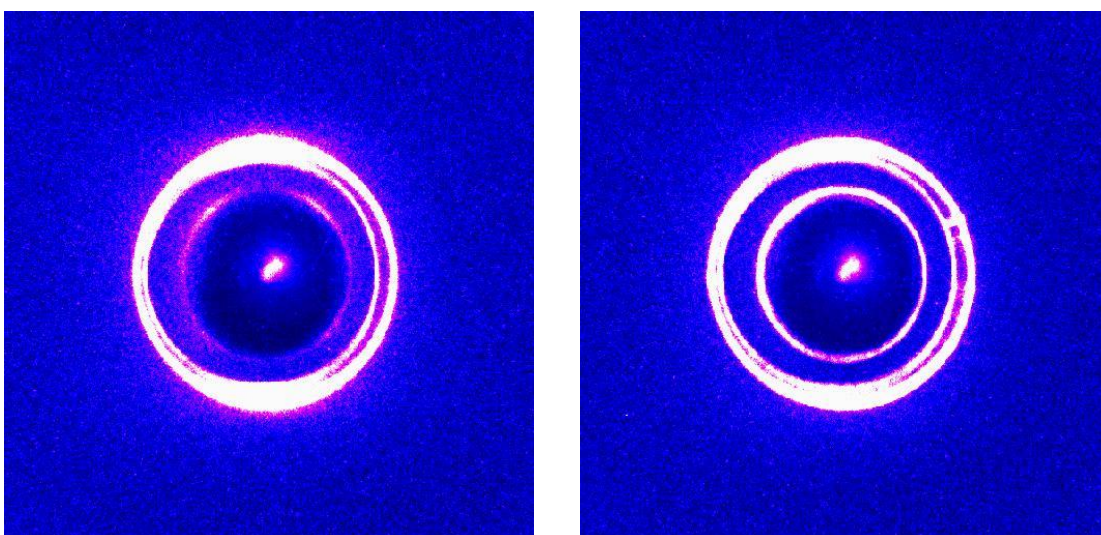


**Figure 59:** Expansion of small angle scattering for compound **35** at 184 °C and 144 °C.

Shown in Figure 59 are the expansions of the small angle scattering, it shows the similarity of the two mesophases. The peaks appear to be at the similar angles which will be discussed later. The presence of domains can be seen at the lower temperature. At 184 °C a sharp signal is observed and some signs of alignment can also be observed with the maxima at 90° and for the smallest angle maxima at 45 °. The asymmetry of the signal is attributed to the shadow of the beam stop. At 144 ° fluctuations can be seen and the alignment appears to be lost. This behaviour can be attributed to the formation of small domains within this mesophase.

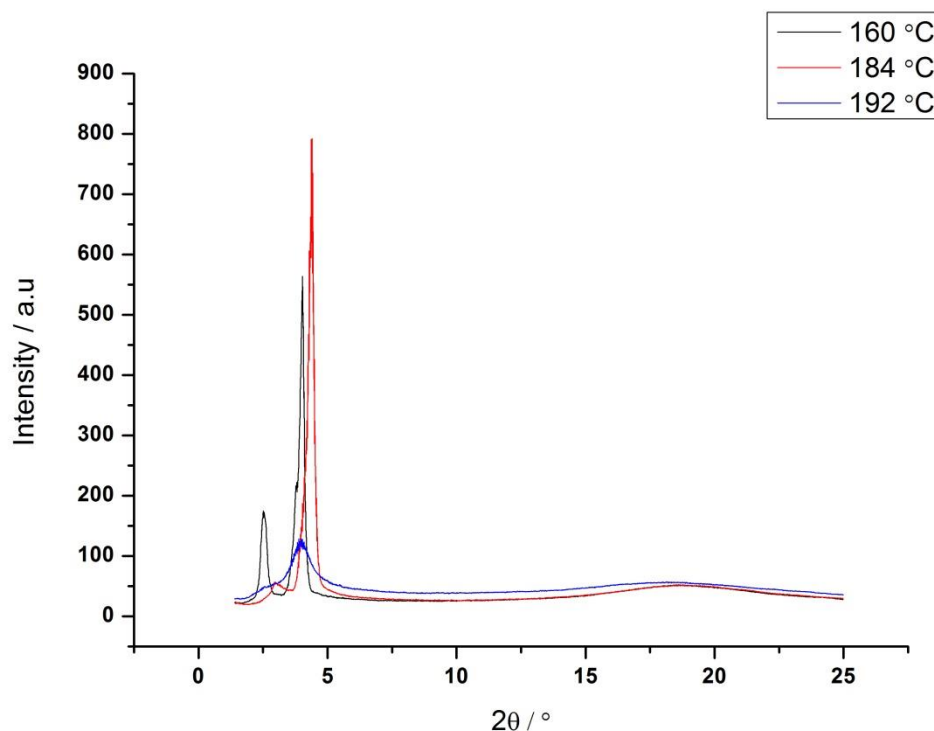


**Figure 60:**  $2\theta$  against intensity plot of compound **35** at all mesophases.

Shown above in Figure 60 are the overlying  $2\theta$  plots of compound **35** in three observed mesophases. The nematic phase has been discussed previously with Figure 56. The most prominent observation is the appearance of a peak at  $2.5\ 2\theta$ . Another important observation is the slight shift of the peak at  $4.0\ 2\theta$  to  $3.95\ 2\theta$  as the temperature is decreased. This change is not very large but is just about observable, and makes a difference of almost  $0.5\ \text{\AA}$ . This change essentially means as the transition from the smectic phase to the lower temperature phase occurs there is a slight increase in the size of the observable lattice. This result is quite surprising, in mesophases as the amount of order increases the size of the observable lattice usually decreases. The d-spacings in the small angle equate to roughly  $22.1\ \text{\AA}$  and  $35.6\ \text{\AA}$ . These values have attempted to be rationalized below in Figure 61 showing the arrangement of molecules in the mesophase. A considerable overlap with molecules flipped vertically and horizontally filling space. As the experiments are recorded at the limits of our instrumentation at such small angles, the possibility of additional signals at lower angles cannot be ruled out. Poor resolution and possibility of smaller angles leaves the XRD data inconclusive regarding the assignment of the lower temperature phase. Kang<sup>93</sup> showed aligning the sample in directions perpendicular and parallel to the

capillary is an effective way of confirming the B6 phase. This is something that will be tried in the future to confirm the structure.

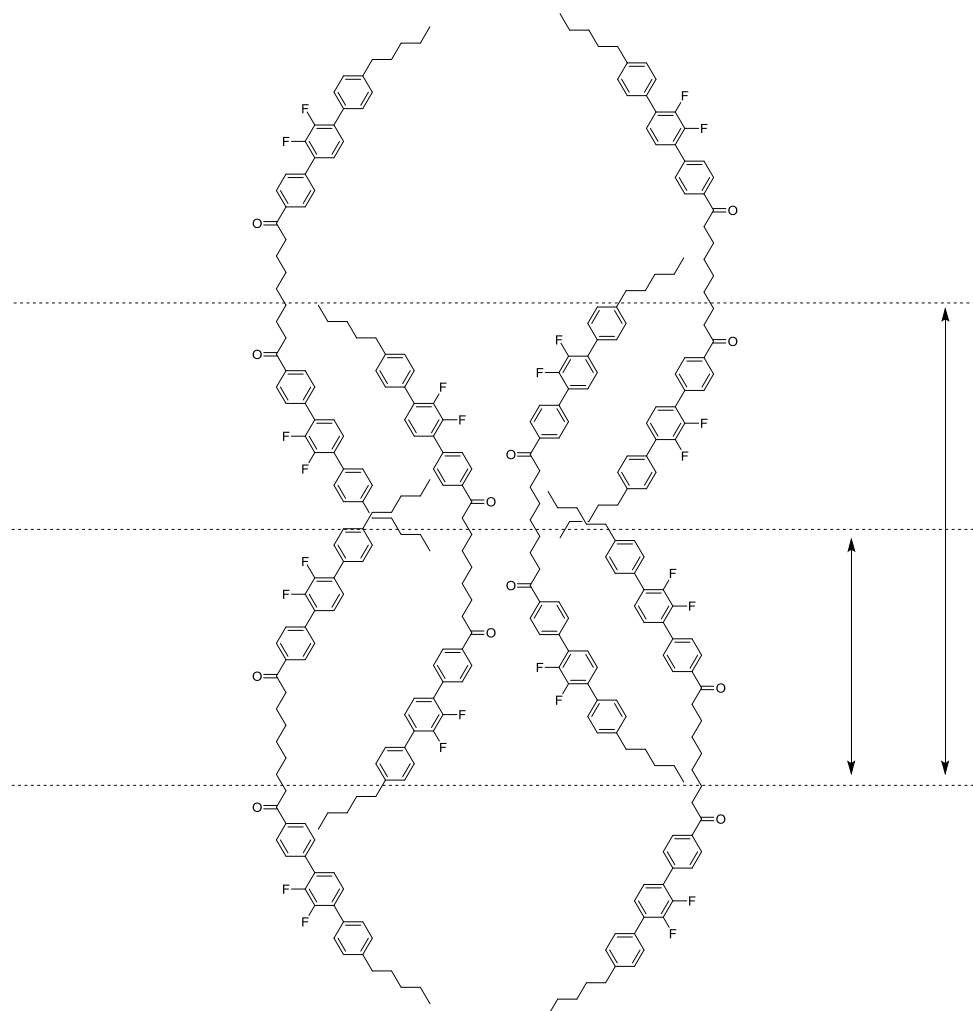


**Figure 61:** Possible molecular arrangement in low temperature mesophase.

Shown below Figure 62 are micrographs of compound **35** cooling from the nematic phase into the lower temperature phase. In the second micrograph the growth of the smectic A phase as batonnets from the nematic phase can be observed. This growth disappears and sections of focal conic growth start to appear in the fourth micrograph.

In the fifth and sixth micrograph the domains grow larger and appear from homeotropically aligned smectic A phase. This growth and very high viscosity point to

the identification of the phase as B6 phase. These micrographs were compared with the ones shown in Figure 63, the similarities lead to the possibilities of this phase in fact being a B6 phase. A very similar molecular arrangement as shown in Figure 61 has also been proposed by Sadashiva *et al*<sup>94</sup>.

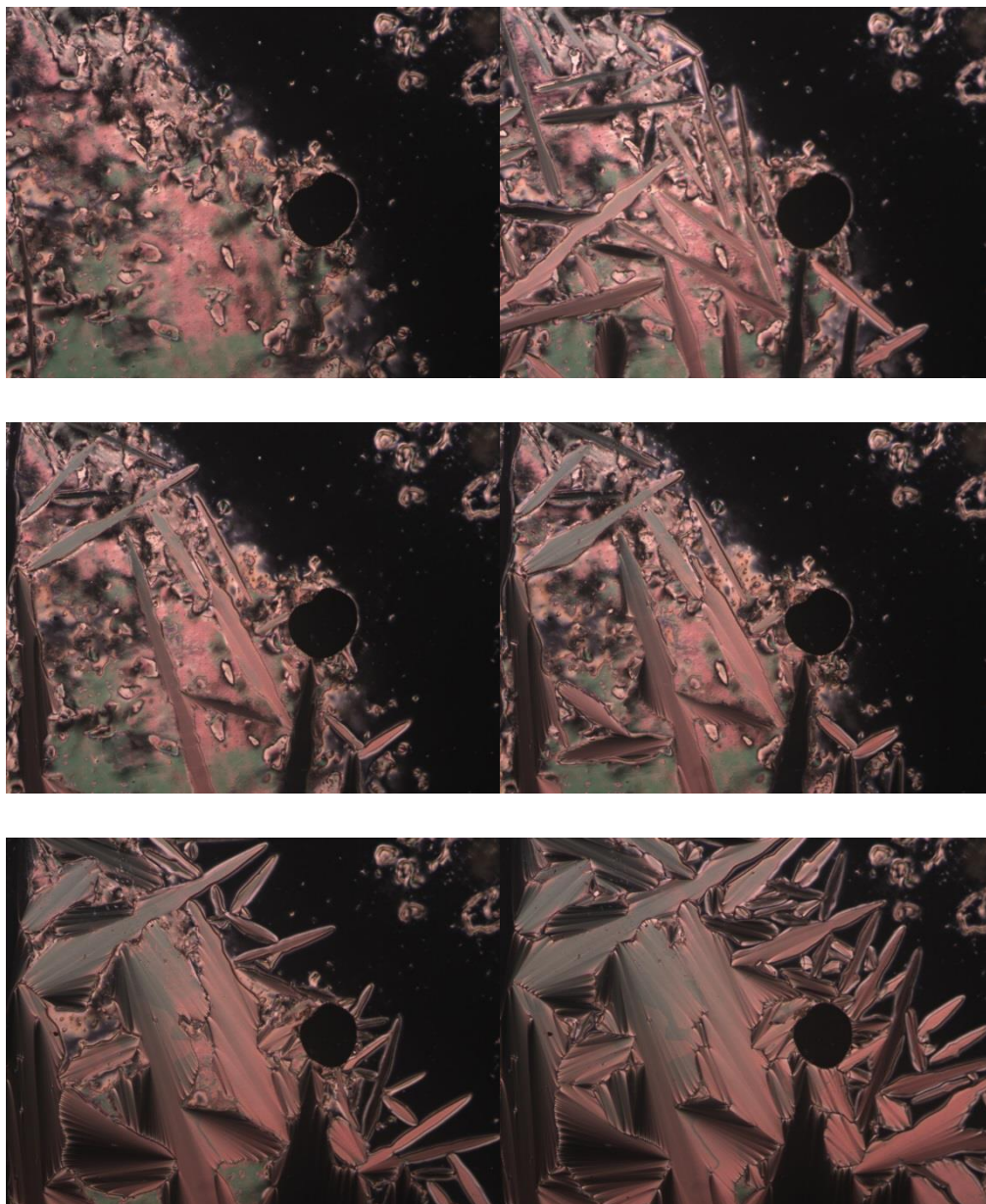


**Figure 62:** Micrographs of compound **35** cooling from 185 °C every 0.5 °C



**Figure 63:** Micrographs of the growth of B6 reported by Sadashiva et al<sup>94</sup> (left) and Achard et al<sup>99</sup> (right).

### Other symmetric systems

Compounds **15** and **17** based on diether spacers with eleven and seven methylene groups long chains respectively and difluoroterphenyl mesogen showed a conventional nematic phase.

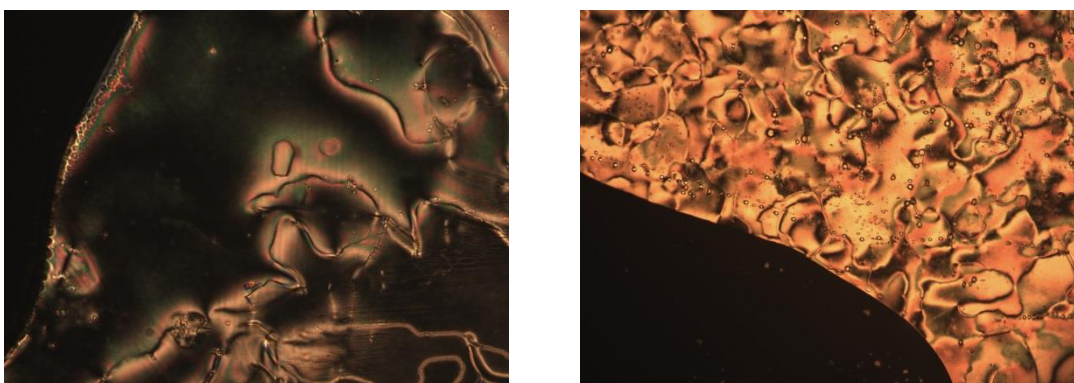


**Figure 64:** Micrographs of compound **15** at 201 °C and compound **17** at 204 °C under crossed polarizers and on untreated slides.

The eleven methylene groups long diether dimer showed a 99 °C wide nematic phase from 105 °C whereas the seven methylene groups long diether dimer showed a 105 °C wide nematic phase from 108 °C. Diether dimers based on cyanobiphenyls have been extensively researched<sup>48</sup> and are found to exhibit 40 °C wide nematic phases from 130 °C in odd spacers of seven to eleven methylene groups long. Compared to this series the difluoroterphenyl compounds crystal – nematic transition is almost 20 °C lower and the phase width is double that of the cyanobiphenyl series.

The aim of the project is to rationalise the design of molecules that exhibit multiple nematic phases. So far all the changes in the design regarding the length of the spacer

and more importantly the group connecting the spacer point to the sensitivity of the  $N_{TB}$  phase to bend. All the systems investigated increased the overall bend of the system with mesogens that are known to exhibit the  $N_{TB}$  phase with odd numbered methylene spacers.

Compound **12** with methylene spacer and trifluoride biphenyl mesogen was investigated as a candidate for a low temperature  $N_{TB}$  compound. Compound **12** did not show a mesophase and had a clearing temperature of 106 °C. It was expected that the end groups play a role in the formation of mesophases with tail to tail interactions.

Compound **31** with methylene spacer and difluoropentylbiphenyl mesogen was investigated, this dimer is a shorter version of the difluoroterphenyl dimer with one ring less per mesogen. No mesophase was observed as the compound was liquid at room temperature. Low temperature investigations have yet to be done.

### **Asymmetric Dimers**

This section is divided into two parts. Dimers based on cyanobiphenyl mesogen and dimers based on the difluoroterphenyl mesogen. Both these mesogens have been used extensively in this research as they exhibit  $N_{TB}$  in symmetric methylene systems and asymmetric dimers with each other. Their symmetric systems can also be mixed with free mesogens like **5CB** and **MCT5**. The investigation regarding the spacer in the previous section suggests that the most likely spacer to form  $N_{TB}$  phase with these mesogens is the methylene spacer. In the symmetric systems based on cyanobiphenyl the nine methylene groups long spacer showed the widest enantiotropic  $N_{TB}$  phase whereas in the difluoroterphenyl systems the eleven methylene groups long spacer showed the widest secondary nematic phase. From this observation it is evident the size of the mesogen compared to the spacer plays a role in the delicate structure of this phase. The eleven methylene groups long spacer on showed a monotropic  $N_{TB}$  phase in the cyanobiphenyl system so it was decided for the investigation of asymmetric systems the nine methylene groups long spacer is our best candidate to exhibit  $N_{TB}$  phase with varying mesogens.

## Cyanobiphenyl asymmetric dimers

Compounds **22**, **23**, **24**, **26** and **34** are asymmetric dimers with a nine methylene spacer and cyanobiphenyl mesogen at one end. The mesogen for the other side was varied and the properties investigated. It is important to note the spacer **21** with cyanobiphenyl mesogen at only one side exhibits a narrow monotropic nematic phase.

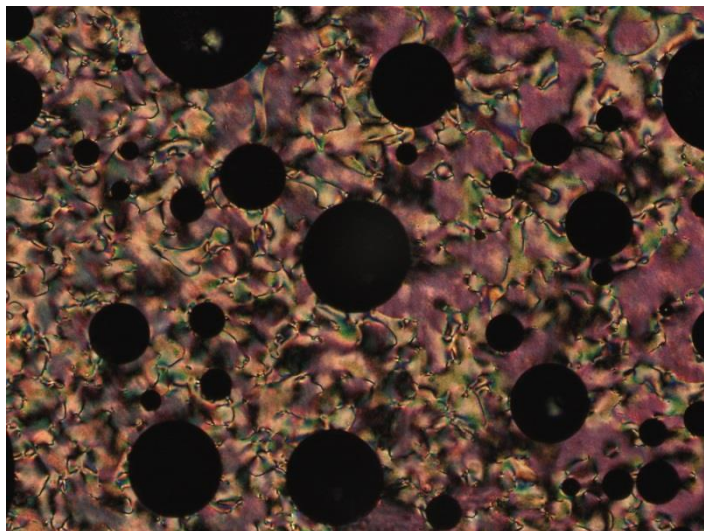
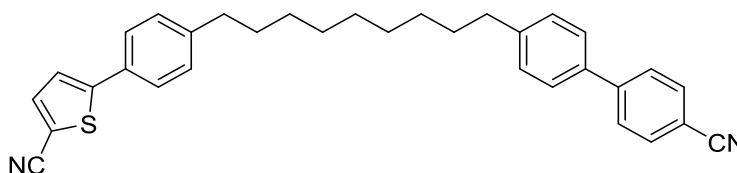


**Figure 65:** Micrograph of intermediate **21** at 20 °C under crossed polarizers and on untreated slide.

### Compound **22**



Compound **22** has a cyanothiophene ring instead of a cyanophenyl ring. This increased the local bend at one side of the dimer. Shown below in Figure 66 is the calorimetric data for compound **22**. It melts at 90 °C into the nematic phase and clears at 101 °C with an isotropisation enthalpy of 2.27 J g<sup>-1</sup>. On cooling the conventional nematic phase comes in at 100 °C with an enthalpy of 2.04 J g<sup>-1</sup>. A secondary phase appears at 89 °C and remains until 62 °C when the compound crystallizes. This phase is identified at the N<sub>TB</sub> which will be discussed later with OPM and XRD. The N-N<sub>TB</sub> enthalpy was observed to be 1.69 J g<sup>-1</sup>.

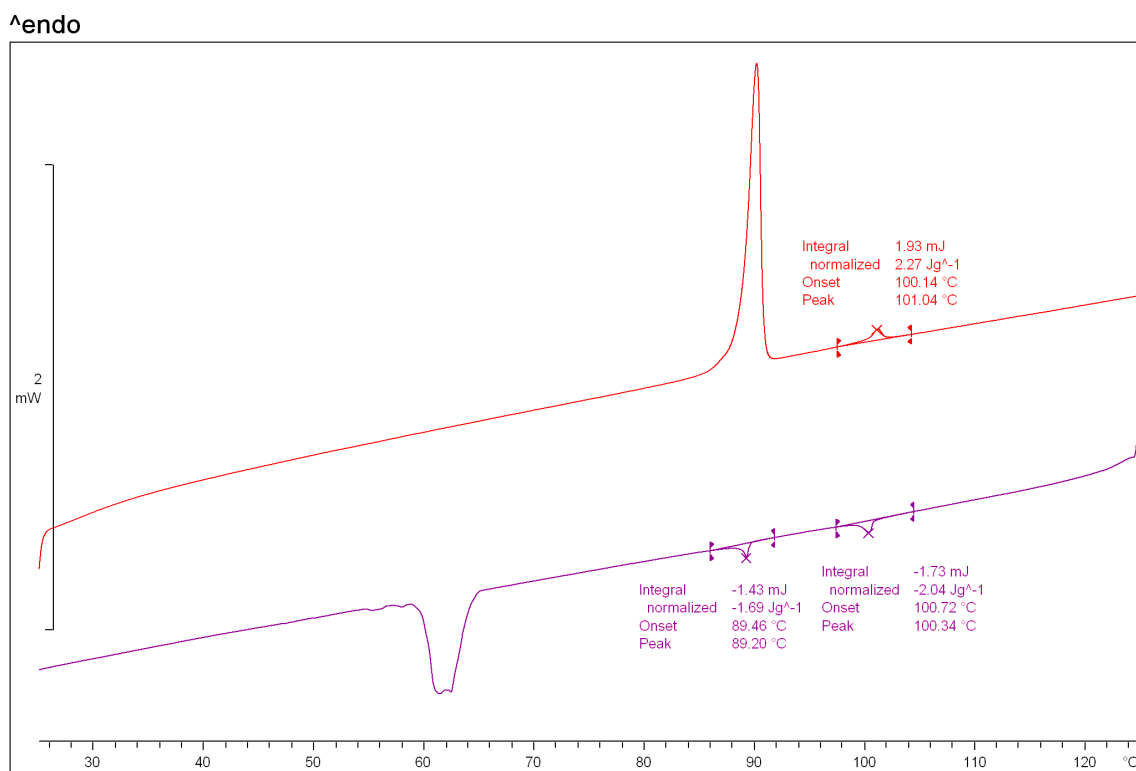


**Figure 66:** Calorimetric data of compound **22**.

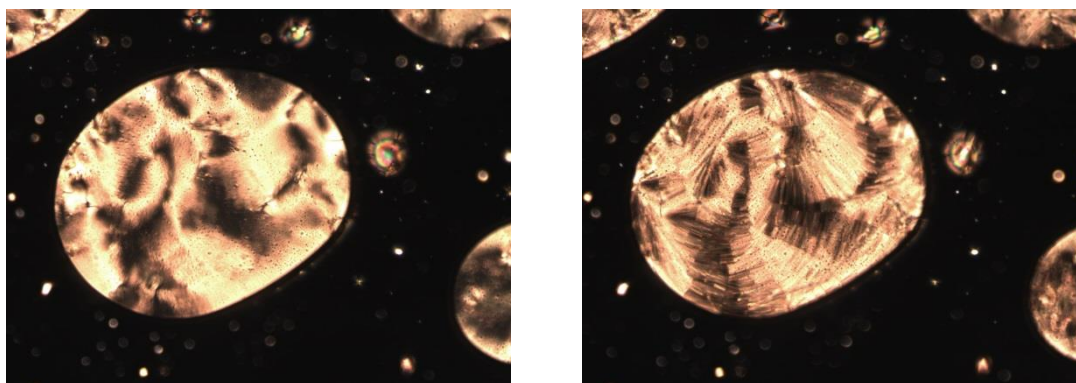
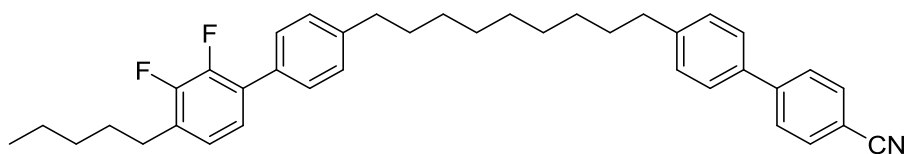


**Figure 67:** Micrographs of compound **22** at 91 °C (left) and 88 °C (right) under crossed polarizers and on untreated slides.

Shown above in Figure 67 are micrographs on compound **22** on cooling from isotropic. At 91 °C a typical nematic textures is observed, some 2 and 4 brush defects can also be observed in the nematic drops. As the temperature decreases into the N<sub>TB</sub> phase the nematic texture is replaced by a plated texture. The sections of the plates can be seen following the defects which shows how little change there is within the molecular organisation of the two phases. XRD studies of compound **22** are currently being undertaken in collaboration with Prof. G. Ungar and ESRF Grenoble.

## Compound **23**



Compound **23** has a difluorobiphenyl mesogen on one end. This is a direct comparison to the asymmetric dimer which incorporates cyanobiphenyl and difluoropentylterphenyl (**CB-C9-DTC**). Compound **23** has one ring less compared to the other system making it a good candidate for a low temperature  $N_{TB}$  phase. **CB-C9-DTC** showed a phase sequence of Cr 68.9  $N_{TB}$  109.8 N 144.1 Iso.

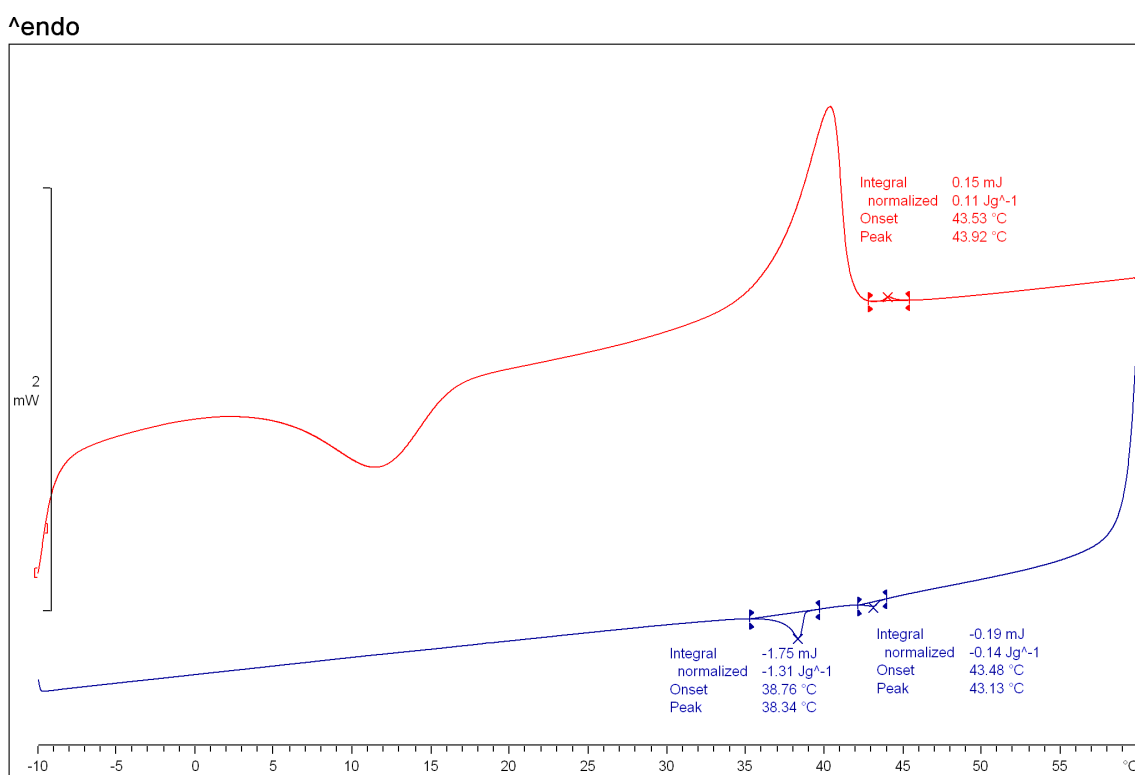


**Figure 68:** Calorimetric data for compound **23**.

Compound **23** showed a 4 °C wide nematic phase from 40 °C on heating, the isotropisation enthalpy of this phase was 0.11 J g<sup>-1</sup>. On cooling the nematic phase reappears at 43 °C with a similar enthalpy as the isotropisation. At 38 °C there is a transition from the nematic phase to the  $N_{TB}$  phase with an enthalpy of 1.31 J g<sup>-1</sup>. This phase was identified by OPM and XRD which will be discussed below. It is important to note here this monotropic phase region is stable up until -10 °C and crystallizes on heating. The phase was also kinetically stable at room temperature for up to 3 weeks.

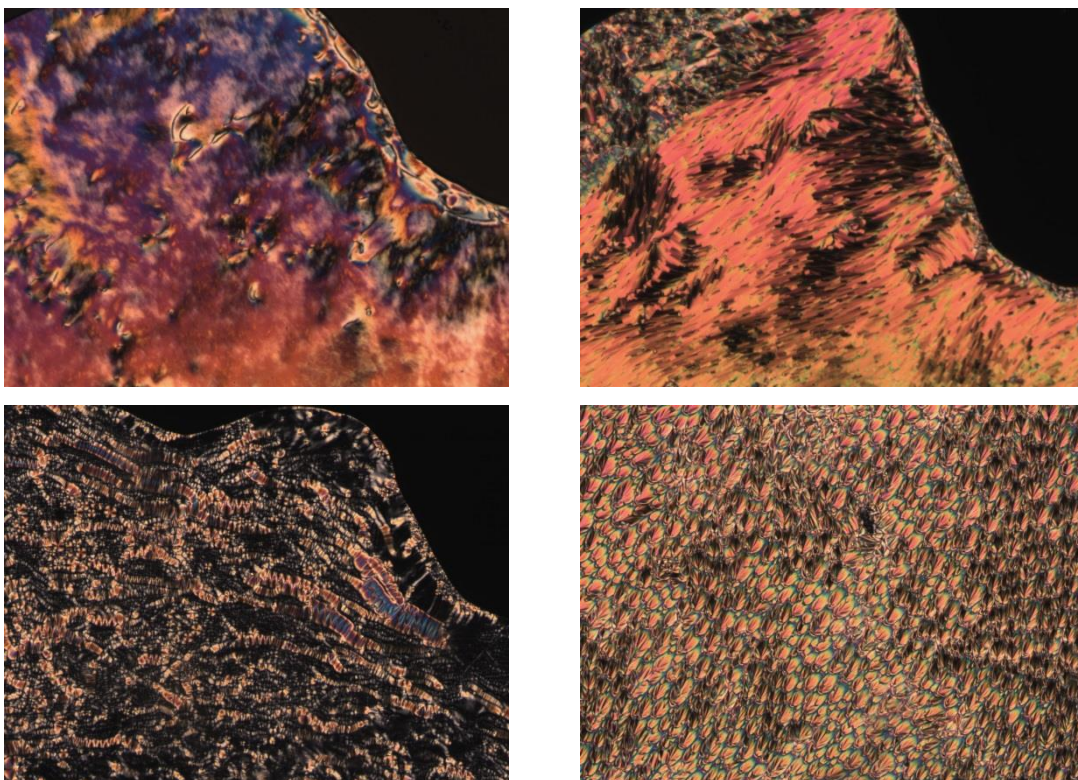


**Figure 69:** Micrographs of compound **23** at 41°C (top left), 36 °C (top right), upon sheering and at 33 °C after sheering. All micrographs were recorded on cooling under crossed polarizers and on untreated slides.

Shown in Figure 69 are the micrographs of compound **23** at various temperatures. The first micrograph shows the marble texture of the nematic phase with some Schlieren defects also visible. At 36 °C in the  $N_{TB}$  phase the marble texture is replaced by the plated texture. Upon sheering this texture homeotropic regions appear that eventually form polygonal fish scale texture.

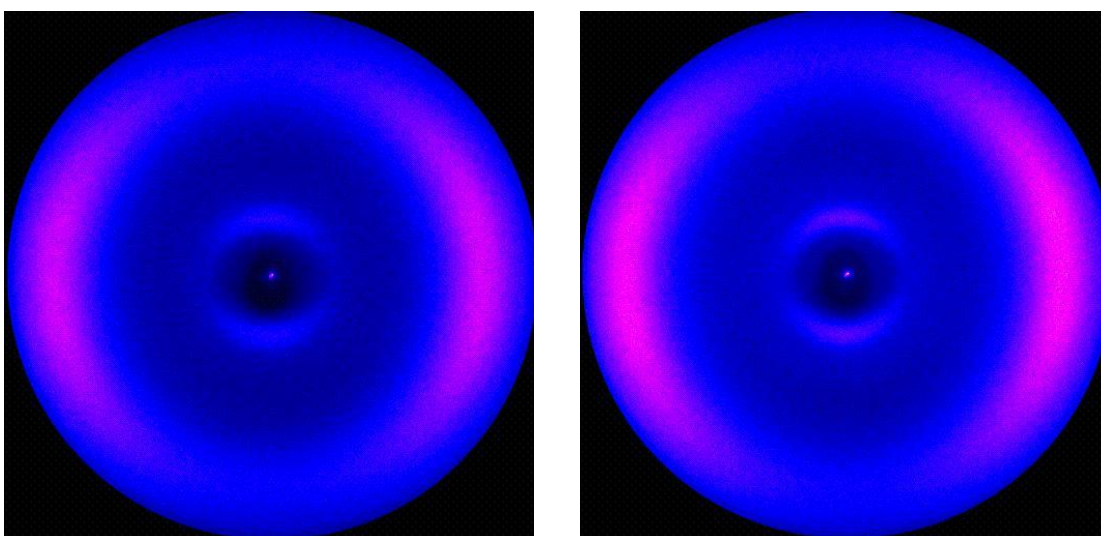


**Figure 70:** XRD scattering data for compound **23** at 41 °C (left) and 36 °C (right).

The XRD scattering data of the two mesophases is shown above in Figure 70. A typical pattern for the nematic phase is observed with very weak small angle scattering and diffused halo in the wide angle. In the  $N_{TB}$  the pattern looks very similar, the wide angle distribution is narrower leading to a more intense signal. This reflects the increase in macroscopic order expected for the  $N_{TB}$  phase.

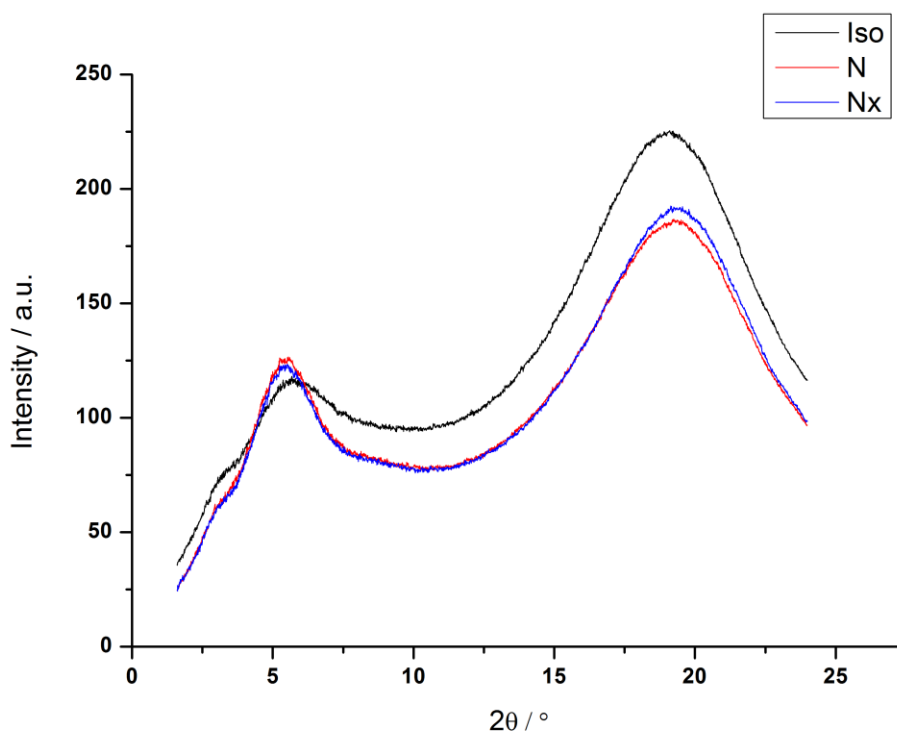
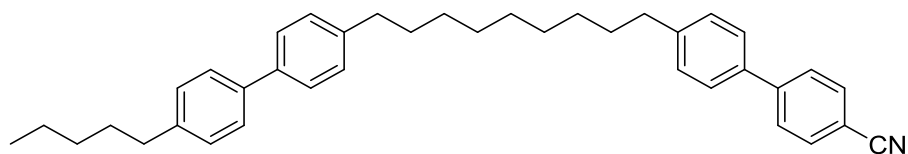


**Figure 71:**  $2\theta$  against intensity plot of compound **23**.

The change in wide angle is better observed in the  $2\theta$  plot shown in Figure 71. As the amount of scattering is equal due to the same amount of sample being diffracted off, the narrowing of the wide angle results in an increase in the height of the peak. A smectic phase is ruled out due to the very low small angle intensity. The small angle peak at 5.6 equals  $15.8 \text{ \AA}$ , this value is roughly half the molecular length. This data points to considerable overlap with in the molecular arrangement of the mesophases.

## Compound **24**



Compound **24** is directly related to compound **23**, it just has two fluorines less making it a pentylbiphenyl mesogen. This compound shows a 5 °C wide nematic phase from 81 °C. This result is surprising by just by removing two fluorines from one side of the mesogen increases the transition temperature by 40 °C and the N<sub>TB</sub> phase is lost.

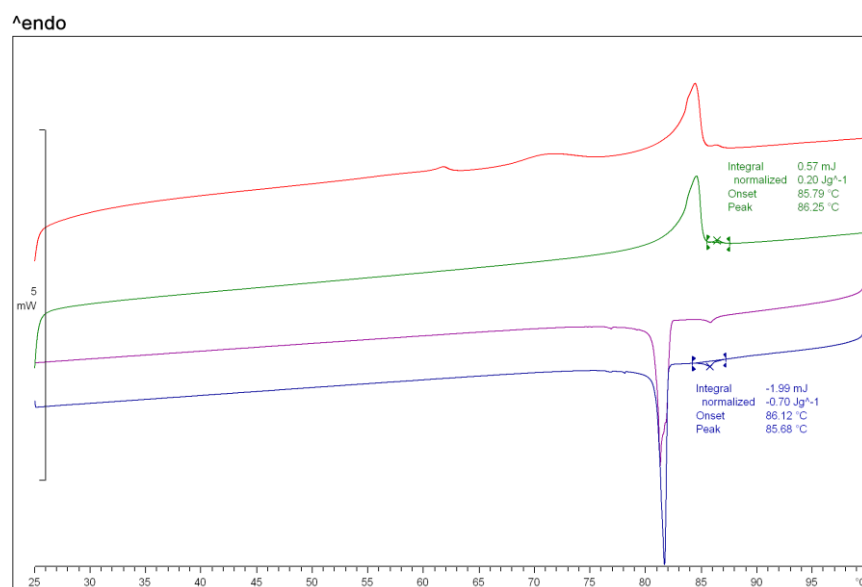


**Figure 72:** Calorimetric data for compound **24**.

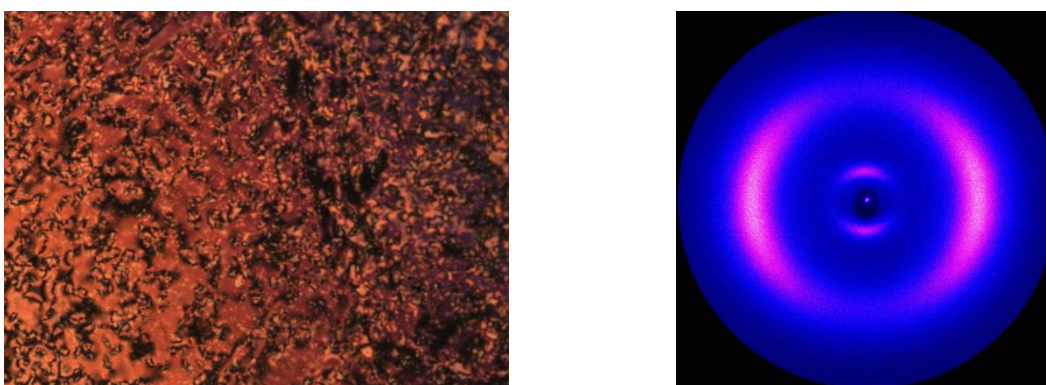
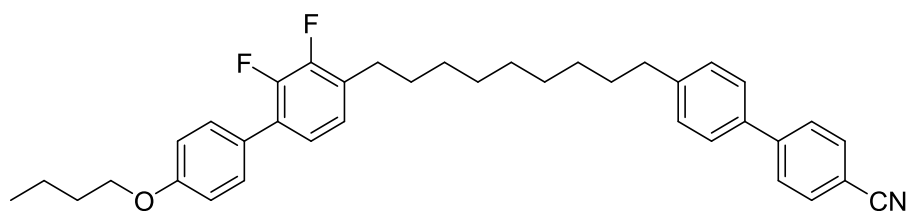


**Figure 73 :** Nematic phase of compound **24** shown by OPM and XRD at 82 °C.

The micrograph of compound **24** shown in Figure 73 shows characteristic Schlieren defects with two and four brushes. The XRD pattern is also typical of that observed for

nematic phase. The peak in the small angle at  $5.1 \text{ } 2\theta$  equals  $17.1 \text{ \AA}$ . This value is slightly larger than half the molecular length. Compared to compound **23** there is less overlap. This information shows the importance of the role lateral fluorines play in the arrangement of molecules within these phases.

#### Compound **26**



Compound **26** is also very similar to compound **23**, the terminal pentyl chain is replaced by a butyloxy chain. The phase transitions observed are very similar to compound **23**. A nematic phase is observed from  $56 \text{ } ^\circ\text{C}$  to  $64 \text{ } ^\circ\text{C}$  on heating. The width of this phase is three times the one seen for compound **23**. Just adding an oxygen atom in the terminal chain increased the transitions by  $16 \text{ } ^\circ\text{C}$  and increased the stability of the nematic phase. On cooling, two phases can be observed between  $62 \text{ } ^\circ\text{C}$  and  $55 \text{ } ^\circ\text{C}$ . The higher temperature phase is identified as a conventional nematic phase with an isotropic-nematic enthalpy of  $0.26 \text{ J g}^{-1}$ . The nematic-nematic transition has a higher enthalpy of  $0.81 \text{ J g}^{-1}$ .

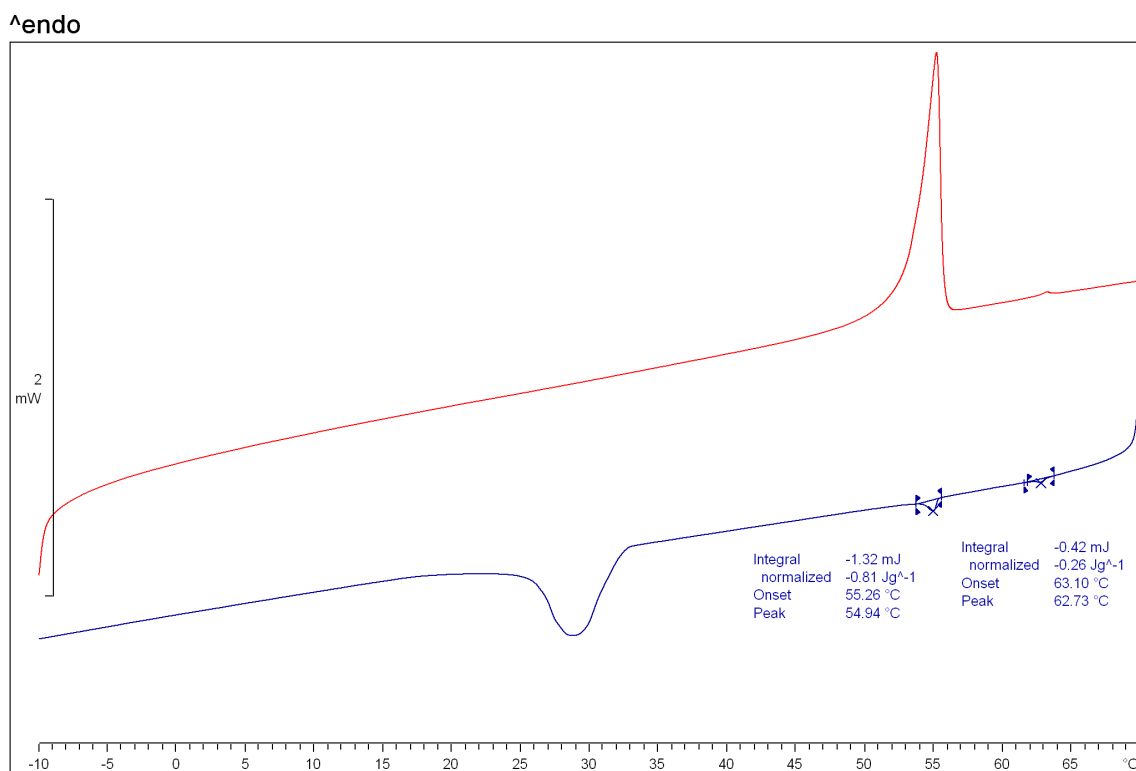


**Figure 74:** Calorimetric data of compound **26**.

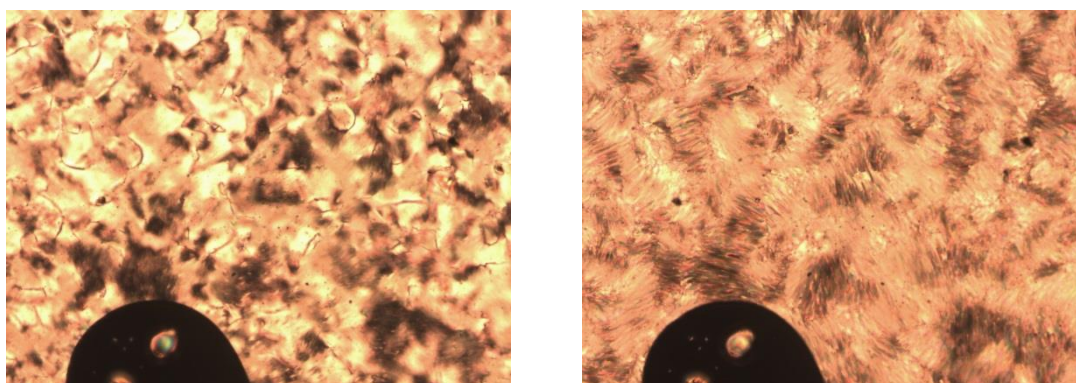


**Figure 75:** Micrographs of compound **26** at 56 °C (left) and 53 °C (right) under crossed polarizers and on untreated slides.

Shown above in Figure 75 are the micrographs of compound **26** in the nematic and  $N_{TB}$  phase. The higher temperature phase exhibits a marble texture with disclinations which is characteristic for a conventional nematic phase. At the lower temperature phase the same region becomes very grainy and a plated texture can be seen. This plated texture does not provide conclusive evidence on its own hence as focal conic domains would give a similar looking texture.

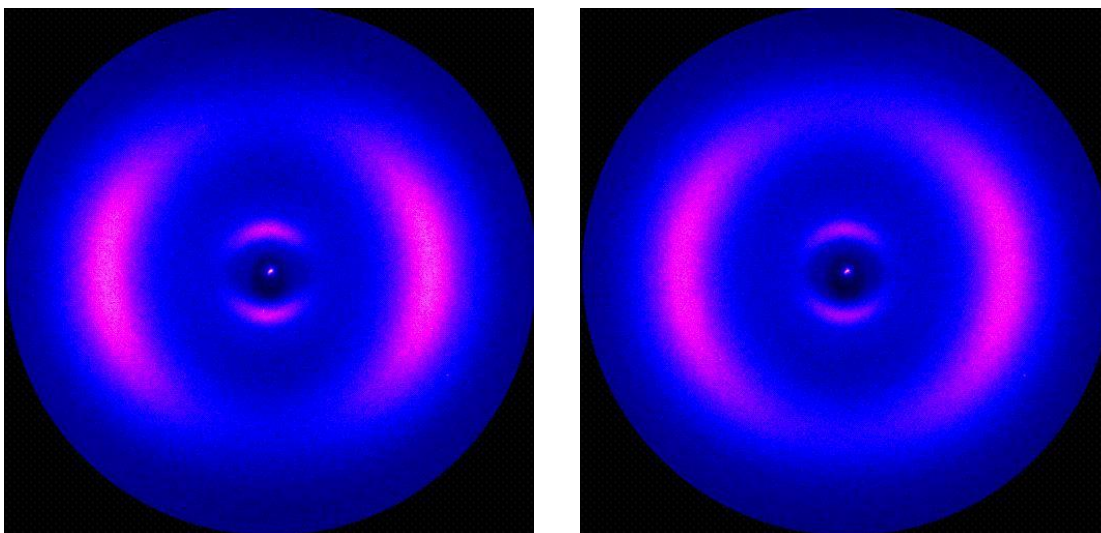


**Figure 76:** XRD scattering data of compound **26** at 58 °C (left) and 52 °C (right) on cooling from isotropic.

Both XRD scattering patterns are typical for nematic phases. The lack of an intense small angle peak points to the phase not being smectic as layer correlations are very strong. The narrowing of the wide angle in the  $N_{TB}$  phase is more obvious in this compound showing the increase in macroscopic order.

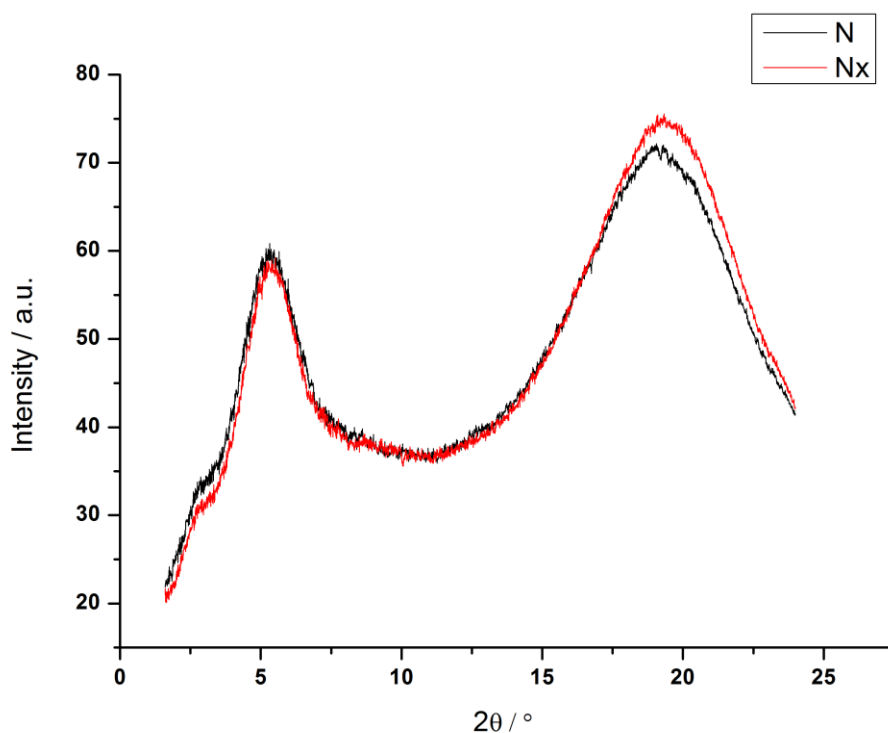
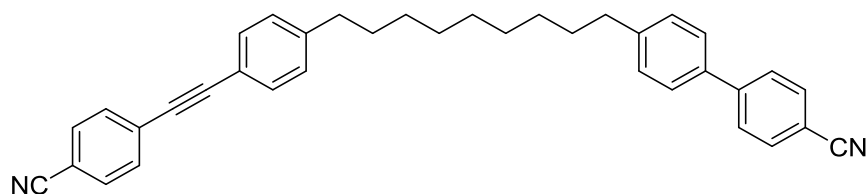


**Figure 77:**  $2\theta$  against intensity plot of compound **26** in the nematic and  $N_{TB}$  phase.

Shown in Figure 77 are the  $2\theta$  plots of the two nematic phases of compound **26**. The difference in the height of the peak is noticeable. As the spread of the wide angle is

narrower more molecules are closer to the value represented by the peak, giving an overall increase in the signal. The small angle peak at 5.3 equals 16.6 Å.

#### Compound **34**



Compound **34** consists of a cyanotolane mesogen on one end of the dimer molecule. Tolane based mesogens have been investigated<sup>95,96</sup> for their high birefringence and low viscosity. Our aim was to see if we can stabilize the  $N_{TB}$  phase by extending the size of the mesogen. Compound **34** is directly comparable with the symmetric cyanobiphenyl dimer **CB-C9-CB** that shows the phase sequence Cr-85- $N_{TB}$ -108-N-124-Iso. Compound **34** shows similar phase sequence of Cr-90- $N_{TB}$ -102-N-125-Iso. The tolane acetylene link is considered the equivalent of a half ring so a 5 °C increase in the Cr- $N_{TB}$  transition can be explained. It is interesting to note that the width of the  $N_{TB}$  has been halved with the change from cyanobiphenyl to cyanotolane. This illustrates how sensitive the  $N_{TB}$  phase is to changes in molecular shape. Ethyne linkages often lead to lower transition temperatures by extending the molecular conjugation which weakens  $\pi$ - $\pi$  stacking, although in this case the clearing point is almost identical to the symmetric system.

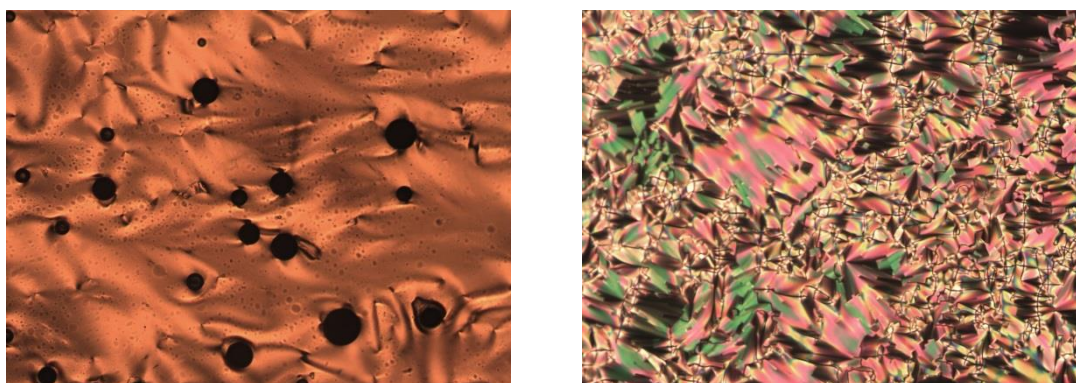


**Figure 78:** Micrographs of compound **34** at 108 °C (left) and 95 °C (right) under crossed polarizers and on untreated slides.

Shown in Figure 78 are micrographs of compound **34** in the two nematic phases. A classical picture is observed for the conventional nematic phase but a ribbon texture is seen for the  $N_{TB}$  phase. This texture is the reason this phase was missed when the symmetric cyanobiphenyl dimers were first investigated. Regions of the micrograph appear to have fan shaped focal conic running along defects lines.

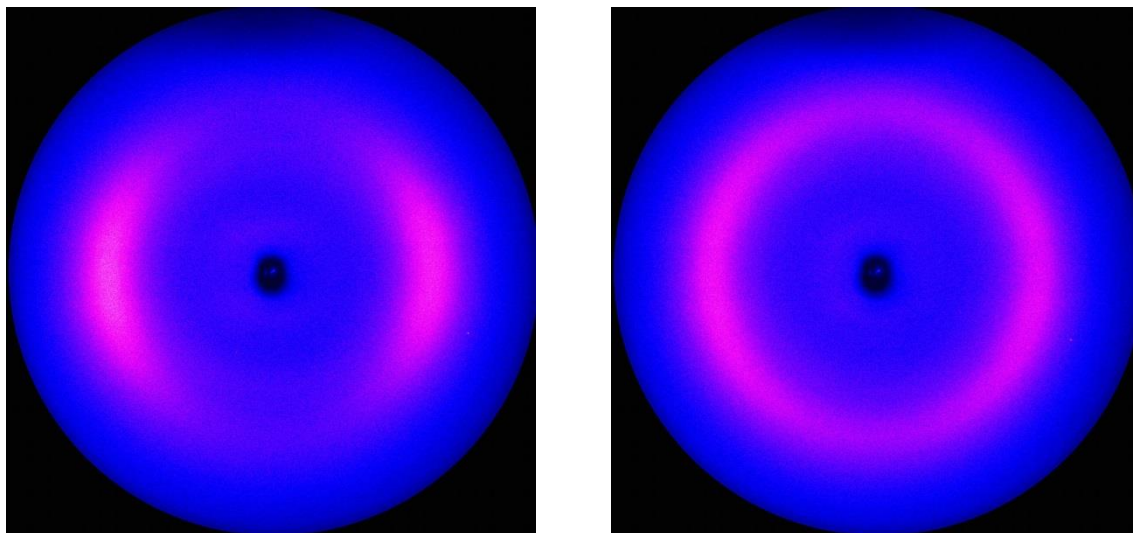


**Figure 79:** XRD scattering data of compound **34** at 115 °C (left) and 95 °C right.

Shown in Figure 79 is the XRD scattering data for compound **34**. This data was acquired over a 3600 second exposure. All the XRD data discussed so far has the exposure time of 300 seconds. This is indicative of how weakly this sample scattered. The absence of a small angle scattering confirms the two phases are not smectic. The lower temperature scattering pattern at 95 °C appears to be the similar to those seen for isotropic samples scattering equally at all angles.

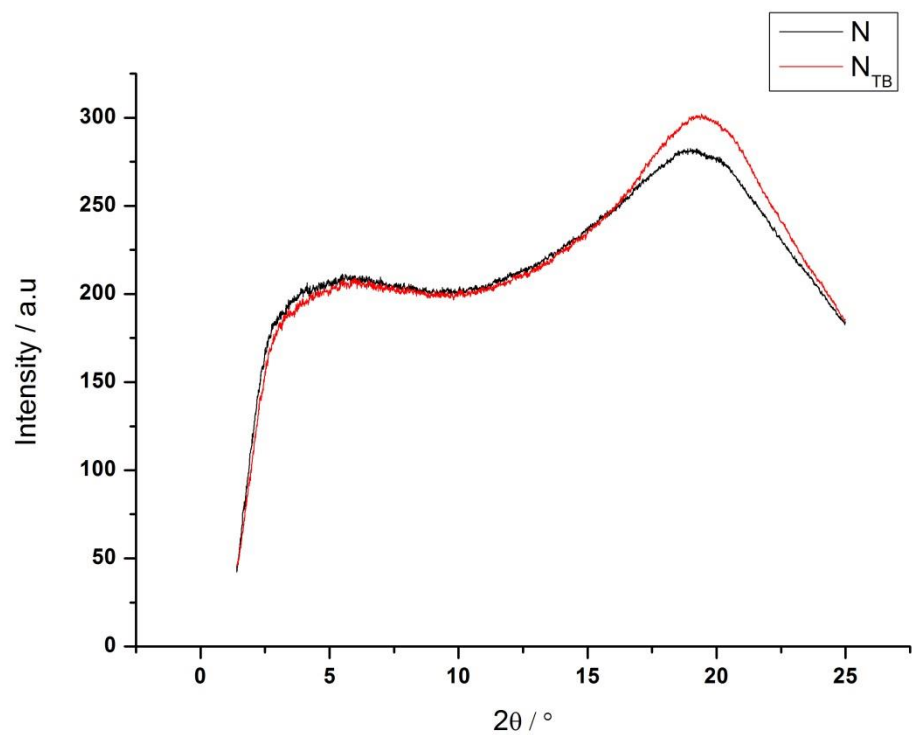


**Figure 80** : Plot of the  $2\theta$  against intensity of compound **34** in the nematic phase at 115°C and nematic twist bend phase at 95 °C.

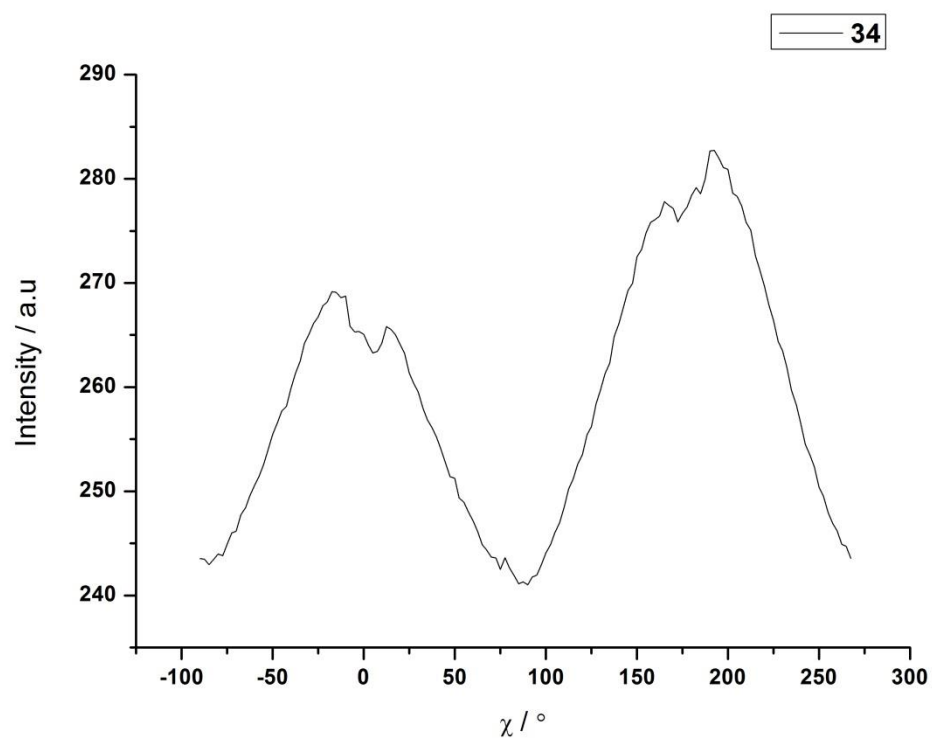


**Figure 81**: Plot of  $\chi$  against intensity of compound **34** at 95 °C of the wide angle.

Shown in Figure 81 is the plot of  $\chi$  scans against intensity of compound **34** at 95 °C in the wide angle. The plot shows the intensities peak at 0 and 180 ° which shows that that scattering is not isotropic. With this information to be able to visualize the data, compound **34** was exposed for 3600 seconds at 140 °C to collect true isotropic scattering. This is then subtracted from the sample. The narrowing of the wide angle scattering representing macroscopic order enables us to assign the phase as N<sub>TB</sub>.

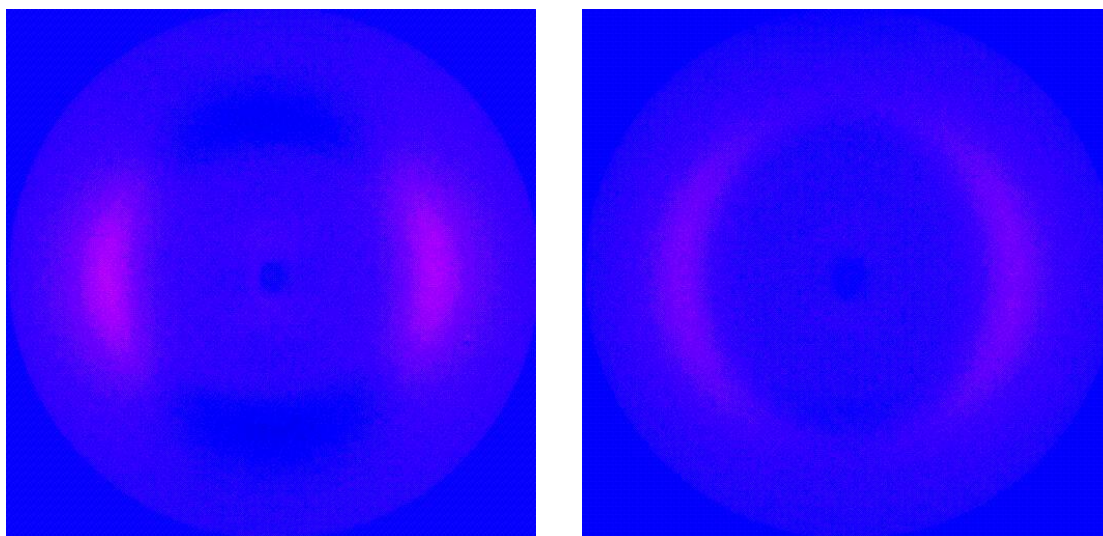


**Figure 82:** XRD scattering data of compound **34** at 115 °C (left) and 95 °C (right) with isotropic scattering subtracted.

### Difluoroterphenyl asymmetric dimers

Compounds **27**, **28**, **29**, and **30** have a nine methylene spacer with a difluoropentylterphenyl mesogen on one end. The other side of the dimer is varied and the properties reported. The dimer intermediate **25** with phenylbromide on one side and the difluoropentylterphenyl mesogen on the other side surprisingly shows an enantiotropic N<sub>TB</sub> phase. The phase sequence shown in Figure 83 below is Cr-42-N<sub>TB</sub>-61-N-85-Iso.

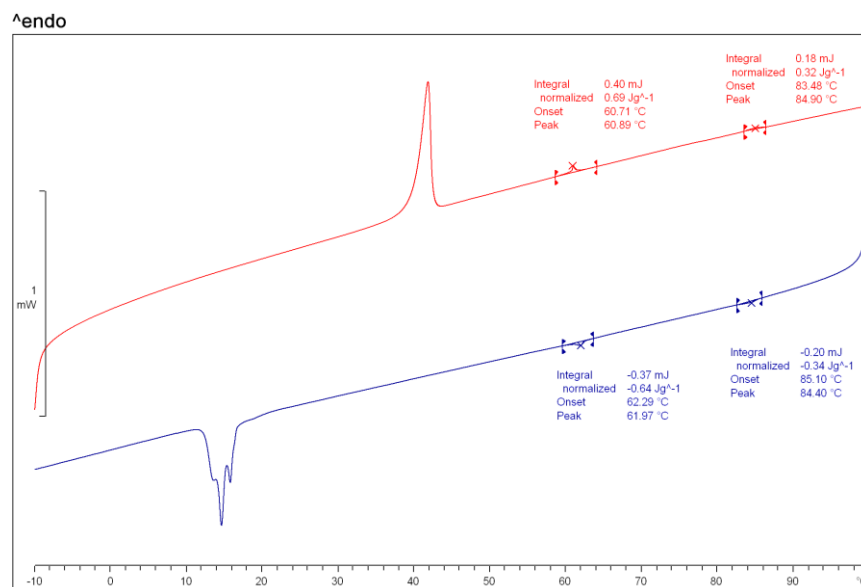
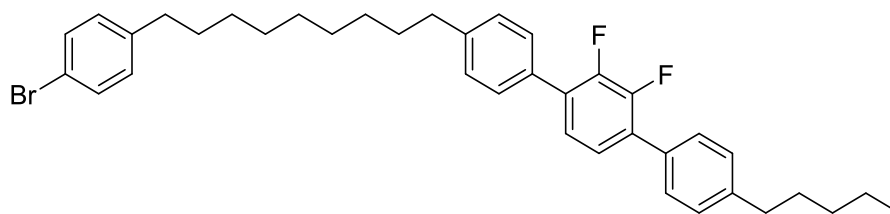


**Figure 83:** Calorimetric data for intermediate **25**.

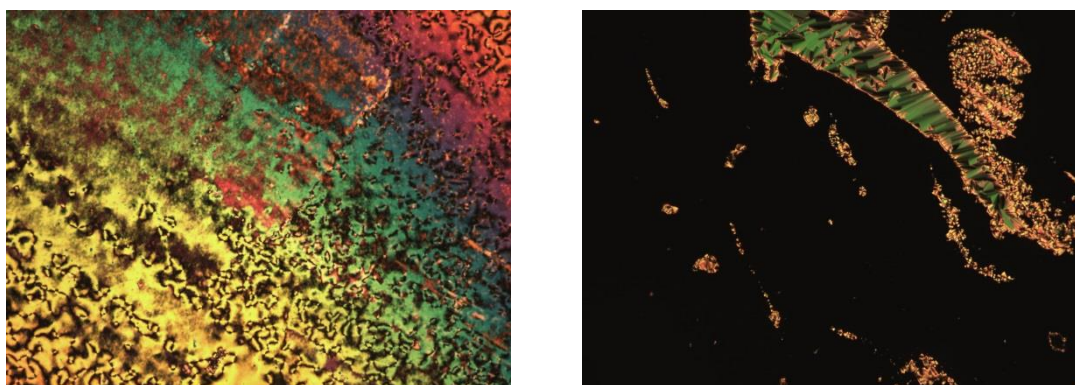
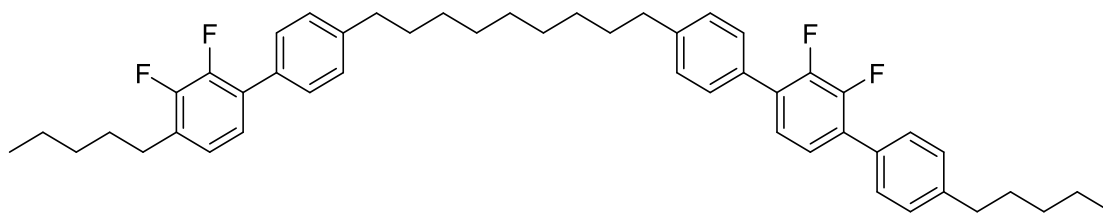


**Figure 84:** Micrographs of intermediate **25** at 77 °C (left) and 60 °C (right) under crossed polarizers and on untreated slides.

The micrographs of intermediate **25** shown in Figure 84 show the two nematic phases. The micrograph on the left shows marble texture with Schlieren defects with two and four brush defects. As the sample approached the nematic-nematic transition, the sample spontaneously aligns homeotropically. The regions that are still birefringent exhibit the plated texture and upon sheering show streaks as expected for a nematic phase.

## Compound **27**



Compound **27** has very similar mesogens on both ends. The smaller mesogen on one end is expected to reduce the transition temperatures. Compound **27** can directly be compared to **DTC-C9-DTC** that shows the phase sequence Cr-96-N<sub>TB</sub>-120-N-165-Iso. Surprisingly compound **27** did not show a second nematic phase. The phase sequence was observed to be Cr-37-N-53-Iso. The mesophase transition was reduced by almost 60 °C and the clearing temperature by almost a 110 °C.

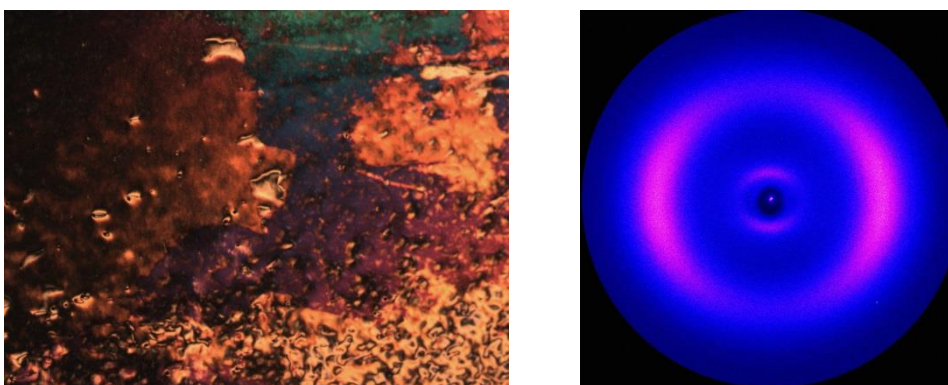
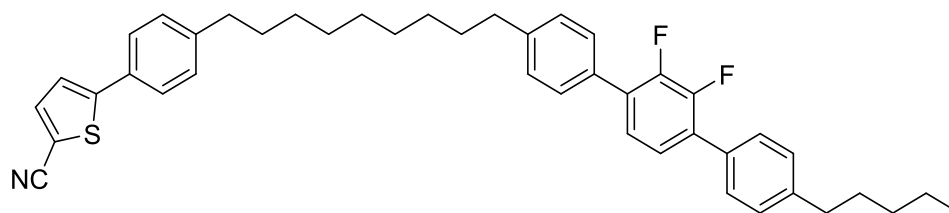


**Figure 85:** Micrograph and XRD scattering data of compound **27** at 50 °C.

Shown in Figure 85 is the micrograph and XRD scattering data for compound **27** at 50 °C. A marble texture is observed and a typical scattering pattern is also observed in scattering experiments. The weak signal in the small angle has a peak at 4.8 2theta and is equal to 18.4 Å. The uneven size of the two mesogens does not allow for even packing which might explain the drastic changes in the transition temperature.

## Compound **28**



Compound **28** introduces a local bend at one side of the dimer with a cyanothiophene based mesogen. A nematic phase from 89 °C to 115 °C is observed on heating. A second phase is observed cooling shown in Figure 86. The isotropic-nematic transition shows an enthalpy of  $0.81 \text{ J g}^{-1}$  and nematic-nematic transition has an enthalpic change of  $0.12 \text{ J g}^{-1}$ .

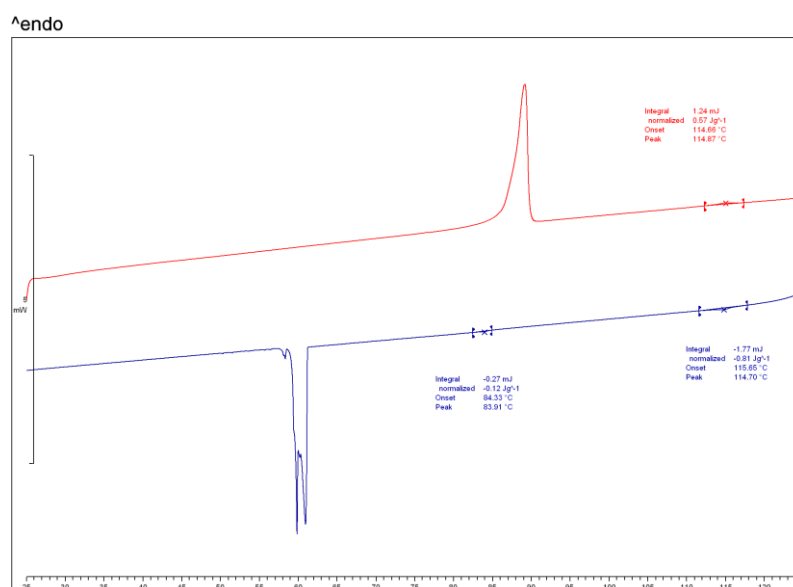


**Figure 86:** Calorimetric data for compound **28**.

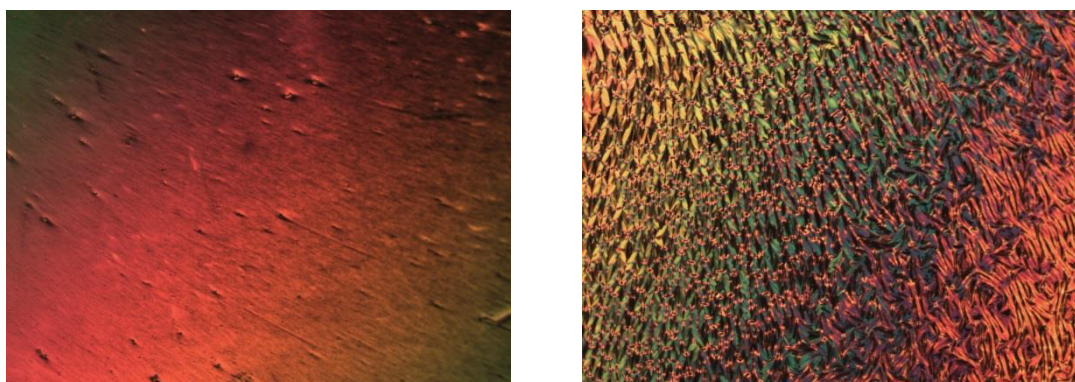


**Figure 87:** Micrographs of compound **28** at 90 °C (left) and 78 °C (right) under crossed polarizers and on untreated slides.

Shown in Figure 87 are the micrographs of compound **28** in the nematic and the  $N_{TB}$  phase. The marble texture of the nematic phase at 90 °C is typical, but the texture observed for the  $N_{TB}$  phase is complicated. The regions near the top left of the image suggest smectic A type focal conic whereas the bottom right of the image almost shows a fibrous texture and in the centre a mixture of the two.

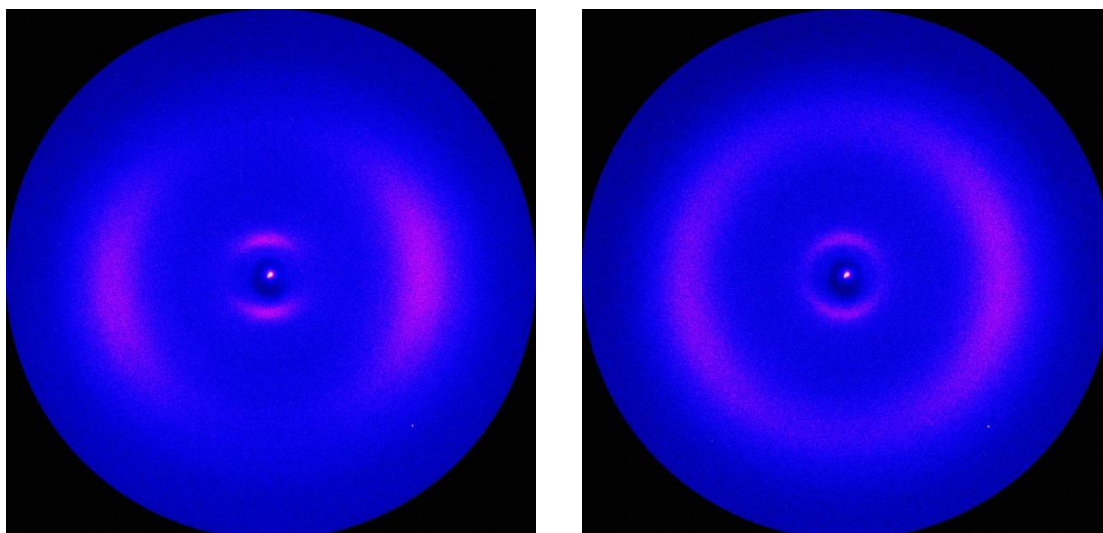


Figure 88: XRD scattering data of compound **28** at 100 °C and 80 °C

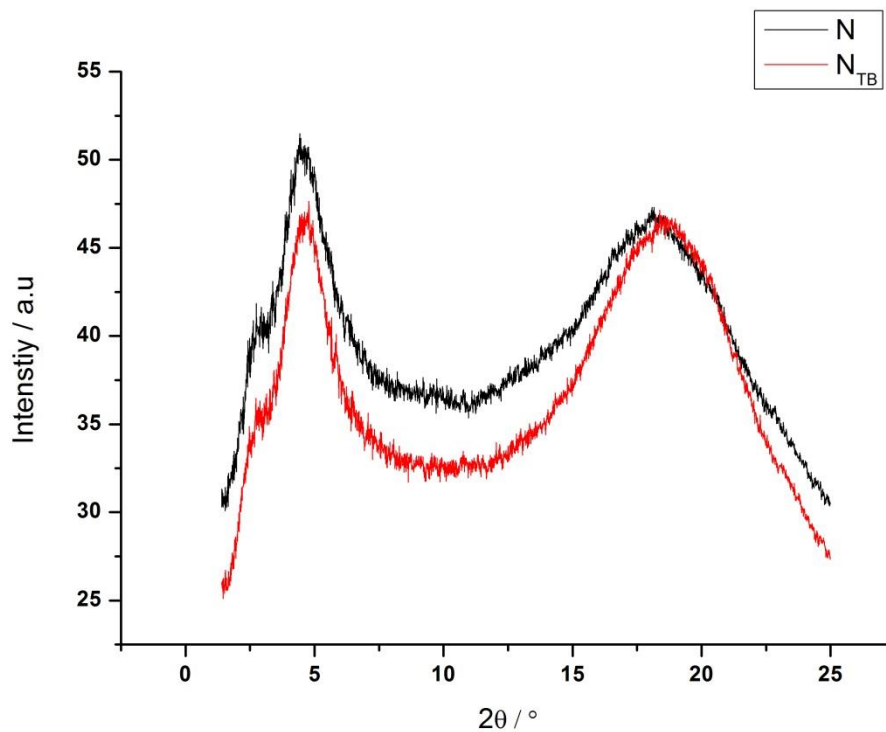
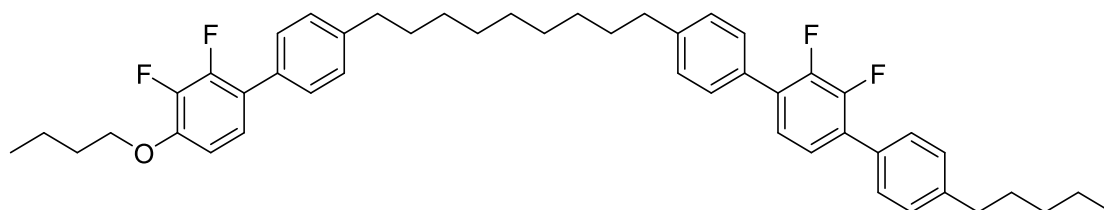


Figure 89: Plot of  $2\theta$  against intensity of compound **28** in both nematic phases.

The  $N_{TB}$  phase can be seen clearly from the narrowing of the wide angle scattering shown in Figure 88 and Figure 89. The mismatch of intensity is attributed to the uneven filling of the capillary, as the temperature is cycled the sample can flow out of the furnace window leading to differences in intensity. If the intensity difference is overlooked in the plot the difference in the width of the two peaks is evident.

### Compound 29



Compound 29 has a difluorobutyloxy biphenyl mesogen on one side of the dimer.

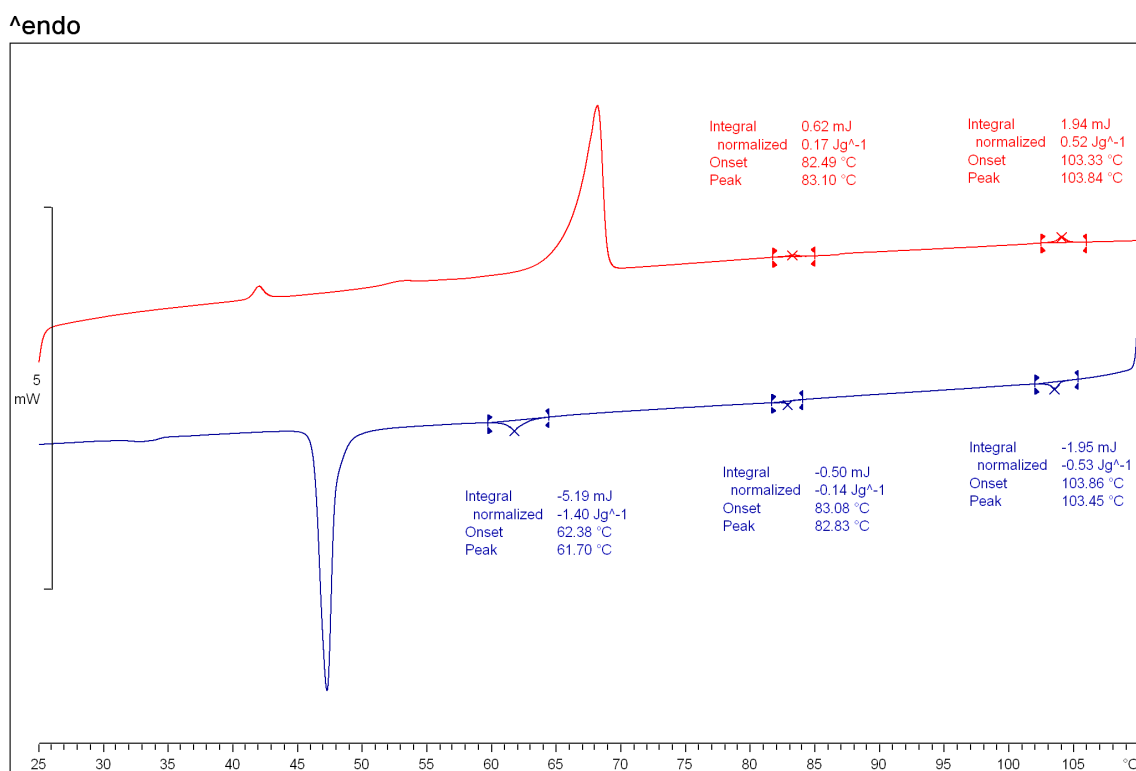
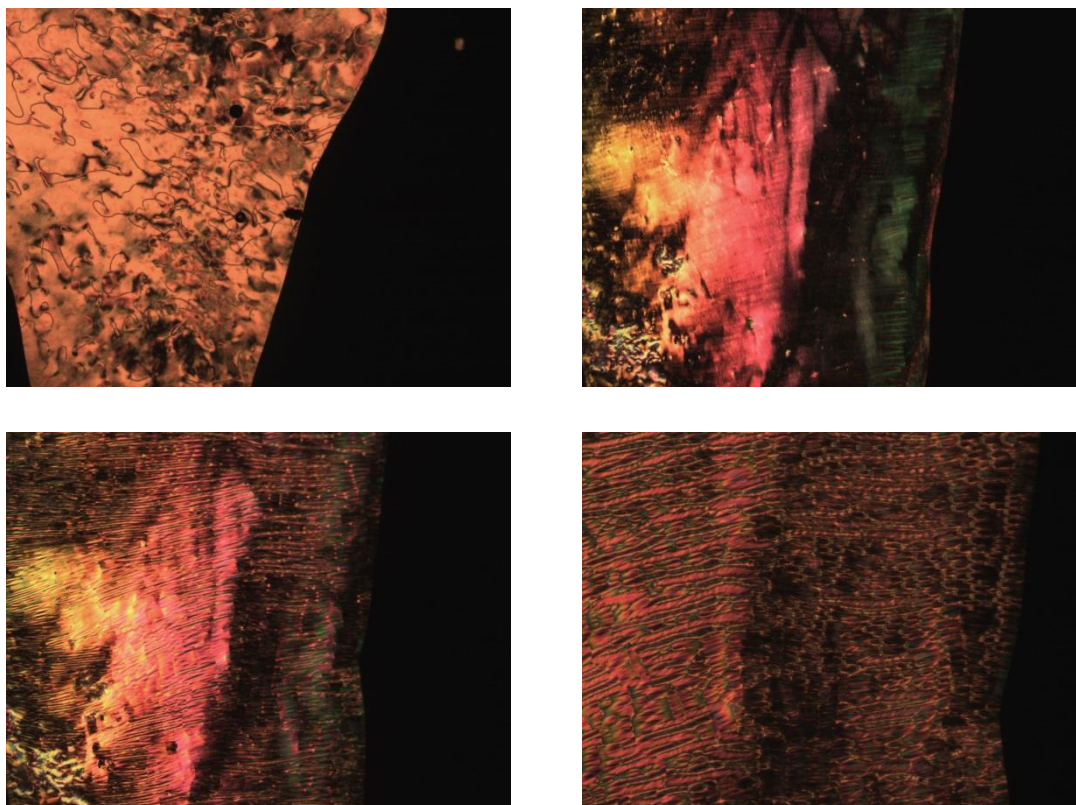


Figure 90: Calorimetric data for compound 29.

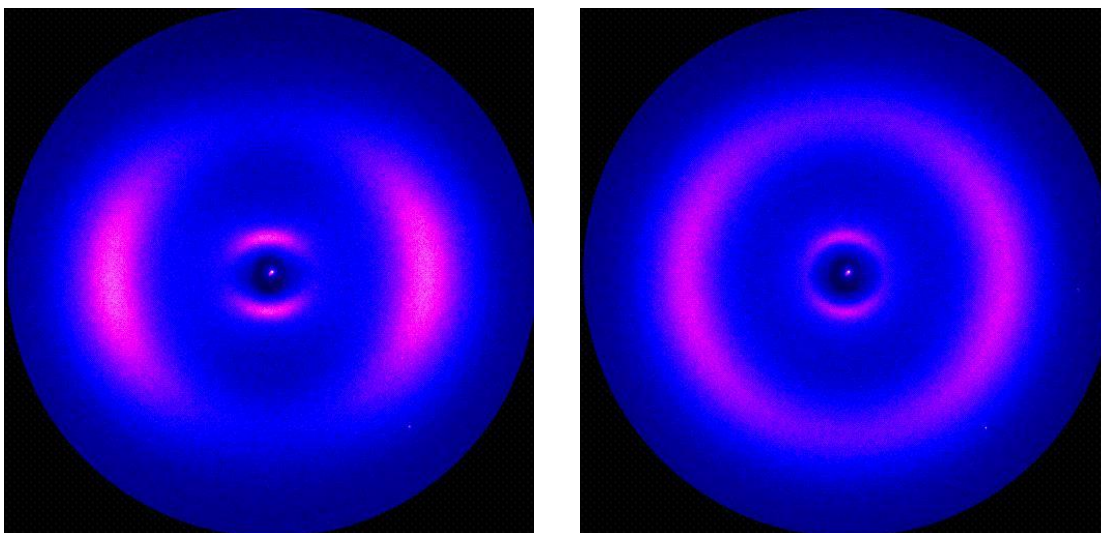
Shown in Figure 90 is calorimetric data for compound 29. Two mesophases can be observed on heating and three mesophases can be observed on cooling. On heating the  $N_{TB}$  phase is observed from 69-83 °C and a conventional nematic phase until 104

°C. The enthalpy change for the nematic-nematic transition was observed to be  $0.17 \text{ J g}^{-1}$  and the nematic-isotropic enthalpy was found to be  $0.52 \text{ J g}^{-1}$ . An additional phase was seen on cooling after the  $N_{TB}$  phase from  $62 \text{ °C}$  to  $47 \text{ °C}$  and is thought to be a smectic phase with an enthalpy of  $1.40 \text{ J g}^{-1}$  associated with the transition.



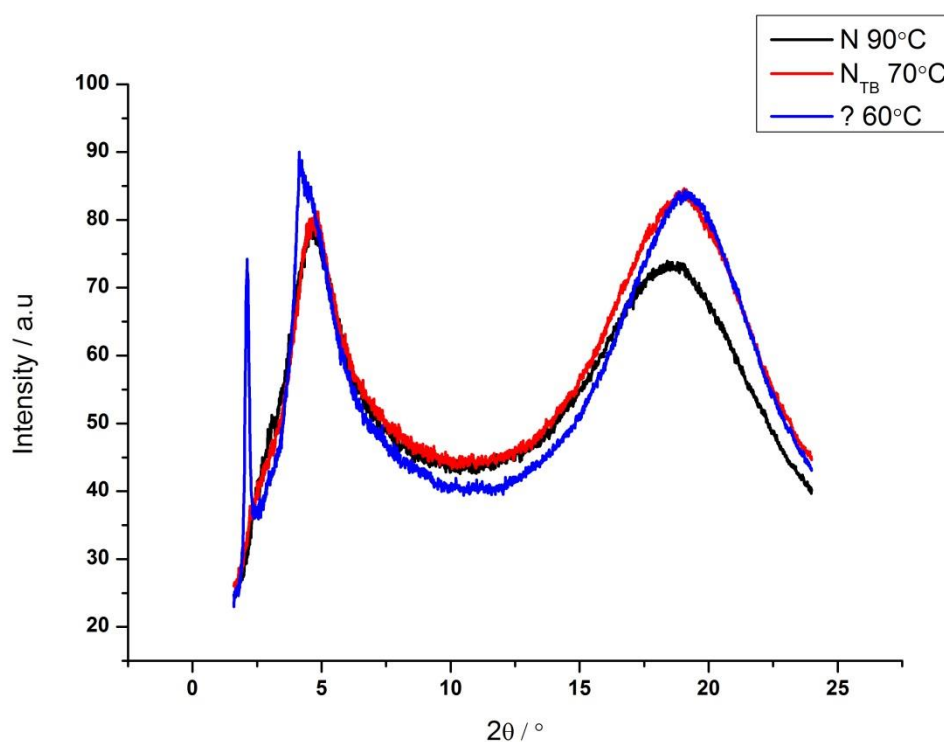
**Figure 91:** Micrographs of compound **29** at  $100 \text{ °C}$  (top left),  $84 \text{ °C}$  (top right),  $81 \text{ °C}$  (bottom left) and  $78 \text{ °C}$  (bottom right) under crossed polarizers and on untreated slides.

Figure 91 shows the micrographs of compound **29** at various temperatures. The first micrograph shows the conventional nematic phase with marble texture and some disclinations. The second micrograph is just before the transition to the  $N_{TB}$  and it can be observed that the phase looks grainy and signs of plates beginning to appear. The third micrograph is just after the transition and the plated texture is fully formed throughout the bulk of the sample. The fourth micrograph is a few degrees into the  $N_{TB}$  phase and the polygonal fish scale like texture forms. The left side of the micrograph is showing a rope like texture that is often observed in rubbed cells.



**Figure 92:** XRD scattering data for compound **29** at 90 °C and 70 °C.

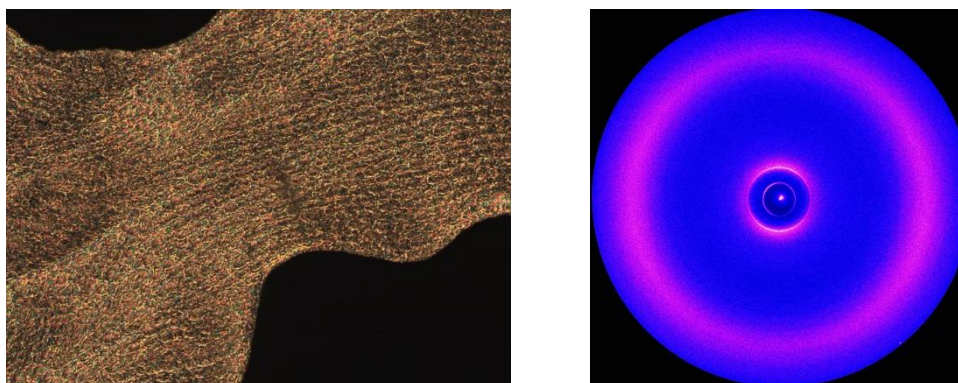
The data shown in Figure 92 shows the two patterns expected for the conventional nematic phase and the twist bend nematic phase exhibited by compound **29**. The peak in the small angle is at 4.7 which equals to 18.8 Å.



**Figure 93:** Plot of  $2\theta$  against intensity for compound **29** at various temperatures.

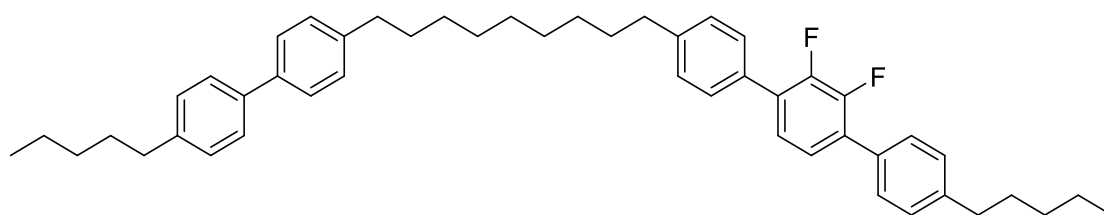
Shown in Figure 93 the plot of  $2\theta$  against intensity for compound **29** in all mesophases on cooling from the isotropic. The narrowing effect of the  $N_{TB}$  in the wide angle is most

evident in this example with a sizeable difference in peak height. Another interesting thing to note is the plot of the unknown phase.



The Two signals in the small angle at 2.1 and 4.3 equal 42 Å and 20.5 Å respectively. The shape of the peak at 4.3 seems to be an intermediate between a Lorentzian peak seen for smectics and those seen for nematics. As the signal is near the limit of the instrumentation it is important to collect the complete data set before a conclusion can be made regarding the assignment of this phase. Recent report by Tamba<sup>97</sup> *et al* has showed evidence of a smectic twist bend phase. This cannot be ruled out and is under investigation.

#### Compound 30



Compound **30** has a pentylbiphenyl mesogen on one side and exhibits two enantiotropic nematic phases. The phase sequence Cr-78-N<sub>TB</sub>-87-N-106-Iso was observed as shown in Figure 94. The nematic-nematic transition had an enthalpy of 0.24 J g<sup>-1</sup> and the nematic-isotropic transition showed an enthalpy of 0.56 J g<sup>-1</sup>.

<sup>endo</sup>

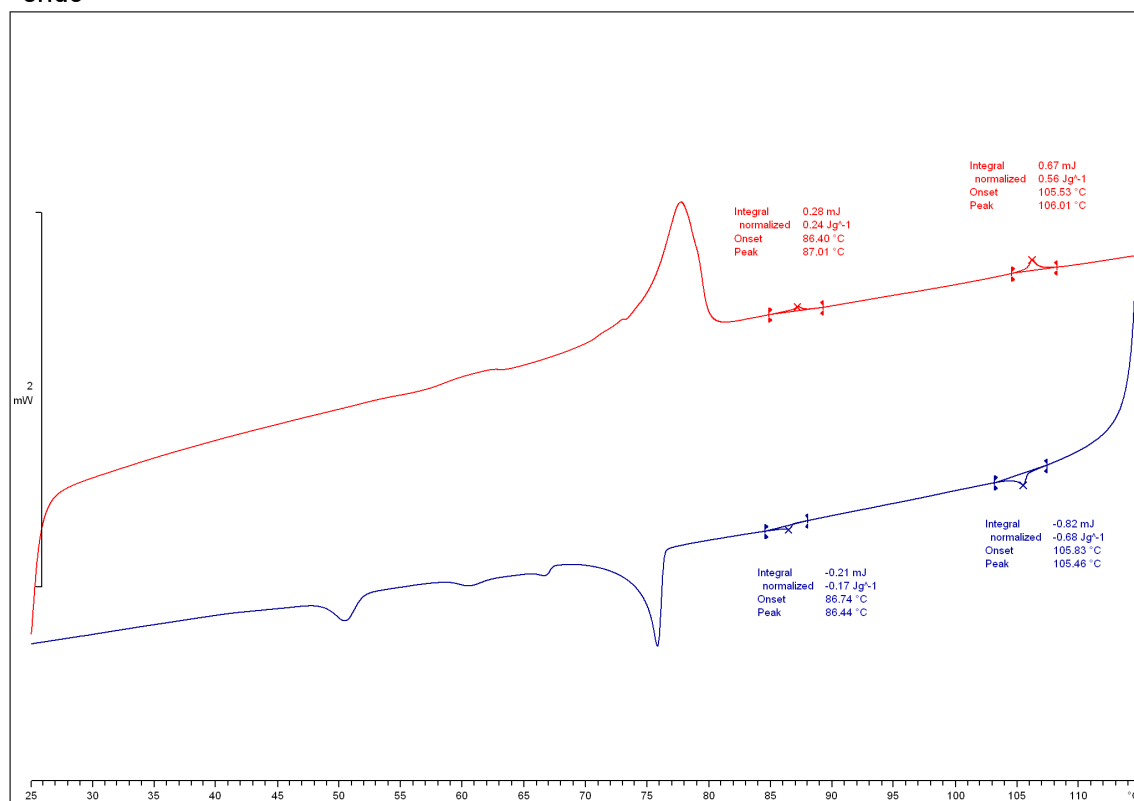


**Figure 94:** Calorimetric data for compound **30**

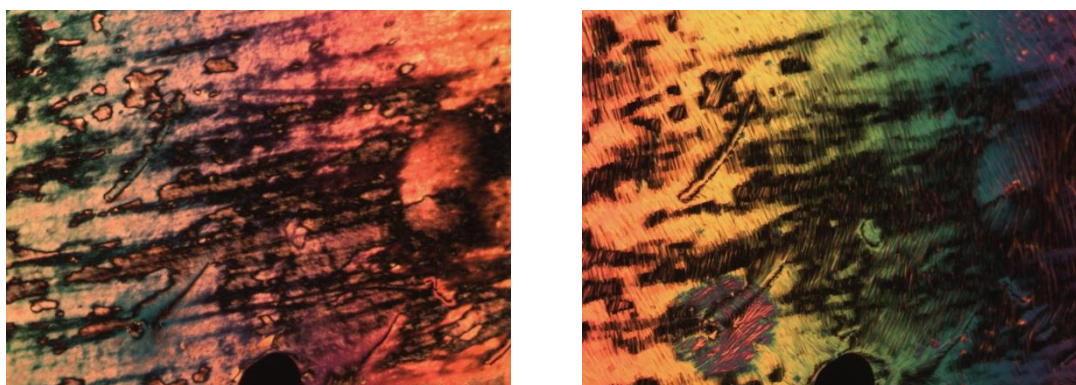


**Figure 95:** Micrographs of compound **30** at 101 °C (left) and 85 °C (right) under crossed polarizers and on untreated slides.

Figure 95 shows the marble texture of the nematic phase at 101 °C and shows the plated texture of the nematic twist bend phase at 85 °C immediately after the transition. After cooling a further 10 °C the plated textures develops into the polygonal fish scale texture as shown in Figure 96 of the same area. A rope like texture can also be observed which has developed spontaneously without any rubbing.

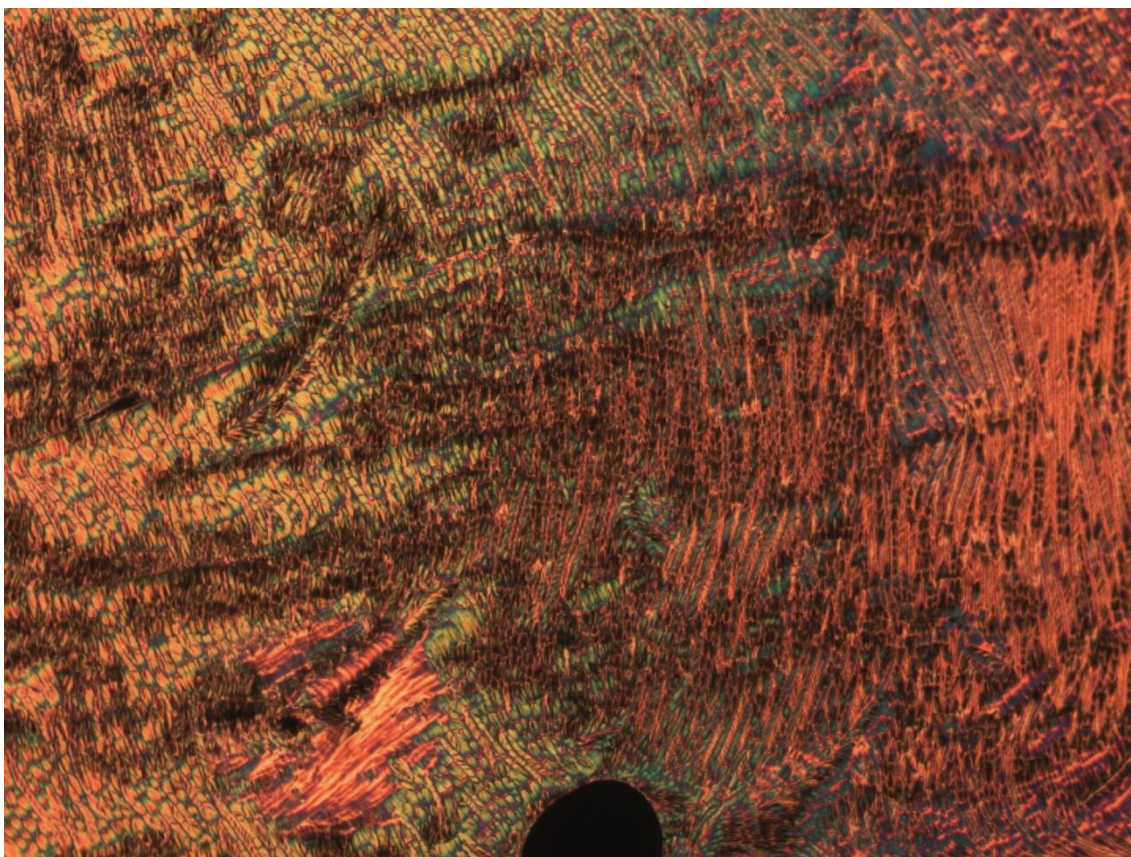


**Figure 96:** Micrograph of compound **30** at 75 °C.

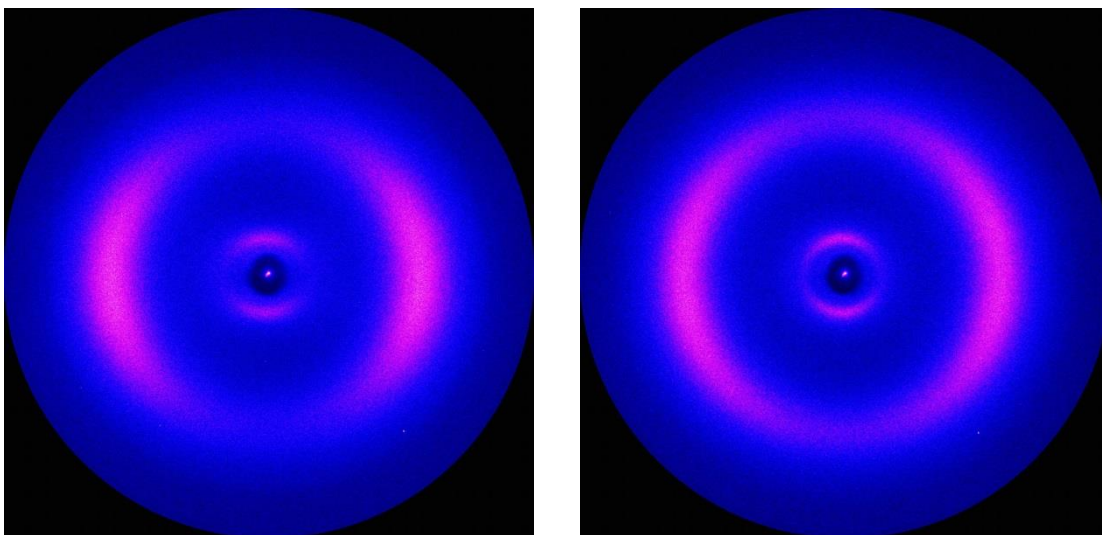


**Figure 97:** XRD scattering data for compound **30** at 103 °C (left) and 83 °C (right).

Figure 97 shows the scattering data for the nematic and the  $N_{TB}$  phase. The narrowing of the wide angle is visible in the  $N_{TB}$  phase. The small angle peak at 4.5 equals to 19.6 Å. 19.6 Å is approximately half the molecular length.

Compound	Structure	Transitions ( °C )	Enthalpy Iso-N( J g <sup>-1</sup> )	Enthalpy N-N <sub>TB</sub> ( J g <sup>-1</sup> )
<b>CB-C9-CB</b>		Cr- 85- N <sub>x</sub> – 107– N – 124 – Iso	2.10	0.86
<b>DTC-C9-CB</b>		Cr- 69- N <sub>x</sub> – 110– N – 144 – Iso	2.25	0.43
<b>22</b>		Cr – (N <sub>x</sub> 89) 90 – N – 101 - Iso	2.04	1.69
<b>23</b>		Cr – (N <sub>x</sub> 38) 40 – N – 44 – Iso	0.14	1.31
<b>24</b>		Cr – 81 – N – 86 – Iso	0.70	-
<b>26</b>		Cr – (N <sub>x</sub> 55) 56 – N – 64 – Iso	0.26	0.81
<b>34</b>		Cr – 90 - N <sub>x</sub> – 102 – N – 125 – Iso	1.89	0.57
<b>27</b>		Cr – 37 – N – 53 – Iso	-	-
<b>28</b>		Cr – (N <sub>x</sub> 84) 89 – N – Iso	0.81	0.12
<b>29</b>		Cr – (SmX 62) 69 – N <sub>x</sub> – 83 – N – 104 – Iso	0.53	0.14
<b>30</b>		Cr- 78- N <sub>x</sub> – 87 – N – 106 – Iso	0.68	0.17

Table showing asymmetric dimers, their structures, transitions and enthalpies.

The enthalpies attributed to the isotropic-nematic transition of compounds **23**, **24**, **26**, **28**, **29** and **30** were observed to be significantly lower than those usually expected for the conventional nematic phase. Expected at 1 to 2 J g<sup>-1</sup> normally, the cyanobiphenyl based asymmetric compounds exhibited almost 10 times smaller enthalpies. The difluoroterphenyl based asymmetric dimers were found to exhibit higher enthalpies for the isotropic-nematic transition compared to the cyanobiphenyl analogues but compared to other systems previously reported in literature these values were still much lower than expected.

At the same time the nematic-nematic transition enthalpies were found to be anomalously high for the cyanobiphenyl based asymmetric dimers with the exception of the cyanotolane dimer. The bent system based on the cyanothiophene mesogen showed an enthalpy that agrees with similar systems for the isotropic-nematic transition but showed a very high nematic-nematic transition enthalpy.

The systems based on difluoroterphenyl also showed a lower nematic-nematic transition enthalpy. This observation is more understandable as the enthalpies of both transitions are consistently lower than expected. The enthalpies exhibited by compounds **28**, **29** and **30** are roughly half of what has been previously reported for dimers shown in the above table.

## Conclusion and Outlook

Several novel compounds exhibiting  $N_{TB}$  phase were synthesized and characterized. For the mesogens investigated, odd numbered methylene spacer was found to promote  $N_{TB}$  behaviour. The inclusion of lateral fluorines in the aromatic groups of the mesogens led to lower transition temperatures and was found to stabilize the  $N_{TB}$  phase formation along with the inclusion of terminal dipoles.

The synthetic routes were found to be efficient and successful in achieving the targeted molecules. The methods of characterisation were successful in differentiating between the two nematic phases.

Striped and elliptical polygonal texture was observed on OPM for the  $N_{TB}$  phase compared to the marble and Schlieren observed for a conventional nematic phase. XRD showed a narrowing of the wide angle signal indicative of an increase of macroscopic order as expected for the  $N_{TB}$  phase.

Novel compounds containing bent mesogens were found to exhibit the  $N_{TB}$ , this is the first example of this double bend behaviour leading to multiple nematic phases. A new material was also found to exhibit monotropic  $N_{TB}$  which was kinetically stable at room temperature for up to 3 weeks. This indicates that even though the knowledge about these materials is at present still very incomplete, as the structure of the  $N_{TB}$  phase is not yet fully understood it is possible to design materials with the desired phase close to room temperature.

Moreover, the materials reared and investigated in this project, show beyond the  $N_{TB}$  phase a number of other higher ordered LC phases. The assignment of the unknown phases is currently underway and should be resolved from X-ray data collected at synchrotron facilities. Investigation in to the presence of a possible smectic twist bend phase will also be carried out. The technological impact of these compounds in devices is yet to be explored.

Several interesting architectures can be investigated for exhibiting the  $N_{TB}$  phase. The asymmetry can be increased by using even smaller and larger mesogens on either side of the spacer. It would also be interesting to investigate mesogens with flexibility, essentially a triple bend molecule.

## Experimental

Most starting reagents and solvents were purchased from Fischer, Sigma Aldrich, Acros Organics and Fluorochem and used without further purification. Boronic acids were purchased from Kingston chemicals and were also used without further purification.

Silica gel for chromatography was purchased from Fluorochem with an estimated pore size of 60 Å formed from 35-70 mesh (particle size 200-500 µm). Thin layer chromatography was performed on Merck Millipore aluminium plates with a 200 µm thick layer of 10-12 µm silica particles. The TLC plates also contain manganese doped zinc silicate also known as fluorescent green indicator F<sub>254</sub>.

The structures after purification were confirmed by <sup>1</sup>H and <sup>13</sup>C nuclear magnetic resonance spectroscopy. The experiments were performed with a Joel JNM-ECP 400 MHz FT-NMR. The chemical shifts reported in this section are relative to tetramethylsilane used as an internal standard and coupling constants *J* are reported in Hertz (Hz). <sup>1</sup>H experiments were performed at 400 MHz, <sup>13</sup>C at 100 MHz and <sup>19</sup>F 376 MHz. In some cases <sup>13</sup>C signals are less than expected, this is most likely due to the signals being lost in the noise or due to overlap.

Low resolution electron ionisation (EI), electro-spray (ES), chemical ionisation (CI), matrix assisted laser deposition ionisation (MALDI) and high resolution mass spectrometry (HRMS) were obtained via the EPSRC National Mass Spectrometry Service Centre at Swansea University, Wales.

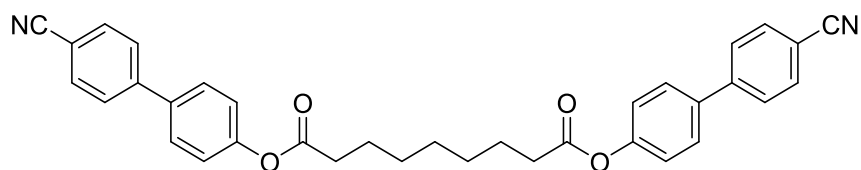
The purity of the final compounds was confirmed by high performance liquid chromatography. The HPLC setup consisted of Gilson 321 pump, Agilent/HP1100 detector with a Phenomex LUNA 18(2) reverse phase C18 column. The column dimensions are 250 mm x 4.6 mm, 5 µm particles and 100 Å pore size.

The thermal properties of the final compounds were investigated on Mettler-Toledo differential scanning calorimetry DSC822e. These experiments were performed under nitrogen and the enthalpies measured against an internal gold standard. The mesophase was optically observed on an Olympus BX-51 optical polarising microscope equipped with a Mettler FP82 hot stage and Mettler 5 central processing unit. The

microscope was also equipped with Lumenera's Infinity X camera and images were captured using Studio86Design's studio capture. All experiments were carried out at 100X magnification unless stated otherwise. All transitions are reported in degrees Celsius.

The structure of the mesophase was also investigated by x-ray diffraction. CuK $\alpha$  radiation of wavelength 1.54 Å was generated using copper tube at 35 KV and 30 mA. The beam is passed through a 300  $\mu\text{m}$  thick beryllium window and is further 2D shaped using Xenocs FOX2D12\_INF optics. The size of the beam is approximately 200  $\mu\text{m}$  x 200  $\mu\text{m}$ . The samples are heated in the presence of a 1 T magnet in a home built graphite furnace consisting of Eurotherm heater. The x-rays were detected on Mar345 2D-image plate. The data was analysed using Paul Heiney's Datasqueeze software and was fitted using OriginLab's Origin pro 8 software. All experiments were conducted with the magnetic field perpendicular to the beam and capillary.

## Synthesis of bis(4'-cyano-[1,1'-biphenyl]-4-yl) nonanedioate (1)



Nonanedioic acid (0.5 g, 2.7 mmol), 4-cyano-4'-hydroxybiphenyl (2.60 g, 13.3 mmol), N,N-diisopropylcarbodiimide (2.70 g, 21.4 mmol) and 4-dimethylaminopyridine (0.65 g, 5.3 mmol) were dissolved in dry tetrahydrofuran (50 mL) under inert atmosphere. The reaction was stirred at room temperature, under darkness and inert atmosphere until completion by thin layer chromatography. The solvent was removed under reduced pressure and the organics separated by silica column chromatography using dichloromethane. The crude compound was recrystallized from methanol to afford the title compound as a white solid (0.91 g, 63%).

Cr – 144 – N – 189 – Iso

$^1\text{H NMR}$ :  $\delta_{\text{H}}$  (400 MHz,  $\text{CDCl}_3$ ) 7.73 (4H, d,  $J$  8.16), 7.65 (4H, d,  $J$  8.16), 7.59 (4H, d,  $J$  8.57), 7.20 (4H, d,  $J$  8.57), 2.61 (4H, t,  $J$  7.45), 1.79 (4H, m), 1.48 (6H, m).

$^{13}\text{C NMR}$ :  $\delta_{\text{C}}$  (100 MHz,  $\text{CDCl}_3$ ) 172.1, 151.1, 144.7, 136.8, 132.6, 128.3, 127.7, 122.3, 118.8, 111.0, 34.3, 28.8, 24.8.  $^{13}\text{C}$  expected 14, found 13.

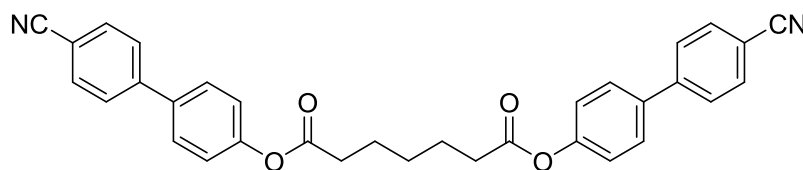
**MS: 542**

$m/z$  (CI) 560 ( $\text{M}+\text{NH}_4^+$ )

HRMS Calc:  $\text{C}_{35}\text{H}_{30}\text{N}_2\text{O}_4+\text{NH}_4$  requires = 560.2549

HRMS Found: 560.2539

## Synthesis of bis(4'-cyano-[1,1'-biphenyl]-4-yl) heptanedioate (2)



Heptanedioic acid (0.75 g, 4.7 mmol), 4-cyano-4'-hydroxybiphenyl (4.57 g, 23.4 mmol), N,N-diisopropylcarbodiimide (4.70 g, 37.2 mmol) and 4-dimethylaminopyridine (0.65 g, 9.3 mmol) were dissolved in dry tetrahydrofuran (50 mL) under inert atmosphere. Reaction was stirred at room temperature, under darkness and inert atmosphere until completion by thin layer chromatography. The solvent was removed under reduced pressure and the organics separated by silica column chromatography using dichloromethane. The crude compound was recrystallized from methanol to afford the title compound as a white solid (0.60 g, 25%).

Cr- (N 189) 209 – Iso

$^1\text{H NMR}$ :  $\delta_{\text{H}}$  (400 MHz,  $\text{CDCl}_3$ ) 7.72 (4H, d,  $J$  8.57), 7.65 (4H, d,  $J$  8.57), 7.59 (4H, d,  $J$  8.57), 7.21 (4H, d,  $J$  8.57), 2.65 (4H, t,  $J$  7.45), 1.86 (4H, m), 1.59 (2H, m).

$^{13}\text{C NMR}$ :  $\delta_{\text{C}}$  (100 MHz,  $\text{CDCl}_3$ ) 171.8, 151.0, 144.7, 136.8, 132.6, 128.3, 127.6, 122.3, 118.8, 111.0, 34.0, 28.5, 24.4.

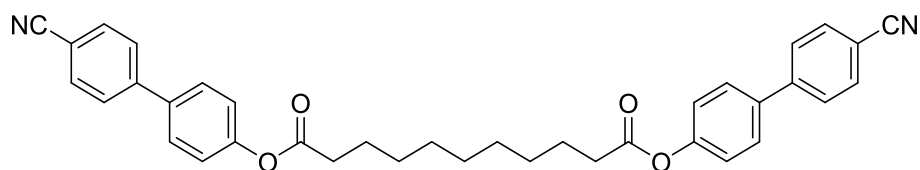
**MS: 514**

$m/z$  (CI) 532 ( $\text{M}+\text{NH}_4^+$ )

HRMS Calc:  $\text{C}_{33}\text{H}_{26}\text{N}_2\text{O}_4+\text{NH}_4$  requires = 532.2236

HRMS Found: 532.2227

### Synthesis of bis(4'-cyano-[1,1'-biphenyl]-4-yl) undecanedioate (3)



Undecanedioic acid (0.5 g, 2.3 mmol), 4-cyano-4'-hydroxybiphenyl (2.26 g, 11.6 mmol), N,N-diisopropylcarbodiimide (2.33 g, 18.5 mmol) and 4-dimethylaminopyridine (0.56 g, 4.5 mmol) were dissolved in dry tetrahydrofuran (50 mL) under inert atmosphere. The reaction was stirred at room temperature, under darkness and inert atmosphere until completion by thin layer chromatography. The solvent was removed under reduced pressure and the organics separated by silica column chromatography using dichloromethane. The crude compound was recrystallized from methanol to afford the title compound as a white solid (0.84 g, 64%).

Cr – 122 – N – 177 – Iso

$^1\text{H NMR}$ :  $\delta_{\text{H}}$  (400 MHz,  $\text{CDCl}_3$ ) 7.71 (4H, d,  $J$  8.16), 7.65 (4H, d,  $J$  8.36), 7.58 (4H, d,  $J$  8.57), 7.20 (4H, d,  $J$  8.57), 2.60 (4H, t,  $J$  7.60), 1.78 (4H, m), 1.42 (10H, m).

$^{13}\text{C NMR}$ :  $\delta_{\text{C}}$  (100 MHz,  $\text{CDCl}_3$ ) 172.2, 151.1, 144.7, 136.7, 132.6, 128.3, 127.6, 122.3, 118.8, 110.9, 34.3, 29.2, 29.1, 29.0, 24.8.

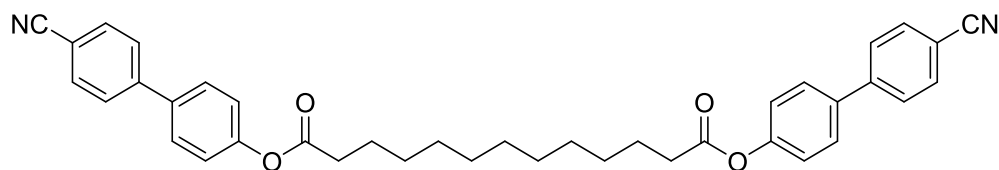
**MS: 570**

$m/z$  (CI) 588 ( $\text{M}+\text{NH}_4^+$ )

HRMS Calc:  $\text{C}_{37}\text{H}_{34}\text{N}_2\text{O}_4+\text{NH}_4$  requires = 588.2862

HRMS Found: 588.2853

## Synthesis of bis(4'-cyano-[1,1'-biphenyl]-4-yl) tridecanedioate (4)



Tridecanedioic acid (0.5 g, 2.0 mmol), 4-cyano-4'-hydroxybiphenyl (2.00 g, 10.2 mmol), N,N-diisopropylcarbodiimide (2.07 g, 16.4 mmol) and 4-dimethylaminopyridine (0.50 g, 4.1 mmol) were dissolved in dry tetrahydrofuran (50 mL) under inert atmosphere. The reaction was stirred at room temperature, under darkness and inert atmosphere until completion by thin layer chromatography. The solvent was removed under reduced pressure and the organics separated by silica column chromatography using dichloromethane. The crude compound was recrystallized from methanol to afford the title compound as a white solid (0.87 g, 71%).

Cr- 132 – N – 169 - Iso

$^1\text{H NMR}$ :  $\delta_{\text{H}}$  (400 MHz,  $\text{CDCl}_3$ ) 7.73 (4H, d,  $J$  8.36), 7.66 (4H, d,  $J$  8.77), 7.59 (4H, d,  $J$  8.77), 7.20 (4H, d,  $J$  8.57), 2.59 (4H, t,  $J$  7.45), 1.79 (4H, m), 1.55-1.34 (14H, m).

$^{13}\text{C NMR}$ :  $\delta_{\text{C}}$  (100 MHz,  $\text{CDCl}_3$ ) 172.1, 151.1, 144.6, 136.6, 132.5, 128.2, 127.5, 122.2, 118.8, 110.8, 34.3, 29.4, 29.3, 29.1, 28.9, 24.8.

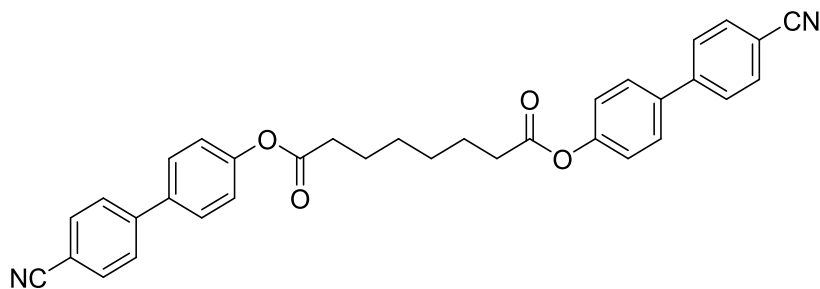
**MS: 598**

$m/z$  (CI) 616 ( $\text{M}+\text{NH}_4^+$ )

HRMS Calc:  $\text{C}_{39}\text{H}_{38}\text{N}_2\text{O}_4+\text{NH}_4$  requires = 616.3175

HRMS Found: 616.3165

## Synthesis of bis(4'-cyano-[1,1'-biphenyl]-4-yl) octanedioate (5)



Octanedioic acid (0.25 g, 1.4 mmol), 4-cyano-4'-hydroxybiphenyl (1.40 g, 7.2 mmol), N,N-diisopropylcarbodiimide (1.45 g, 11.5 mmol) and 4-dimethylaminopyridine (0.35 g, 2.8 mmol) were dissolved in dry tetrahydrofuran (20 mL) under inert atmosphere. The reaction was stirred at room temperature, under darkness and inert atmosphere until completion by thin layer chromatography. The solvent was removed under reduced pressure and the organics separated by silica column chromatography using dichloromethane to afford the title compound as a white solid (0.52 g, 68%).

Cr- 205 – N – 226 – Iso

$^1\text{H NMR}$ :  $\delta_{\text{H}}$  (400 MHz,  $\text{CDCl}_3$ ) 7.72 (4H, d,  $J$  8.16), 7.65 (4H, d,  $J$  8.36), 7.59 (4H, d,  $J$  8.57), 7.20 (4H, d,  $J$  8.57), 2.63 (4H, t,  $J$  7.45), 1.82 (4H, m), 1.52 (4H, m).

$^{13}\text{C NMR}$ :  $\delta_{\text{C}}$  (100 MHz,  $\text{CDCl}_3$ ) 172.0, 151.1, 144.7, 136.7, 132.6, 128.3, 127.6, 122.3, 118.8, 111.0, 34.2, 28.7, 24.6.

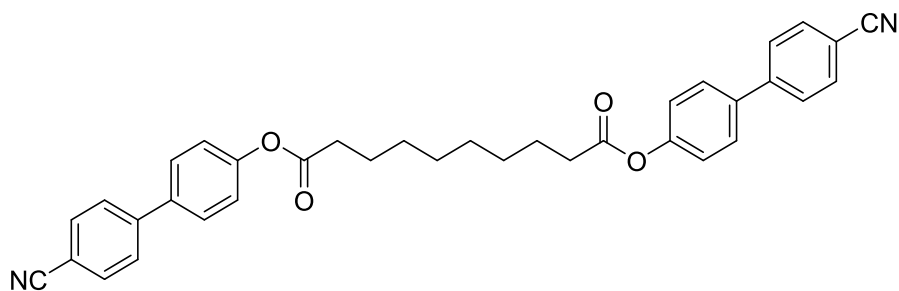
**MS: 528**

$m/z$  (CI) 546 ( $\text{M}+\text{NH}_4^+$ )

HRMS Calc:  $\text{C}_{34}\text{H}_{28}\text{N}_2\text{O}_4+\text{NH}_4$  requires = 546.2387

HRMS Found: 546.2378

## Synthesis of bis(4'-cyano-[1,1'-biphenyl]-4-yl) decanedioate (6)



Decanedioic acid (0.25 g, 1.2 mmol), 4-cyano-4'-hydroxybiphenyl (1.21 g, 6.2 mmol), N,N-diisopropylcarbodiimide (1.25 g, 9.9 mmol) and 4-dimethylaminopyridine (0.65 g, 2.7 mmol) were dissolved in dry tetrahydrofuran (20 mL) under inert atmosphere. The reaction is stirred at room temperature, under darkness and inert atmosphere until completion by thin layer chromatography. The solvent was removed under reduced pressure and the organics separated by silica column chromatography using dichloromethane to afford the title compound as a white solid (0.52 g, 76%).

Cr- 151 - Iso

$^1\text{H NMR}$ :  $\delta_{\text{H}}$  (400 MHz,  $\text{CDCl}_3$ ) 7.72 (4H, d,  $J$  8.16), 7.65 (4H, d,  $J$  8.16), 7.59 (4H, d,  $J$  8.36), 7.20 (4H, d,  $J$  8.36), 2.62 (4H, t,  $J$  7.45), 1.82 (4H, m), 1.61-1.25 (8H, m).

$^{13}\text{C NMR}$ :  $\delta_{\text{C}}$  (100 MHz,  $\text{CDCl}_3$ ) 172.1, 151.1, 144.7, 136.7, 132.6, 128.3, 127.6, 122.3, 118.8, 111.0, 34.3, 29.0, 28.9, 24.8.

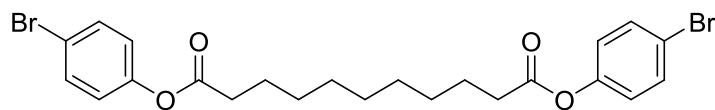
**MS: 556**

$m/z$  (CI) 574( $\text{M}+\text{NH}_4^+$ )

HRMS Calc:  $\text{C}_{36}\text{H}_{32}\text{N}_2\text{O}_4+\text{NH}_4$  requires = 574.2700

HRMS Found: 574.2693

## Synthesis of bis(4-bromophenyl) undecanedioate (7)



Undecanedioic acid (1.40 g, 6.5 mmol), bromophenol (3.36 g, 19.4 mmol), N,N-diisopropylcarbodiimide (6.54 g, 51.8 mmol) and 4-dimethylaminopyridine (1.58 g, 12.9 mmol) were dissolved in dry tetrahydrofuran (50 mL) under inert atmosphere. The reaction was stirred at room temperature, under darkness and inert atmosphere until completion by thin layer chromatography. The solvent was removed under reduced pressure and the organics separated by silica column chromatography using dichloromethane to afford the title compound as a white solid (2.53 g, 74%).

**<sup>1</sup>H NMR:**  $\delta_{\text{H}}$  (400 MHz, CDCl<sub>3</sub>) 7.49 (4H, d, *J* 8.57), 6.97 (4H, d, *J* 8.57), 2.55 (4H, t, *J* 7.5), 1.73 (4H, q, *J* 7.14), 1.38 (10H, m).

**<sup>13</sup>C NMR:**  $\delta_{\text{C}}$  (100 MHz, CDCl<sub>3</sub>) 171.9, 149.7, 132.4, 123.4, 118.8, 34.3, 29.2, 29.1, 29.0, 24.8.

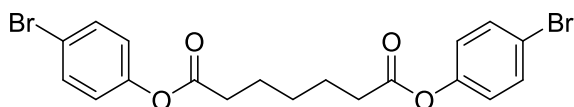
**MS: 526**

*m/z* (CI) 544 (M+NH<sub>4</sub><sup>+</sup>)

HRMS Calc: C<sub>23</sub>H<sub>26</sub>Br<sub>2</sub>O<sub>4</sub>+NH<sub>4</sub> requires = 542.0541

HRMS Found: 542.0532

## Synthesis of bis(4-bromophenyl) heptanedioate (8)



Heptanedioic acid (1.00 g, 6.2 mmol), bromophenol (3.24 g, 18.7 mmol), N,N-diisopropylcarbodiimide (6.30 g, 49.9 mmol) and 4-dimethylaminopyridine (1.58 g, 12.5 mmol) were dissolved in dry tetrahydrofuran (50 mL) under inert atmosphere. The reaction was stirred at room temperature, under darkness and inert atmosphere until completion by thin layer chromatography. The solvent was removed under reduced pressure and the organics separated by silica column chromatography using dichloromethane to afford the title compound as a white solid (2.71 g, 92%).

<sup>1</sup>H NMR:  $\delta_{\text{H}}$  (400 MHz, CDCl<sub>3</sub>) 7.48 (4H, d, *J* 8.36), 6.97 (4H, d, *J* 8.36), 2.59 (4H, t, *J* 7.55), 1.81 (4H, q, *J* 7.75), 1.53 (2H, m).

<sup>13</sup>C NMR:  $\delta_{\text{C}}$  (100 MHz, CDCl<sub>3</sub>) 171.6, 149.6, 132.4, 123.3, 118.8, 34.0, 28.4, 24.4.

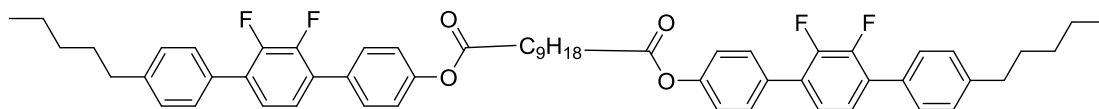
**MS: 470**

*m/z* (CI) 488 (M+NH<sub>4</sub><sup>+</sup>)

HRMS Calc: C<sub>19</sub>H<sub>18</sub>Br<sub>2</sub>O<sub>4</sub>+ NH<sub>4</sub> requires = 485.9915

HRMS Found: 485.9911

## Synthesis of bis (2',3'-difluoro-4''-pentyl-[1,1':4',1''-terphenyl]-4-yl) undecanedioate (9)



Bis(4-bromophenyl)undecanedioate (0.50 g, 1.0 mmol), 2,3-difluoro-4'-pentylbiphenyl-4-boronic acid (1.70 g, 5.6 mmol) and tetrakis(triphenylphosphine)palladium(0) (0.055 g, 47.6  $\mu\text{mol}$ ) were dissolved in tetrahydrofuran (40 mL) under inert atmosphere. The reaction was stirred at room temperature, with nitrogen being bubbled through the solvent. After an hour an aqueous solution of sodium carbonate (0.30 g, 2.8 mmol) was added drop wise and the reaction was heated under reflux overnight. The solvent was removed under reduced pressure and the organics separated by silica column chromatography using a mixture of dichloromethane and hexane 1:2 to afford the title compound as a white solid (0.62 g, 74%).

Cr – 136 - N – 222 – Iso

$^1\text{H NMR}$ :  $\delta_{\text{H}}$  (400 MHz,  $\text{CD}_2\text{Cl}_2$ ) 7.46 (8H, d,  $J$  7.96), 7.29 (8H, d,  $J$  7.96), 7.23-7.13 (4H, m), 2.66 (4H, t,  $J$  7.76), 1.66 (4H, m), 1.50-1.27 (10H, m), 0.91 (6H, t,  $J$  6.94). 60 H expected, 44 found.

$^{13}\text{C NMR}$ :  $\delta_{\text{C}}$  (100 MHz,  $\text{CDCl}_3$ ) 172.2, 150.6, 143.2, 130.0, 129.9, 128.7, 124.7, 124.6, 121.8, 35.7, 34.4, 31.5, 31.0, 29.2, 29.1, 29.0, 24.9, 22.5, 14.0.  $^{13}\text{C}$  expected 24, found 19.

$^{19}\text{F NMR}$ :  $\delta_{\text{F}}$  (376 MHz,  $\text{CDCl}_3$ ) -142.9 (2F, dd  $J$  20.81, 6.94), -143.1 (2F, dd  $J$  18.50, 6.94)

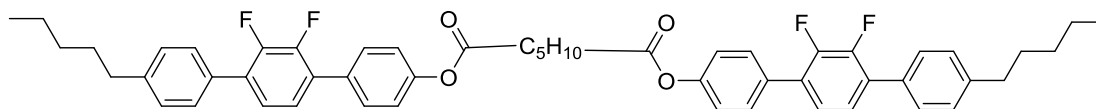
**MS: 885**

$m/z$  (CI) 902 ( $\text{M}+\text{NH}_4^+$ )

HRMS Calc:  $\text{C}_{57}\text{H}_{60}\text{F}_4\text{O}_4+\text{NH}_4$  requires = 902.4771

HRMS Found: 902.4753

## Synthesis of bis (2',3'-difluoro-4''-pentyl-[1,1':4',1''-terphenyl]-4-yl) heptanedioate (10)



Bis(4-bromophenyl) heptanedioate (0.50 g, 1.1 mmol), 2,3-difluoro-4'-pentylbiphenyl-4-boronic acid (1.30 g, 4.3 mmol) and tetrakis(triphenylphosphine)palladium(0) (0.055 g, 47.6  $\mu$ mol) were dissolved in tetrahydrofuran (40 mL) under inert atmosphere. The reaction was stirred at room temperature, with nitrogen being bubbled through the solvent. After an hour an aqueous solution of sodium carbonate (0.30 g, 2.8 mmol) was added drop wise and the reaction was heated under reflux overnight. The solvent was removed under reduced pressure and the organics separated by silica column chromatography using a mixture of dichloromethane and hexane 1:2 to afford the title compound as a white solid (0.20 g, 23%).

Cr- 147-(SmA 151) N – 239 - Iso

<sup>1</sup>H NMR:  $\delta_{\text{H}}$  (400 MHz, CDCl<sub>3</sub>) 7.51-7.48 (8H, m), 7.30 (4H, d, *J* 8.36), 7.26-7.24 (4H, m), 6.95 (4H, d, *J* 8.77), 2.66 (4H, t, *J* 7.86), 1.66 (4H, m), 1.37-1.34 (8H, m), 0.91 (6H, t, *J* 6.94). 52 H expected, 42 found.

<sup>13</sup>C NMR:  $\delta_{\text{C}}$  (100 MHz, CDCl<sub>3</sub>) 172.0, 150.6, 143.2, 129.97, 192.95, 128.7, 124.7, 124.6, 121.8, 35.7, 34.1, 31.5, 31.0, 28.5, 24.5, 22.5, 14.0. <sup>13</sup>C expected 22, found 17.

<sup>19</sup>F NMR:  $\delta_{\text{F}}$  (376 MHz, CDCl<sub>3</sub>) -142.9 (2F, dd *J* 18.50, 6.94), -143.0 (2F, dd *J* 18.50, 6.94)

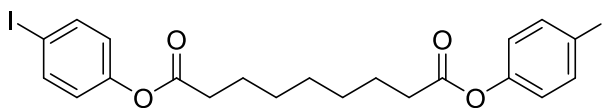
**MS: 828**

*m/z* (CI) 846 (M+NH<sub>4</sub><sup>+</sup>)

HRMS Calc: C<sub>53</sub>H<sub>52</sub>F<sub>4</sub>O<sub>4</sub>+NH<sub>4</sub> requires = 846.4145

HRMS Found: 846.4139

## Synthesis of bis(4-iodophenyl) nonanedioate (11)



Nonanedioic acid (2.00 g, 10.6 mmol), iodophenol (7.00 g, 31.8 mmol), N,N-diisopropylcarbodiimide (10.7 g, 84.8 mmol) and 4-dimethylaminopyridine (2.60 g, 21.3 mmol) were dissolved in dry tetrahydrofuran (50 mL) under inert atmosphere. The reaction was stirred at room temperature, under darkness and inert atmosphere until completion by thin layer chromatography. The solvent was removed under reduced pressure and the organics separated by silica column chromatography using a mixture of 3:1 dichloromethane and hexane to afford the title compound as a white solid (4.43 g, 70%).

$^1\text{H NMR}$ :  $\delta_{\text{H}}$  (400 MHz,  $\text{CDCl}_3$ ) 7.68 (4H, d,  $J$  8.77), 6.85 (4H, d,  $J$  8.77), 2.55 (4H, t,  $J$  7.45), 1.75 (4H, m), 1.43 (6H, m).

$^{13}\text{C NMR}$ :  $\delta_{\text{C}}$  (100 MHz,  $\text{CDCl}_3$ ) 171.8, 150.5, 138.4, 123.7, 89.7, 34.2, 28.8, 24.7, 18.0.

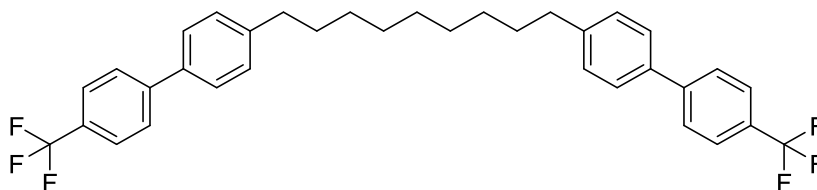
**MS: 592**

$m/z$  (CI) 610 ( $\text{M}+\text{NH}_4^+$ )

HRMS Calc:  $\text{C}_{21}\text{H}_{22}\text{I}_2\text{O}_4+\text{NH}_4$  requires = 609.9951

HRMS Found: 609.9944

## Synthesis of 1,9-bis(4'-(trifluoromethyl)-[1,1'-biphenyl]-4-yl)nonane (12)



4-Bromobenzotrifluoride (0.50 g, 2.1 mmol), (nonane-1,9-diylbis(4,1-phenylene) diboronic acid (0.20 g, 0.5 mmol) and tetrakis(triphenylphosphine)palladium(0) (0.030 g, 26.0  $\mu$ mol) were dissolved in tetrahydrofuran (40 mL) under inert atmosphere. The reaction was stirred at room temperature, with nitrogen being bubbled through the solvent. After an hour an aqueous solution of sodium carbonate (0.17 g, 1.6 mmol) was added drop wise and the reaction was heated under reflux overnight. The solvent was removed under reduced pressure and the organics separated by silica column chromatography using a mixture of dichloromethane and hexane 1:2 to afford the title compound as a white solid (0.17 g, 56%).

Cr – 106 – Iso

$^1\text{H NMR}$ :  $\delta_{\text{H}}$  (400 MHz,  $\text{CD}_2\text{Cl}_2$ ) 7.68 (8H, m), 7.53 (4H, d,  $J$  8.16), 7.29 (4H, d,  $J$  7.96), 2.67 (4H, t,  $J$  7.76), 1.66 (4H, m), 1.36 (10H, m).

$^{13}\text{C NMR}$ :  $\delta_{\text{C}}$  (100 MHz,  $\text{CDCl}_3$ ) 144.6, 143.2, 137.0, 129.0, 127.2, 127.0, 125.7, 125.6, 35.6, 31.4, 29.5, 29.3.  $^{13}\text{C}$  expected 14, found 12.

$^{19}\text{F NMR}$ :  $\delta_{\text{F}}$  (376 MHz,  $\text{CDCl}_3$ ) -62.2 (3F, s)

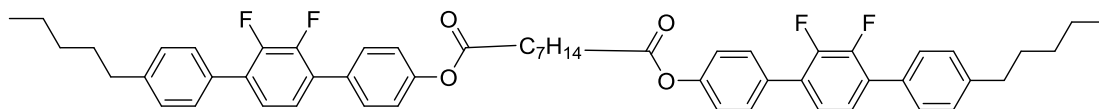
**MS: 568**

$m/z$  (CI) 586 ( $\text{M}+\text{NH}_4^+$ )

HRMS Calc:  $\text{C}_{35}\text{H}_{34}\text{F}_6+\text{NH}_4$  requires = 586.2908

HRMS Found: 586.2905

## Synthesis of bis(2',3'-difluoro-4''-pentyl-[1,1':4',1''-terphenyl]-4-yl) nonanedioate (13)



Bis(4-iodophenyl) nonanedioate (0.40 g, 0.7 mmol), 2,3-difluoro-4'-pentylbiphenyl-4-boronic acid (0.82 g, 2.7 mmol) and tetrakis(triphenylphosphine)palladium(0) (0.040 g, 37.2  $\mu$ mol) were dissolved in tetrahydrofuran (20 mL) under inert atmosphere. The reaction was stirred at room temperature, with nitrogen being bubbled through the solvent. After an hour an aqueous solution of sodium carbonate (0.43 g, 4.1 mmol) was added drop wise and the reaction was heated under reflux overnight. The solvent was removed under reduced pressure and the organics separated by silica column chromatography using a mixture of dichloromethane and hexane 2:1 to afford the title compound as a white solid (0.12 g, 21%).

Cr- 125 - Cr - 169 - Cr- 182 - Iso

$^1\text{H NMR}$ :  $\delta_{\text{H}}$  (400 MHz,  $\text{CD}_2\text{Cl}_2$ ) 7.49 (8H, m), 7.30 (4H, d,  $J$  8.36), 7.25 (4H, dt,  $J$  4.28, 0.82), 2.66 (4H, t,  $J$  8.36), 1.65 (4H, m), 1.36 (6H, m).

$^{13}\text{C NMR}$ :  $\delta_{\text{C}}$  (100 MHz,  $\text{CDCl}_3$ ) 155.6, 143.1, 130.3, 130.2, 128.7, 124.5, 124.3, 35.7, 31.5, 31.1, 22.5, 14.0.  $^{13}\text{C}$  expected 22, found 12.

$^{19}\text{F NMR}$ :  $\delta_{\text{F}}$  (376 MHz,  $\text{CDCl}_3$ ) -143.2 (2F, dd,  $J$  18.50, 6.94), -143.5 (2F, dd,  $J$  18.50, 6.94).

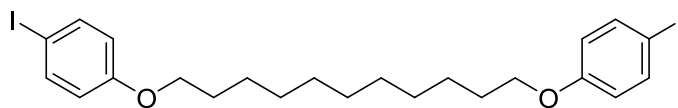
**MS: 857**

$m/z$  (CI) 875 ( $\text{M}+\text{NH}_4^+$ )

HRMS Calc:  $\text{C}_{55}\text{H}_{56}\text{F}_4\text{O}_4+\text{NH}_4$  requires = 874.4458

HRMS Found: 874.4462

## Synthesis of 1,11-bis(4-iodophenoxy)undecane (14)



Dibromoundecane (1.0 g, 3.2 mmol), iodophenol (2.80 g, 12.7 mmol) and potassium carbonate (1.36 g, 12.8 mmol) were dissolved in butanone (50 mL). The reaction was heated under reflux with stirring until completion by thin layer chromatography. The solvent was removed under reduced pressure and the organics extracted into dichloromethane. This was then washed with water twice and dried over an excess of magnesium sulphate. The organics were separated by silica column chromatography using a 1:3 mixture of dichloromethane and hexane to afford the title compound as a white solid (1.46 g, 77%).

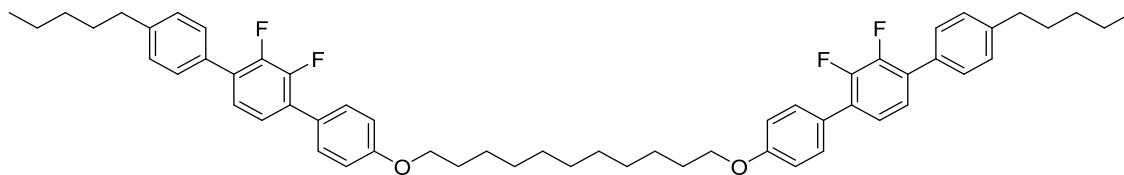
$^1\text{H NMR}$ :  $\delta_{\text{H}}$  (400 MHz,  $\text{CDCl}_3$ ) 7.54 (4H, d,  $J$  8.98), 6.67 (4H, d,  $J$  8.98), 3.91 (4H, t,  $J$  6.53), 1.76 (4H, m), 1.45-1.30 (16H, m).

$^{13}\text{C NMR}$ :  $\delta_{\text{C}}$  (100 MHz,  $\text{CDCl}_3$ ) 159.0, 138.1, 116.9, 82.4, 68.0, 29.60, 29.56, 29.4, 29.3, 25.9.

**MS: 592**

$m/z$  (CI) 593 ( $\text{M}+\text{H}^+$ ) 610 ( $\text{M}+\text{NH}_4^+$ )

## Synthesis of 1,11-bis((2',3'-difluoro-4''-pentyl-[1,1':4',1''-terphenyl]-4-yl)oxy)undecane (15)



1,11-bis(4-Bromophenoxy)undecane (0.33 g, 0.56 mmol), 2,3-difluoro-4'-pentylbiphenyl-4- boronic acid (0.68 g, 2.2 mmol) and tetrakis(triphenylphosphine) palladium(0) (0.030 g, 30.0  $\mu$ mol) were dissolved in tetrahydrofuran (20 mL) under inert atmosphere. The reaction was stirred at room temperature, with nitrogen being bubbled through the solvent. After an hour an aqueous solution of sodium carbonate (0.18 g, 1.7 mmol) was added drop wise and the reaction was heated under reflux overnight. The solvent was removed under reduced pressure and the organics separated by silica column chromatography using a mixture of dichloromethane and hexane 2:1 to afford the title compound as a white solid (0.37 g, 77%).

Cr- 105 – N – 204 – Iso

$^1\text{H NMR}$ :  $\delta_{\text{H}}$  (400 MHz,  $\text{CD}_2\text{Cl}_2$ ) 7.49 (8H, dt,  $J$  8.98, 1.43), 7.28 (4H, d,  $J$  8.36), 7.23 (4H, d,  $J$  5.51), 6.98 (4H, d,  $J$  8.77), 3.99 (4H, t,  $J$  6.63), 2.64 (4H, t,  $J$  7.76), 1.79 (4H, m), 1.63 (4H, m), 1.48-1.32 (22H, m), 0.89 (6H, t,  $J$  7.04).

$^{13}\text{C NMR}$ :  $\delta_{\text{C}}$  (100 MHz,  $\text{CDCl}_3$ ) 159.1, 143.0, 132.0, 130.0, 129.9, 128.70, 128.66, 126.8, 124.5, 124.3, 114.6, 68.1, 35.7, 31.6, 29.52, 29.50, 29.48, 29.35, 29.2, 26.0, 22.5, 14.0.  $^{13}\text{C}$  expected 23, found 22.

$^{19}\text{F NMR}$ :  $\delta_{\text{F}}$  (376 MHz,  $\text{CDCl}_3$ ) -143.2 (2F, dd,  $J$  18.50, 6.94), -143.5 (2F, dd,  $J$  18.50, 6.94).

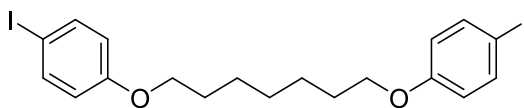
**MS: 856**

$m/z$  (CI) 857 ( $\text{M}+\text{H}^+$ ) 875 ( $\text{M}+\text{NH}_4^+$ )

HRMS Calc: -  $\text{C}_{57}\text{H}_{64}\text{F}_4\text{O}_2$  requires = 856.4842

HRMS Found: 856.4827

## Synthesis of 1,7-bis(4-bromophenoxy)heptane (16)



Dibromoheptane (0.5 g, 1.9 mmol), iodophenol (1.70 g, 7.7 mmol) and potassium carbonate (1.07 g, 7.7 mmol) were dissolved in butanone (50 mL). The reaction was heated under reflux with stirring until completion by thin layer chromatography. The solvent was removed under reduced pressure and the organics extracted into dichloromethane. This was then washed with water twice and dried over an excess of magnesium sulphate. The organics were separated by silica column chromatography using a 1:3 mixture of dichloromethane and hexane to afford the title compound as a white solid (0.99 g, 95%).

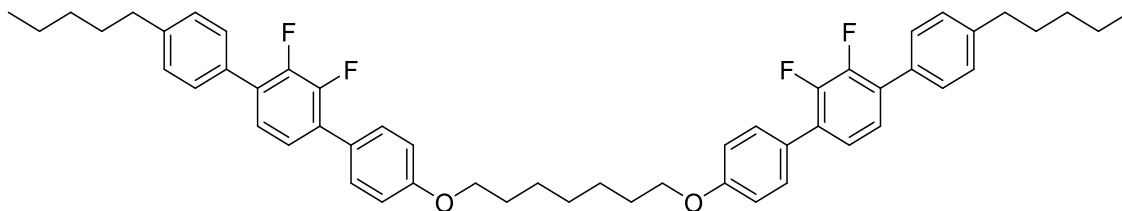
$^1\text{H NMR}$ :  $\delta_{\text{H}}$  (400 MHz,  $\text{CDCl}_3$ ) 7.54 (4H, d,  $J$  8.98), 6.67 (4H, d,  $J$  8.98), 3.91 (4H, t,  $J$  6.53), 1.78 (4H, m), 1.45 (6H, m).

$^{13}\text{C NMR}$ :  $\delta_{\text{C}}$  (100 MHz,  $\text{CDCl}_3$ ) 159.0, 138.1, 116.9, 82.4, 67.9, 29.0, 25.9.  $^{13}\text{C}$  expected 8, found 7.

**MS: 536**

$m/z$  (CI) 536 ( $\text{M}+\text{H}^+$ ) 554 ( $\text{M}+\text{NH}_4^+$ )

## Synthesis of 1,7-bis((2',3'-difluoro-4''-pentyl-[1,1':4',1''-terphenyl]-4-yl)oxy)heptane (17)



1,7-Bis(4-bromophenoxy)heptane (0.40 g, 0.7 mmol), 2,3-difluoro-4'-pentylbiphenyl-4-boronic acid (0.90 g, 2.9 mmol) and tetrakis(triphenylphosphine)palladium(0) (0.043 g, 37.2  $\mu\text{mol}$ ) were dissolved in tetrahydrofuran (20 mL) under inert atmosphere. The reaction was stirred at room temperature, with nitrogen being bubbled through the solvent. After an hour an aqueous solution of sodium carbonate (0.23 g, 2.2 mmol) was added drop wise and the reaction was heated under reflux overnight. The solvent was removed under reduced pressure and the organics separated by silica column chromatography using a mixture of dichloromethane and hexane 2:1 to afford the title compound as a white solid (0.40 g, 68%).

Cr- 108 – N – 213 – Iso

$^1\text{H NMR}$ :  $\delta_{\text{H}}$  (400 MHz,  $\text{CD}_2\text{Cl}_2$ ) 7.49 (8H, dt,  $J$  8.98, 1.63), 7.28 (4H, d,  $J$  8.16), 7.23 (4H, d,  $J$  5.31), 6.98 (4H, d,  $J$  8.77), 4.01 (4H, t,  $J$  6.63), 2.64 (4H, t,  $J$  7.75), 1.81 (4H, m), 1.64 (4H, m), 1.48-1.32 (14H, m), 0.89 (6H, t,  $J$  6.94).

$^{13}\text{C NMR}$ :  $\delta_{\text{C}}$  (100 MHz,  $\text{CDCl}_3$ ) 159.1, 143.0, 132.0, 130.0, 129.9, 128.69, 129.65, 126.9, 124.5, 124.3, 114.6, 68.0, 35.7, 31.6, 31.1, 29.15, 29.07, 26.0, 22.5, 14.0.  $^{13}\text{C}$  expected 23, found 20.

$^{19}\text{F NMR}$ :  $\delta_{\text{F}}$  (376 MHz,  $\text{CDCl}_3$ ) -143.3 (1F, dd,  $J$  20.81, 6.94), -143.5 (1F, dd,  $J$  20.81, 6.94)

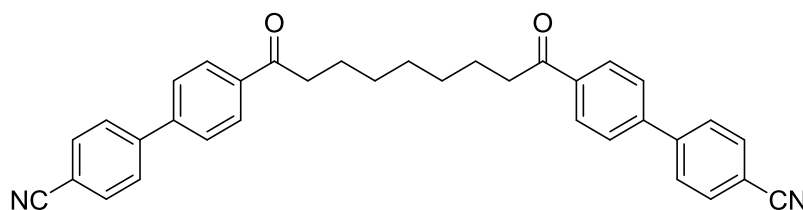
**MS: 800**

$m/z$  (CI) 818 ( $\text{M}+\text{NH}_4^+$ )

HRMS Calc: -  $\text{C}_{53}\text{H}_{56}\text{F}_4\text{O}_2 + \text{NH}_4$  requires = 818.4560

HRMS Found: 818.4562

## Synthesis of 4',4''-nonanedioylbis([1,1'-biphenyl]-4-carbonitrile) (18)



1,9-bis(4-Bromophenyl)nonane-1,9-dione (0.14 g, 0.3 mmol), (4-cyanophenyl)boronic acid (0.18 g, 1.2 mmol) and tetrakis(triphenylphosphine)palladium(0) (0.017 g, 14.7  $\mu\text{mol}$ ) were dissolved in tetrahydrofuran (20 mL) under inert atmosphere. The reaction was stirred at room temperature, with nitrogen being bubbled through the solvent. After 1 hour an aqueous solution of sodium carbonate (0.095 g, 0.9 mmol) was added drop wise and the reaction was heated under reflux overnight. The solvent was removed under reduced pressure and the organics separated by silica column chromatography using dichloromethane to afford the title compound as a white solid (0.087 g, 57%).

Cr – 167 – N – 186 – Iso

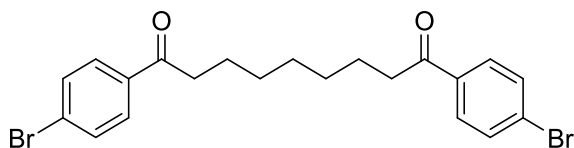
$^1\text{H NMR}$ :  $\delta_{\text{H}}$  (400 MHz,  $\text{CD}_2\text{Cl}_2$ ) 8.07 (4H, d,  $J$  8.36), 7.75 (8H, q,  $J$  8.57), 7.67 (4H, d,  $J$  8.36), 3.01 (4H, t,  $J$  7.34), 1.78 (4H, m), 1.43 (6H, m).

$^{13}\text{C NMR}$ :  $\delta_{\text{C}}$  (100 MHz,  $\text{CDCl}_3$ ) 199.8, 144.3, 143.3, 136.8, 132.7, 128.9, 127.9, 127.5, 118.6, 111.9, 38.7, 29.3, 29.2, 24.2.

**MS: 510**

$m/z$  (CI) 511 ( $\text{M}+\text{H}^+$ ), 528 ( $\text{M}+\text{NH}_4^+$ )

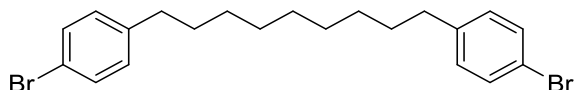
## Synthesis of 1,9-bis(4-bromophenyl)nonane-1,9-dione **(19)** <sup>98</sup>



Nonanedioic acid (20.0 g, 0.10 mol) was dissolved in dry dichloromethane under nitrogen. Oxalyl chloride (27.0 g, 0.21 mol) was added drop wise. The reaction was then cooled to 0 °C and a drop of N,N-dimethylformamide was added to initiate the reaction. The reaction was stirred overnight at 45 °C. The solvent was removed under reduced pressure and the acid chloride was used immediately without any purification. Bromobenzene (13.0 g, 95 mmol) and aluminium chloride (12.8 g, 95 mmol) are stirred under nitrogen for 1 hour. A solution of the acid chloride in an excess of bromobenzene was added drop wise with rapid stirring over 2 hours. The reaction was stirred at room temperature under nitrogen overnight. Upon completion the reaction was poured onto a mixture of hydrochloric acid and ice (1:1) and was extracted into dichloromethane and washed with water multiple times. The organic layer was dried over magnesium sulphate and the solvent was removed under reduced pressure. The organics are purified by column chromatography using a mixture of dichloromethane and hexane 1:2. Further purified by recrystallizing from ethanol afforded the title compound as a white solid (21.4 g, 43%).

<sup>1</sup>H NMR:  $\delta_{\text{H}}$  (400 MHz, CD<sub>2</sub>Cl<sub>2</sub>) 7.82 (4H, d, *J* 8.57), 7.60 (4H, *J* 8.57), 2.92 (4H, t, *J* 7.34), 1.73 (4H, m), 1.39 (6H, m).

## Synthesis of 1,9-bis(4-bromophenyl)nonane (20) <sup>98</sup>



1,9-Bis(4-bromophenyl)nonane-1,9-dione (21.4 g, 45.9 mmol) and hydrazine hydrate (5.51 g, 0.11 mol) were dissolved in diethylene glycol by stirring at 130 °C for 1 hour. Potassium hydroxide (15.4 g, 0.27 mol) was added carefully and stirred at 130 °C for 4 hours. The condenser was removed and the reaction was stirred at 200 °C to remove the excess hydrazine overnight. Upon completion the reaction was cooled and diluted with water and poured onto a mixture of concentrated hydrochloric acid and ice. The organics were extracted into dichloromethane and washed with water and brine. After drying over magnesium sulphate the solvent was removed under reduced pressure. The organics separated by silica column chromatography using hexane afford the title compound as a white solid (18.2 g, 91%).

<sup>1</sup>H NMR:  $\delta_{\text{H}}$  (400 MHz, CD<sub>2</sub>Cl<sub>2</sub>) 7.38 (4H, d, *J* 8.36), 7.04 (4H, d, *J* 8.36), 2.54 (4H, t, *J* 7.76), 1.54 (4H, m), 1.27 (10H, m).

<sup>13</sup>C NMR:  $\delta_{\text{C}}$  (100 MHz, CDCl<sub>3</sub>) 141.8, 131.2, 130.2, 119.2, 35.3, 31.3, 29.41, 29.39, 29.1.

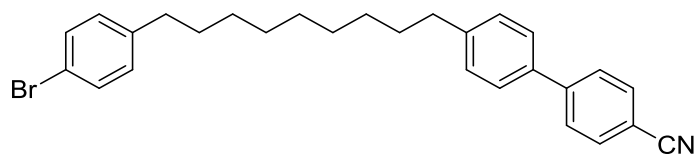
**MS: 438**

*m/z* (CI) 439 (M+H<sup>+</sup>)

HRMS Calc: C<sub>21</sub>H<sub>26</sub>Br<sub>2</sub>+<sub>4</sub> requires = 437.0479

HRMS Found: 437.0477

## Synthesis of 4'-(9-(4-bromophenyl)nonyl)-[1,1'-biphenyl]-4-carbonitrile (21)



1,9-Bis(4-Bromophenyl)nonane (1.80 g, 4.1 mmol), (4-cyanophenyl)boronic acid (0.20 g, 1.4 mmol) and tetrakis(triphenylphosphine)palladium(0) (0.030 g, 26.0  $\mu\text{mol}$ ) were dissolved in tetrahydrofuran (40 mL) under inert atmosphere. The reaction was stirred at room temperature, with nitrogen being bubbled through the solvent. After 1 hour an aqueous solution of sodium carbonate (0.21 g, 2.0 mmol) was added drop wise and the reaction was heated under reflux overnight. The solvent was removed under reduced pressure and the organics separated by silica column chromatography using a mixture of dichloromethane and hexane 1:3 to afford the title compound as a white solid (0.41 g, 65%).

**$^1\text{H NMR}$ :**  $\delta_{\text{H}}$  (400 MHz,  $\text{CD}_2\text{Cl}_2$ ) 7.69 (4H, q,  $J$  8.56), 7.51 (2H, d,  $J$  8.16), 7.38 (2H, d,  $J$  8.36), 7.29 (2H, d,  $J$  8.16), 7.04 (2H, d,  $J$  8.36), 2.65 (2H, t,  $J$  7.75), 2.54 (2H, t,  $J$  7.65), 1.65-1.55 (4H, m), 1.40-1.20 (10H, m).

**$^{13}\text{C NMR}$ :**  $\delta_{\text{C}}$  (100 MHz,  $\text{CDCl}_3$ ) 145.6, 143.8, 141.8, 136.4, 132.6, 131.2, 130.1, 129.2, 127.5, 127.1, 119.2, 119.0, 110.5, 35.6, 35.3, 31.4, 31.3, 29.43, 29.39, 29.3, 29.1.  $^{13}\text{C}$  expected 22, found 21.

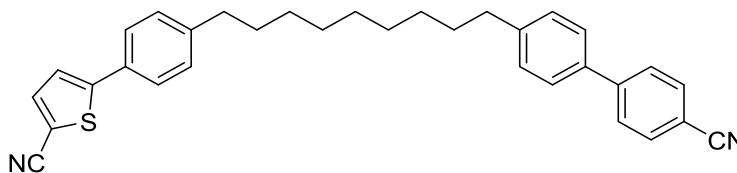
**MS: 460**

$m/z$  (CI) 461 ( $\text{M}+\text{H}^+$ )

HRMS Calc:  $\text{C}_{28}\text{H}_{30}\text{BrN}+\text{H}$  requires = 460.1634

HRMS Found: 460.1625

## Synthesis of 5-(4-(9-(4'-cyano-[1,1'-biphenyl]-4-yl)nonyl)phenyl)thiophene-2-carbonitrile (22)



4'-(9-(4-Bromophenyl)nonyl)-[1,1'-biphenyl]-4-carbonitrile (0.20 g, 0.43 mmol), (5-cyanothiophen-2-yl)boronic acid (0.20 g, 1.3 mmol) and tetrakis(triphenylphosphine)palladium(0) (0.025 g, 21.6  $\mu$ mol) were dissolved in tetrahydrofuran (20 mL) under inert atmosphere. The reaction was stirred at room temperature, with nitrogen being bubbled through the solvent. After 1 hour an aqueous solution of sodium carbonate (0.070 g, 0.66 mmol) was added drop wise and the reaction was heated under reflux overnight. The solvent was removed under reduced pressure and the organics separated by silica column chromatography using a mixture of dichloromethane and hexane 1:1 to afford the title compound as a white solid (0.09 g, 42%).

Cr – (N<sub>x</sub> 89) 90 – N – 101 - Iso

<sup>1</sup>H NMR:  $\delta_{\text{H}}$  (400 MHz, CD<sub>2</sub>Cl<sub>2</sub>) 7.62 (4H, m), 7.52 (1H, m), 7.44 (4H, dd, *J* 6.32, 1.94), 7.18 (5H, m), 2.55 (4H, m), 1.54 (4H, m), 1.33-1.12 (10H, m).

**MS: 488**

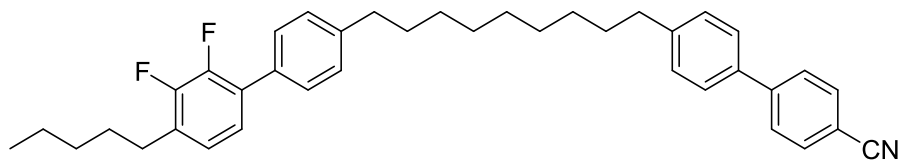
*m/z* (CI) 489 (M+H<sup>+</sup>)

HRMS Calc: C<sub>33</sub>H<sub>32</sub>N<sub>2</sub>S+H requires = 489.2364

HRMS Found: 489.2349

**HPLC trace = 98.3 %**

## Synthesis of 4'-(9-(2',3'-difluoro-4'-pentyl-[1,1'-biphenyl]-4-yl)nonyl)-[1,1'-biphenyl]-4-carbonitrile (23)



4'-(9-(4-Bromophenyl)nonyl)-[1,1'-biphenyl]-4-carbonitrile (0.23 g, 0.50 mmol), (2,3-difluoro-4-pentylphenyl) boronic acid (0.34 g, 1.5 mmol) and tetrakis(triphenylphosphine) palladium(0) (0.028 g, 24.2  $\mu$ mol) were dissolved in tetrahydrofuran (20 mL) under inert atmosphere. The reaction was stirred at room temperature, with nitrogen being bubbled through the solvent. After 1 hour an aqueous solution of sodium carbonate (0.080 g, 0.7 mmol) was added and the reaction was heated under reflux overnight. The solvent was removed under reduced pressure and the organics separated by silica column chromatography using a mixture of dichloromethane and hexane 1:2 to afford the title compound as a white solid (0.2 g, 71%).

Cr – (N<sub>x</sub> 38) 40 – N – 44 – Iso

<sup>1</sup>H NMR:  $\delta_{\text{H}}$  (400 MHz, CD<sub>2</sub>Cl<sub>2</sub>) 7.68 (4H, m), 7.50 (2H, d, *J* 8.16), 7.44 (2H, dd, *J* 6.53, 1.53), 7.26 (4H, m), 7.08 (1H, dt, *J* 7.50, 1.63), 6.96 (1H, dt, *J* 7.50, 1.63), 2.65 (6H, m), 1.63 (6H, m), 1.42-1.26 (14H, m), 0.88 (3H, t, *J* 6.84).

<sup>13</sup>C NMR:  $\delta_{\text{C}}$  (100 MHz, CDCl<sub>3</sub>) 145.6, 143.8, 142.7, 136.5, 132.6, 129.2, 128.70, 128.68, 128.6, 127.5, 127.0, 124.6, 124.1, 119.1, 110.5, 35.7, 35.6, 31.46, 31.38, 29.7, 29.5, 29.32, 29.28, 28.7, 22.5, 14.0.

<sup>19</sup>F NMR:  $\delta_{\text{F}}$  (376 MHz, CDCl<sub>3</sub>) -143.7 (1F, dd, *J* 20.81, 6.94), -144.3 (1F, dd, *J* 20.81, 6.94).

**MS: 563**

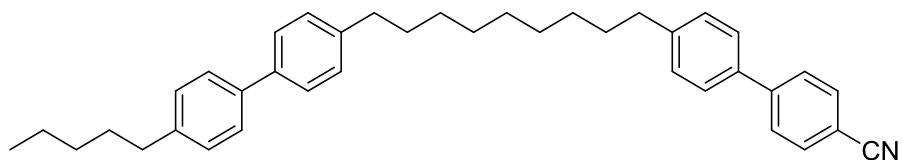
*m/z* (CI) 564 (M+H<sup>+</sup>)

HRMS Calc: C<sub>39</sub>H<sub>43</sub>F<sub>2</sub>N+H requires = 564.3441

HRMS Found: 564.3425

**HPLC trace = 97.8 %**

## Synthesis of 4'-(4'-pentyl-[1,1'-biphenyl]-4-ylnonyl)-[1,1'-biphenyl]-4-carbonitrile (24)



4'-(9-(4-Bromophenyl)nonyl)-[1,1'-biphenyl]-4-carbonitrile (0.23 g, 0.50 mmol), (4-pentylphenyl)boronic acid (0.28 g, 1.5 mmol) and tetrakis(triphenylphosphine)palladium(0) (0.028 g, 24.2  $\mu$ mol) were dissolved in tetrahydrofuran (20 mL) under inert atmosphere. The reaction was stirred at room temperature, with nitrogen being bubbled through the solvent. After 1 hour an aqueous solution of sodium carbonate (0.080 g, 0.7 mmol) was added drop wise and the reaction was heated under reflux overnight. The solvent was removed under reduced pressure and the organics separated by silica column chromatography using a mixture of dichloromethane and hexane 1:2 to afford the title compound as a white solid (0.15 g, 61%).

Cr – 81 – N – 86 – Iso

$^1\text{H NMR}$ :  $\delta_{\text{H}}$  (400 MHz,  $\text{CD}_2\text{Cl}_2$ ) 7.66 (4H, m), 7.49 (6H, d,  $J$  7.96), 7.27(2H, d,  $J$  8.16), 7.22 (4H, dd,  $J$  8.06, 2.34), 2.63 (6H, m), 1.64 (6H, m), 1.39-1.23 (16H, m), 0.91 (3H, t,  $J$  6.94).

$^{13}\text{C NMR}$ :  $\delta_{\text{C}}$  (100 MHz,  $\text{CDCl}_3$ ) 145.6, 143.8, 141.8, 141.7, 138.5, 138.4, 136.4, 132.5, 129.2, 128.75, 128.73, 127.5, 127.0, 126.79, 126.77, 119.0, 110.5, 35.61, 35.57, 31.56, 31.46, 31.4, 31.2, 29.5, 29.32, 29.26, 22.6, 14.0.  $^{13}\text{C}$  expected 30, found 28.

**MS: 527**

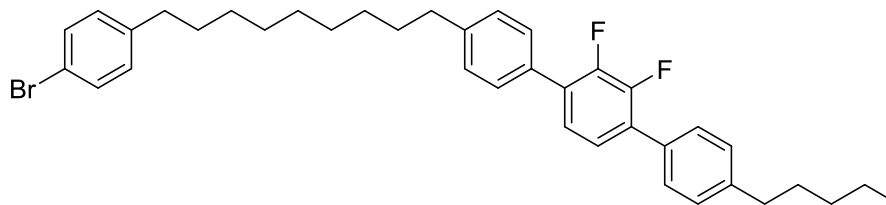
$m/z$  (CI) 528 ( $\text{M}+\text{H}^+$ ) 545 ( $\text{M}+\text{NH}_4^+$ )

HRMS Calc:  $\text{C}_{39}\text{H}_{45}\text{N}+\text{H}$  requires = 528.3630

HRMS Found: 528.3620

**HPLC trace = 99.0 %**

## Synthesis of 4-(9-(4-bromophenyl)nonyl)-2',3'-difluoro-4''-pentyl-1,1':4',1''-terphenyl (25)



1,9-bis(4-Bromophenyl)nonane (4.3 g, 9.8 mmol), (2,3-difluoro-4'-pentyl-[1,1'-biphenyl]-4-yl)boronic acid (1.0 g, 3.3 mmol) and tetrakis(triphenylphosphine)palladium(0) (0.076 g, 65.7  $\mu$ mol) were dissolved in tetrahydrofuran (100 mL) under inert atmosphere. The reaction was stirred at room temperature, with nitrogen being bubbled through the solvent. After 1 hour an aqueous solution of sodium carbonate (0.52 g, 4.9 mmol) was added drop wise and the reaction was heated under reflux overnight. The solvent was removed under reduced pressure and the organics separated by silica column chromatography using a mixture of dichloromethane and hexane 1:5 to afford the title compound as a white solid (2.03 g, 65%).

Cr – 42 – N<sub>x</sub> – 61 – N – 85 – Iso

<sup>1</sup>H NMR:  $\delta_{\text{H}}$  (400 MHz, CD<sub>2</sub>Cl<sub>2</sub>) 7.51 (4H, d, *J* 7.75), 7.38 (2H, d, *J* 8.36), 7.31 (2H, d, *J* 2.45), 7.29 (2H, d, *J* 2.45), 7.27 (2H, dd, *J* 1.74, 3.37), 7.07 (2H, d, *J* 8.57), 2.66 (4H, dt, *J* 2.04, 7.14), 2.56 (2H, t, *J* 7.75), 1.70-1.50 (4H, m), 1.38-1.31 (16H, m), 0.91 (3H, t, *J* 6.94).

<sup>13</sup>C NMR:  $\delta_{\text{C}}$  (100 MHz, CDCl<sub>3</sub>) 149.8, 149.6, 147.3, 147.2, 143.4, 143.1, 143.0, 141.8, 132.0, 131.2, 130.2, 129.5, 129.4, 128.69, 128.66, 124.5, 119.2, 35.7, 35.3, 31.5, 31.36, 31.29, 31.1, 29.5, 29.4, 29.3, 29.1, 22.5, 14.0. <sup>13</sup>C expected 32, found 29.

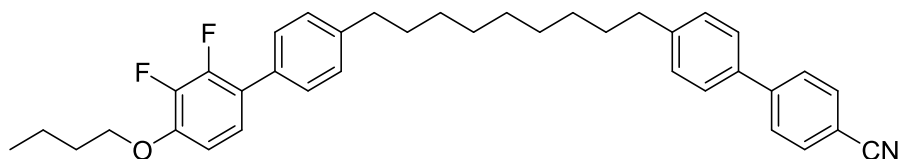
**MS: 617**

*m/z* (Cl) 618 (M+H<sup>+</sup>)

HRMS Calc: C<sub>38</sub>H<sub>43</sub>BrF<sub>2</sub> +H requires = 617.2594

HRMS Found: 617.2591

## Synthesis of 4'-(9-(4'-butoxy-2',3'-difluoro-[1,1'-biphenyl]-4-yl)nonyl)-[1,1'-biphenyl]-4-carbonitrile (26)



4'-(9-(4-Bromophenyl)nonyl)-[1,1'-biphenyl]-4-carbonitrile (0.23 g, 0.50 mmol), (4-butoxy-2,3-difluorophenyl)boronic acid (0.34 g, 1.5 mmol) and tetrakis(triphenylphosphine) palladium(0) (0.028 g, 24.2  $\mu$ mol) were dissolved in tetrahydrofuran (20 mL) under inert atmosphere. The reaction was stirred at room temperature, with nitrogen being bubbled through the solvent. After 1 hour an aqueous solution of sodium carbonate (0.080 g, 0.7 mmol) was added drop wise and the reaction was heated under reflux overnight. The solvent was removed under reduced pressure and the organics separated by silica column chromatography using a mixture of dichloromethane and hexane 1:2 to afford the title compound as a white solid (0.16 g, 68%).

Cr – (N<sub>x</sub> 55) 56 – N – 64 – Iso

<sup>1</sup>H NMR:  $\delta_{\text{H}}$  (400 MHz, CDCl<sub>3</sub>) 7.69 (4H, m), 7.50 (2H, d, *J* 8.16), 7.41 (2H, dd, *J* 8.16, 1.43), 7.29 (2H, d, *J* 8.16), 7.24 (2H, d, *J* 8.16), 7.07 (1H, dt, *J* 8.47, 1.31), 6.78 (1H, dt, *J* 8.16, 1.84), 4.08 (2H, t, *J* 6.53), 2.64 (4H, m), 1.81 (2H, m), 1.63 (4H, m), 1.55 1.40-1.26 (10H, m), 0.88 (3H, t, *J* 7.34).

<sup>13</sup>C NMR:  $\delta_{\text{C}}$  (100 MHz, CDCl<sub>3</sub>) 148.9, 145.6, 143.8, 142.4, 141.9, 136.4, 132.5, 132.2, 129.2, 128.6, 128.5, 127.4, 127.0, 123.5, 123.42, 123.39, 123.0, 122.9, 119.0, 110.5, 109.50, 109.48, 69.5, 35.62, 35.60, 31.37, 31.35, 31.2, 29.4, 29.28, 29.25, 19.1, 13.8.

<sup>19</sup>F NMR:  $\delta_{\text{F}}$  (376 MHz, CDCl<sub>3</sub>) -141.8 (1F, dd, *J* 18.50, 6.94), -158.8 (1F, dd, *J* 20.81, 6.94).

**MS: 565**

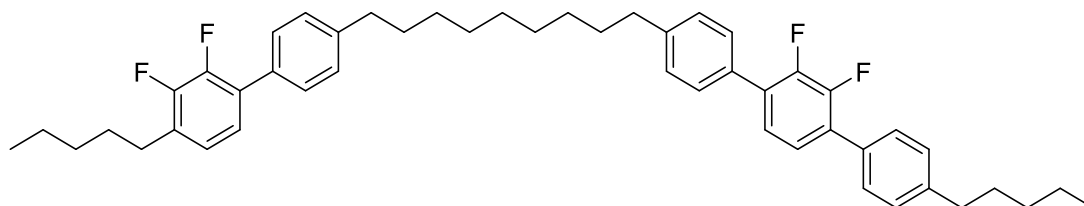
*m/z* (CI) 566 (M+H<sup>+</sup>) 583 (M+NH<sub>4</sub><sup>+</sup>)

HRMS Calc: C<sub>38</sub>H<sub>41</sub>F<sub>2</sub>NO+H requires = 566.3234

HRMS Found: 566.3226

**HPLC trace = 99.5 %**

**Synthesis of 4-(9-(2',3'-difluoro-4'-pentyl-[1,1'-biphenyl]-4-yl)nonyl)-2',3'-difluoro-4''-pentyl-1,1':4',1''-terphenyl (27)**



4-(9-(4-Bromophenyl)nonyl)-2',3'-difluoro-4''-pentyl-1,1':4',1''-terphenyl (0.22 g, 0.35 mmol), (2,3-difluoro-4-pentylphenyl)boronic acid (0.24 g, 1.05 mmol) and tetrakis(triphenylphosphine) palladium(0) (0.020 g, 17.3  $\mu$ mol) were dissolved in tetrahydrofuran (20 mL) under inert atmosphere. The reaction was stirred at room temperature, with nitrogen being bubbled through the solvent. After 1 hour an aqueous solution of sodium carbonate (0.052 g, 0.49 mmol) was added drop wise and the reaction was heated under reflux overnight. The solvent was removed under reduced pressure and the organics separated by silica column chromatography using a mixture of dichloromethane and hexane 1:5 to afford the title compound as a white solid (0.13 g, 52%).

Cr – 37 – N – 53 – Iso

**$^1\text{H NMR}$ :**

$\delta_{\text{H}}$  (400 MHz,  $\text{CD}_2\text{Cl}_2$ ) 7.50 (4H, d,  $J$  7.96), 7.343(2H, dd,  $J$  8.26, 1.73), 7.30 (4H, d,  $J$  8.16), 7.27 (4H, m), 7.11 (1H, dt,  $J$  8.16, 1.70), 7.00 (1H, dt,  $J$  7.45, 1.63), 2.66 (8H, m), 1.64 (8H, m), 1.38-1.31 (18H, m), 0.91 (6H, m).

**$^{13}\text{C NMR}$ :**

$\delta_{\text{C}}$  (100 MHz,  $\text{CDCl}_3$ ) 149.5, 148.5, 148.00, 143.4, 143.06, 142.7.0, 132.3, 132.0, 130.6, 130.5, 129.5, 128.70, 128.68, 128.4, 128.3, 124.7, 124.6, 124.2, 35.7, 31.6, 31.5, 31.4, 31.1, 29.7, 29.5, 29.3, 28.7, 22.6, 22.5, 14.04, 14.00.

**$^{19}\text{F NMR}$ :**  $\delta_{\text{F}}$  (376 MHz,  $\text{CDCl}_3$ ) -143.2 (2F, s), -143.8 (1F, dd,  $J$  20.81, 6.94), -144.2 (1F, dd,  $J$  20.81, 6.94).

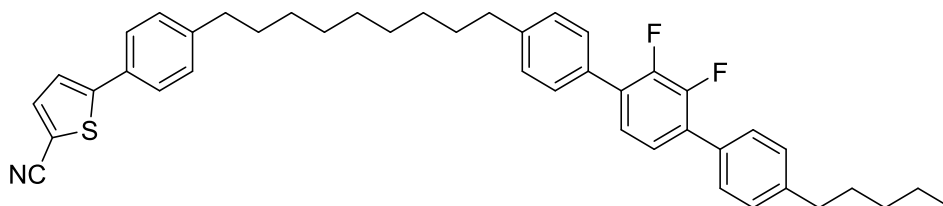
**MS: 720**  $m/z$  (Cl) 721 ( $\text{M}+\text{H}^+$ )

HRMS Calc:  $\text{C}_{49}\text{H}_{56}\text{F}_4 + \text{H}$  requires = 721.4396

HRMS Found: 721.4385

**HPLC trace** = 98.6 %

**Synthesis of 5-(4-(9-(2',3'-difluoro-4''-pentyl-[1,1':4',1''-terphenyl]-4-yl)nonyl)phenyl)thiophene-2-carbonitrile (28)**



4-(9-(4-Bromophenyl)nonyl)-2',3'-difluoro-4''-pentyl-1,1':4',1''-terphenyl (0.20 g, 0.32 mmol), (5-cyanothiophen-2-yl)boronic acid (0.15 g, 0.98 mmol) and tetrakis(triphenylphosphine)palladium(0) (0.020 g, 17.3  $\mu$ mol) were dissolved in tetrahydrofuran (20) mL under inert atmosphere. The reaction was stirred at room temperature, with nitrogen being bubbled through the solvent. After 1 hour an aqueous solution of sodium carbonate (0.052 g, 0.49 mmol) was added drop wise and the reaction was heated under reflux overnight. The solvent was removed under reduced pressure and the organics separated by silica column chromatography using a mixture of dichloromethane and hexane 1:5 to afford the title compound as a white solid (0.09 g, 44%).

Cr – (N<sub>x</sub> 84) 89 – N – Iso

<sup>1</sup>H NMR:  $\delta_{\text{H}}$  (400 MHz, CD<sub>2</sub>Cl<sub>2</sub>) 7.50 (1H, d, *J* 3.88), 7.46-7.40 (6H, m), 7.21 (4H, dd, *J* 8.16, 2.96), 7.18-7.15 (5H, m), 2.60-2.53 (6H, m), 1.55 (6H, m), 1.34-1.18 (14H, m), 0.83 (3H, t, *J* 6.94).

<sup>13</sup>C NMR:  $\delta_{\text{C}}$  (100 MHz, CDCl<sub>3</sub>) 149.0, 144.8, 143.1, 143.0, 138.4, 132.0, 129.7, 129.3, 128.69, 128.68, 126.3, 124.6, 122.7, 114.5, 35.7, 31.6, 31.4, 31.3, 31.1, 29.4, 29.3, 29.2, 22.6, 14.0.

<sup>19</sup>F NMR:  $\delta_{\text{F}}$  (376 MHz, CDCl<sub>3</sub>) -143.2 (2F, s).

**MS: 645**

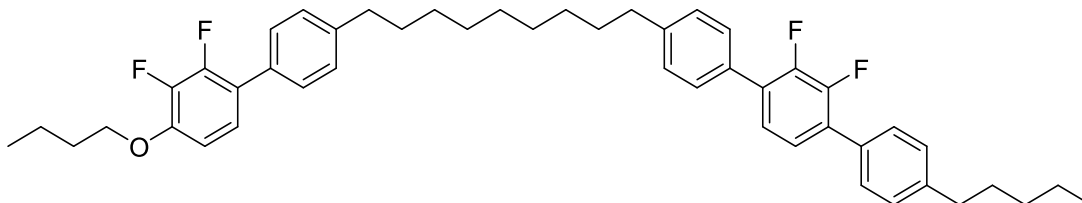
*m/z* (CI) 646 (M+H<sup>+</sup>)

HRMS Calc: C<sub>43</sub>H<sub>45</sub>F<sub>2</sub>NS +H requires = 646.3319

HRMS Found: 646.3305

**HPLC trace = 98.6 %**

## Synthesis of 4-(9-(2',3'-difluoro-4'-butyloxy-[1,1'-biphenyl]-4-yl)nonyl)-2',3'-difluoro-4''-pentylterphenyl (29)



4-(9-(4-bromophenyl)nonyl)-2',3'-difluoro-4''-pentyl-1,1':4',1''-terphenyl (0.16 g, 0.26 mmol), (2,3-difluoro-4butyloxyphenyl)boronic acid ( 0.18 g, 0.78 mmol) and tetrakis(triphenylphosphine)palladium(0) ( 0.020 g, 17.3  $\mu$ mol) were dissolved in tetrahydrofuran (20 mL) under inert atmosphere. The reaction was stirred at room temperature, with nitrogen being bubbled through the solvent. After an hour an aqueous solution of sodium carbonate (0.052 g, 0.49 mmol) was added drop wise and the reaction was heated under reflux overnight. The solvent was removed under reduced pressure and the organics separated by silica column chromatography using a mixture of dichloromethane and hexane 1:5 to afford the title compound as a white solid (0.11 g, 57%).

Cr – (SmX 62) 69 – N<sub>x</sub> – 83 – N – 104 – Iso

<sup>1</sup>H NMR:  $\delta_{\text{H}}$  (400 MHz, CD<sub>2</sub>Cl<sub>2</sub>) 7.50 (4H, d, *J* 7.96), 7.40 (2H, dd, *J* 8.16, 1.43), 7.27 (4H, d, *J* 7.14), 7.23 (4H, d, *J* 8.36), 7.06 (1H, dt, *J* 8.46, 2.24), 6.76 (1H, dt, *J* 8.16, 1.63), 4.05 (2H, t, *J* 6.53), 2.64 (6H, m), 1.82 (2H, m), 1.65 (6H, m), 1.51 (2H, m), 1.38-1.31 (14H, m), 0.98 (3H, t, *J* 7.45), 0.91 (3H, t, *J* 6.94).

<sup>13</sup>C NMR:  $\delta_{\text{C}}$  (100 MHz, CDCl<sub>3</sub>) 148.8, 148.4, 143.1, 143.0, 142.4, 132.2, 132.0, 129.5, 128.69, 128.66, 128.6, 128.5, 124.5, 123.4, 123.0, 122.9, 109.51, 109.49, 69.6, 35.69, 35.68, 35.6, 31.5, 31.39, 31.37, 31.2, 31.1, 29.5, 29.3, 22.5, 19.1, 14.0, 13.8. <sup>13</sup>C expected 42, found 34.

<sup>19</sup>F NMR:  $\delta_{\text{F}}$  (376 MHz, CDCl<sub>3</sub>) -141.8 (1F, dd, *J* 20.81, 6.94), -143.2 (2F, s), -158.8 (1F, dd, *J* 20.81, 6.94).

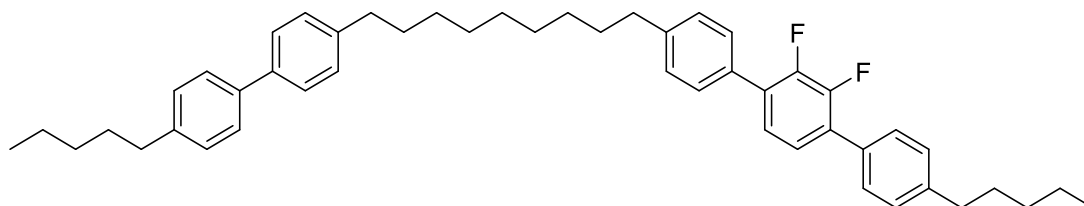
**MS: 722**  $m/z$  (CI) 723 (M+H<sup>+</sup>) 740 (M+NH<sub>4</sub><sup>+</sup>)

HRMS Calc: C<sub>48</sub>H<sub>54</sub>F<sub>4</sub>O+H requires = 723.4189

HRMS Found: 723.4178

HPLC trace = 99.0 %

**Synthesis of 2',3'-difluoro-4-pentyl-4''-(9-(4'-pentyl-[1,1'-biphenyl]-4-yl)nonyl)-1,1':4',1''-terphenyl (30)**



4-(9-(4-Bromophenyl)nonyl)-2',3'-difluoro-4''-pentyl-1,1':4',1''-terphenyl (0.16 g, 0.26 mmol), (pentylphenyl)boronic acid (0.15 g, 0.78 mmol) and tetrakis(triphenylphosphine)palladium(0) (0.020 g, 17.3  $\mu$ mol) were dissolved in tetrahydrofuran (20 mL) under inert atmosphere. The reaction was stirred at room temperature, with nitrogen being bubbled through the solvent. After 1 hour an aqueous solution of sodium carbonate (0.052 g, 0.49 mmol) was added drop wise and the reaction was heated under reflux overnight. The solvent was removed under reduced pressure and the organics separated by silica column chromatography using a mixture of dichloromethane and hexane 1:4 to afford the title compound as a white solid (0.14 g, 77%).

Cr- 78- N<sub>x</sub> – 87 – N – 106 – Iso

<sup>1</sup>H NMR:  $\delta_{\text{H}}$  (400 MHz, CDCl<sub>3</sub>) 7.50 (8H, m), 7.28 (4H, dd, *J* 8.25, 1.94), 7.23, (6H, m), 2.65 (8H, m), 1.66 (8H, m), 1.35 (18H, m), 0.91 (6H, m).

<sup>13</sup>C NMR:  $\delta_{\text{C}}$  (100 MHz, CDCl<sub>3</sub>) 148.5, 143.09, 143.08, 141.8, 141.7, 138.50, 138.48, 132.0, 129.5, 128.75, 128.72, 128.68, 128.4, 128.2, 126.8, 125.5, 124.6, 35.72, 35.71, 35.60, 35.58, 31.6, 31.5, 31.4, 31.2, 31.1, 29.5, 29.4, 22.6, 14.0.

<sup>19</sup>F NMR:  $\delta_{\text{F}}$  (376 MHz, CDCl<sub>3</sub>) -143.2 (2F, s).

**MS: 684**

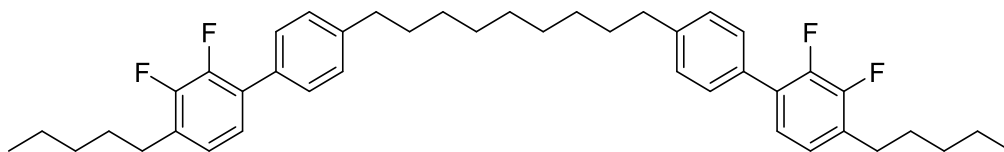
*m/z* (CI) 685 (M+H<sup>+</sup>) 702 (M+NH<sub>4</sub><sup>+</sup>)

HRMS Calc: C<sub>49</sub>H<sub>58</sub>F<sub>2</sub> +Hrequires = 685.4584

HRMS Found: 685.4570

**HPLC trace = 96.3 %**

## Synthesis of 1,9-bis(2',3'-difluoro-4'-pentyl-[1,1'-biphenyl]-4-yl)nonane (31)



1,9-bis(4-Bromophenyl)nonane (0.20 g, 0.46 mmol), (2,3-difluoro-4-pentylphenyl)boronic acid (0.41 g, 1.8 mmol) and tetrakis(triphenylphosphine)palladium(0) (0.026 g, 22.5  $\mu$ mol) were dissolved in tetrahydrofuran (20 mL) under inert atmosphere. The reaction was stirred at room temperature, with nitrogen being bubbled through the solvent. After 1 hour an aqueous solution of sodium carbonate (0.070 g, 0.66 mmol) was added drop wise and the reaction was heated under reflux overnight. The solvent was removed under reduced pressure and the organics separated by silica column chromatography using a mixture of dichloromethane and hexane 1:4 to afford the title compound as a white solid (0.19 g, 65%).

$^1\text{H NMR}$ :  $\delta_{\text{H}}$  (400 MHz,  $\text{CDCl}_3$ ) 7.44 (4H, d,  $J$  7.96), 7.25 (2H, m), 7.09 (2H, t,  $J$  7.96), 6.97 (2H, t,  $J$  7.96), 2.66 (8H, m), 1.66 (8H, m), 1.35 (18H, m), 0.91 (6H, t,  $J$  6.94).

$^{13}\text{C NMR}$ :  $\delta_{\text{C}}$  (100 MHz,  $\text{CDCl}_3$ ) 149.5, 148.0, 142.7, 132.3, 130.6, 130.5, 128.7, 128.64, 128.56, 128.4, 128.3, 124.6, 124.2, 35.7, 31.44, 31.38, 29.7, 29.5, 29.3, 28.7, 22.4, 14.0.

$^{19}\text{F NMR}$ :  $\delta_{\text{F}}$  (376 MHz,  $\text{CDCl}_3$ ) -143.2 (4F, s).

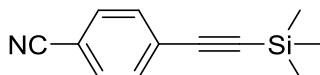
**MS: 644**

$m/z$  (CI) 645 ( $\text{M}+\text{H}^+$ ) 662 ( $\text{M}+\text{NH}_4^+$ )

HRMS Calc:  $\text{C}_{43}\text{H}_{52}\text{F}_4 + \text{H}$  requires = 645.4083

HRMS Found: 645.4065

## Synthesis of 4-((trimethylsilyl)ethynyl)benzonitrile (32) <sup>99</sup>



4-Bromobenzonitrile (8.0 g, 43.9 mmol), tetrakis(triphenyl)phosphine palladium (II) chloride (0.62 g, 0.88 mmol), copper iodide (0.20 g, 1.1 mmol) and degassed triethylamine were added to a flask, sealed and air was evacuated. The reaction was heated to 50 °C and trimethylsilylacetylene (17.2 g, 0.18 mol) was added drop wise. Upon completion of the addition the reaction was heated to 70 °C over night. The solvent was removed under reduced pressure and the organics separated by silica column chromatography using a mixture of dichloromethane and hexane 1:1 to afford the title compound as a white solid (8.65 g, 99%).

<sup>1</sup>H NMR:  $\delta_{\text{H}}$  (400 MHz, CDCl<sub>3</sub>) 7.56 (4H, m), 0.26 (9H, s).

<sup>13</sup>C NMR:  $\delta_{\text{C}}$  (100 MHz, CDCl<sub>3</sub>) 132.7, 132.2, 128.3, 118.7, 112.0, 103.2, 99.8, 0.01.

## Synthesis of 4-ethynylbenzonitrile (33)<sup>100</sup>

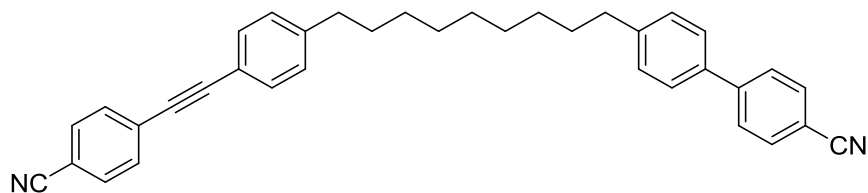


4-((Trimethylsilyl)ethynyl)benzonitrile (8.65 g, 43.4 mmol) was dissolved in *N,N*-dimethylformamide (100 mL). Potassium fluoride (10.1 g, 0.17 mol) was added as an aqueous solution drop wise. Upon completion by TLC organics are extracted into diethyl ether and washed repeatedly with water followed by brine. After drying over magnesium sulphate the solvent was removed under reduced pressure to afford the title compound as a brown solid (5.16 g, 94%).

<sup>1</sup>H NMR:  $\delta_{\text{H}}$  (400 MHz, CDCl<sub>3</sub>) 7.59 (4H, q, *J* 11.83, 8.57), 3.30 (1H, s).

<sup>13</sup>C NMR:  $\delta_{\text{C}}$  (100 MHz, CDCl<sub>3</sub>) 132.7, 132.0, 127.0, 118.2, 112.3, 81.8, 81.5.

**Synthesis of 4'-(9-(4-((4-cyanophenyl)ethynyl)phenyl)nonyl)-[1,1'-biphenyl]-4-carbonitrile (34)**

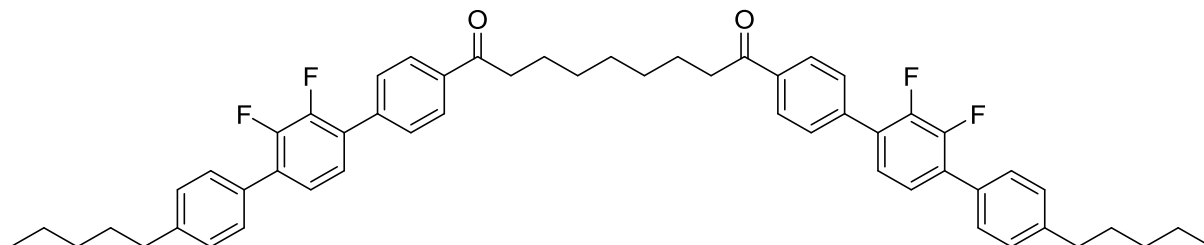


4'-(9-(4-Bromophenyl)nonyl)-[1,1'-biphenyl]-4-carbonitrile (0.20 g, 0.43 mmol), 4-ethynylbenzonitrile (0.16 g, 1.3 mmol), bis(triphenylphosphine)palladium(II) chloride (0.015 g, 21.5  $\mu$ mol), copper iodide (0.004 g, 21.5  $\mu$ mol) and triethylamine (20 mL) were added to a flask and sealed. The air was evacuated and the reaction was heated at 70 °C over night. The solvent was removed under reduced pressure and the organics separated by silica column chromatography using a mixture of dichloromethane and hexane 1:4 to afford the title compound as a white solid (0.042 g, 19%).

Cr – 90 - N<sub>x</sub> – 102 – N – 125 – Iso

<sup>1</sup>H NMR:  $\delta_{\text{H}}$  (400 MHz, CDCl<sub>3</sub>) 7.68 (4H, q, *J* 8.57, 8.16), 7.60 (4H, q, *J* 8.57, 8.57), 7.50 (2H, d, *J* 8.16), 7.45 (2H, d, *J* 8.16), 7.29 (2H, d, *J* 8.16), 7.18 (2H, d, *J* 8.36), 2.63 (4H, m). Found 20, expected 34.

**Synthesis of 1,9-bis(2,3'-difluoro-4''-pentyl-[1,1':4',1''-terphenyl]-4-yl)nonane-1,9-dione (35)**



1,9-bis(4-Bromophenyl)nonane-1,9-dione (0.069 g, 0.15 mmol), (2,3-difluoro-4'-pentyl-[1,1'-biphenyl]-4-yl)boronic acid (0.2 g, 0.65 mmol) and tetrakis(triphenylphosphine) palladium(0) (0.008 g, 7.5  $\mu$ mol) were dissolved in tetrahydrofuran (20 mL) under inert atmosphere. The reaction was stirred at room temperature, with nitrogen being bubbled through the solvent. After 1 hour an aqueous solution of sodium carbonate (0.124 g, 0.9 mmol) was added drop wise and the reaction was heated under reflux overnight. The solvent was removed under reduced pressure and the organics separated by silica column chromatography using a mixture of dichloromethane and hexane 1:4 to afford the title compound as a white solid (0.063 g, 52%).

Cr – 129 – B6 – 183 – SmC – 186 – N – 223 - Iso

$^1\text{H NMR}$ :  $\delta_{\text{H}}$  (400 MHz,  $\text{CD}_2\text{Cl}_2$ ) 8.03 (4H, d,  $J$  8.57), 7.68 (4H, dd,  $J$  8.57, 1.63), 7.48 (4H, dd,  $J$  8.16 1.63), 7.28 (8H, m), 2.99 (4H, t,  $J$  7.35), 2.63 (4H, t,  $J$  7.75), 1.72 (4H, m), 1.63 (4H, m), 1.41 (6H, m), 1.33 (8H, m), 0.88 (6H, m).

- 
- <sup>1</sup> Collins, P. J., Hird, M., *Introduction to Liquid Crystals*. Taylor & Francis: London, 1997.
- <sup>2</sup> Demus, D., Goodby, J. W., Gray, G. W., Spiess, H. W., Vill, V., *Handbook of Liquid Crystals Vol 1*. Wiley-VCH: 1998.
- <sup>3</sup> Lehmann, O., *Z. Phys. Chem.* (1889), **4**, 462.
- <sup>4</sup> Reinitzer, F., *Montasch. Chem.* (1888), **9**, 421.
- <sup>5</sup> Friedel, G., *Ann. Phys* (1922), **18**, 273.
- <sup>6</sup> Mauguin, C., *Physik Zeitschrift* (1911), **12**, 1011.
- <sup>7</sup> Gray, G. W. Harrison, K. J.; Nash, J. A., *Electron. Lett.* (1973), **9**, 130.
- <sup>8</sup> [www.marketsandmarkets.com/pressreleases/display.asp](http://www.marketsandmarkets.com/pressreleases/display.asp)
- <sup>9</sup> Gray, G. W., *Mol. Cryst. Liq. Cryst.*, (1973), **21**, 161.
- <sup>10</sup> Boden, N., Borner, R., Brown, D. R., Bushby R. J., Clements J., *Liq. Crysts.*, (1992), **11**, 325.
- <sup>11</sup> Niori, T., Sekine, T., Watanabe, J., Furukawa, T., Takazoe, H., *J. Mater Chem.*, (1996), **6**, 1231.
- <sup>12</sup> Vorlander, D., Apel, A., *Ber. Dtsch. Chem. Ges.*, (1929), **62**, 2831.
- <sup>13</sup> Plezl, G., Wirth, I., Weissflog, W., *Liq. Cryst.*, (2001), **28**, 969.
- <sup>14</sup> Vorlander, D., *Z.Phys. Chem.*, (1923), **105**, 211.
- <sup>15</sup> Nguyen, H. T., Destrade, H., Gasparoux, H., *Phys. Lett. A.*, (1979), **72**, 251.
- <sup>16</sup> Luckhurst, G., Fukuda, A. and Dunmur, D., *Physical properties of liquid crystals*. 1st ed., IEE: 2001
- <sup>17</sup> [http://www.doitpoms.ac.uk/tlplib/liquid\\_crystals/order\\_disorder\\_position.php](http://www.doitpoms.ac.uk/tlplib/liquid_crystals/order_disorder_position.php)
- <sup>18</sup> Freiser, M. J., *Phys. Rev. Lett.*, (1970), **24**, 1041.
- <sup>19</sup> Yu, L.J., Saupe, A., *Phys. Rev. Lett.*, (1980), **45**, 1000.
- <sup>20</sup> Wensink, H. H., Vroege, J. G., Lekkerkerker, H. N. W., *Phys. Rev. E*, (2002), **66**, 041704.
- <sup>21</sup> Wensink, H. H., Vroege, J. G., *J. Chem. Phys.*, (2003), **119**, 6868.
- <sup>22</sup> Wensink, H. H., Vroege, J. G., *Phys. Rev. E*, (2005), **72**, 031708.
- <sup>23</sup> Hessel, F., Finkelmann, H., *Polym. Bull.*, (1986), **15**, 349.
- <sup>24</sup> Hessel, F., Herr, R-P., Finkelmann, H., *Macromol. Chem. Phys.*, (1987), **188**, 1597.
- <sup>25</sup> Leube, F., Finkelmann, H., *Macromol. Chem. Phys.*, (1990), **191**, 2707.
- <sup>26</sup> Leube, F., Finkelmann, H., *Macromol. Chem. Phys.*, (1991), **192**, 1317.
- <sup>27</sup> Madsen, L. A., Dingemans, T. J., Nakata, M., Samulski, E. T., *Phys. Rev. Lett.*, (2004), **92**, 145505.
- <sup>28</sup> Yelamaggad, C. V., Krishna, P. S., Nair, G. G., Shashikala, I. S., Rao, D. S. S., Lobo, C. V., Chandrasekhar, S., *Angew. Chem. Intl. Ed.*, (2004), **43**, 3429.
- <sup>29</sup> Merkel, K., Kocot, A., Vij, J. K., Korlacki, R., Mehl, G. H., Meyer, T., *Phys. Rev. Lett.*, (2004), **93**, 237801.
- <sup>30</sup> Vries, A. D., *Mol. Cryst. Liq. Cryst.*, (1970), **10**, 219.
- <sup>31</sup> Karahaliou, P. K., Kouwer, P. H., Meyer, T., Mehl, G. H., Photinos, D. J., *Soft Matter*, (2007), **3**, 857.
- <sup>32</sup> Francescangeli, O., Samulski, E. T., *Soft Matter*, (2010), **6**, 2413.
- <sup>33</sup> Francescangeli, O., Laus, M., Galli, G., *Phys. Rev. E*, (1997), **55**, 481.
- <sup>34</sup> Kouwer, P. H., Picken, S. J., Mehl, G. H., *J. Mater. Chem.*, (2007), **17**, 4196.
- <sup>35</sup> Nishiya, W., Takanishi, Y., Yamamoto, J., Yoshizawa, A., *J. Mater. Chem. C*, (2014), **2**, 3677.
- <sup>36</sup> Meyer, R. B. in *Molecular Fluids. Les Houches Lectures*, 1973. (eds Balian, R. & Weill, G.) 271-343 (Gordon and Breach, 1976).
- <sup>37</sup> Dozov, I. *Eur. Phys. Lett.*, (2001), **56**, 24.
- <sup>38</sup> Ungar, G. *Macromolecules*, (1992), **25**, 75.
- <sup>39</sup> Schroder, M. W., Diele, S., Pelzl, G., Dunemann, U., Kresse, H., Weisflog, W., *J. Mater. Chem.*, (2003), **13**, 1877.
- <sup>40</sup> Sepelj, M., Lesac, A., Baumierster, U., Diele, S., Bruce, D. W., *Chem. Mater.*, (2006), **18**, 2050.
- <sup>41</sup> Panov, V. P., Nagaraj, M., Vij, J. K., Panarin, Y. P., Kohlmeier A., Tamba, M. G., Lewis, R. A., Mehl G. H., *Phys. Rev. Lett.*, (2010), **105**, 167801.
- <sup>42</sup> Zep, A., Aya, S., Aihara, K., Ema, K., Poeicha, D., Madrak, K., Bernatowicz, P., Takezoe, H., Gorecka, E., *J. Mater. Chem. C.*, (2013), **1**, 46.
- <sup>43</sup> Borshch, V., Kim, Y. K., Xiang, J., Gao, M., Jakli, A., Panov, V. P., Vij, J. K., Imrie, C. T., Tamba, M. G., Mehl, G. H., Lavrentovich, O. D., *Nat. Comm.*, (2013), **4**, 2635.
- <sup>44</sup> Clark, N. A, Chen, D., Porada, J. H., Hooper, J. B., Klitnick, A., Shen, Y., Tuchband, M. R., Korblova, E., Bedrov, D., Walba, D. M., Glaser, M. A., Mclennan, J. E., *Proc. Natl. Acad. Sci. U.S.A.*, (2013), **110**, 15931.
- <sup>45</sup> Hori, K., Imouro, M., Nakao, A., Toriumi, H., *J. Mol. Struct.*, (2004), **699**, 23.
- <sup>46</sup> Gorecka, E., Zep, A., Ahmed, Z., Welch, C., Mehl, G., *In Publication*, (2014),  
[Dx.Doi.org/10.1080/02678292.2014.984646](https://doi.org/10.1080/02678292.2014.984646).

- <sup>47</sup> Hoffmann, A., Vanakaras, A. G., Kohlmeier A., Mehl, G. H., Photinos D. J., *Arxiv.2014*, **1401**, 5445.
- <sup>48</sup> Emsley, J. W., Luckhurst, G., Shilstone, G. N., Sage, I., *Liq. Cryst.*, (1984), **102**, 223.
- <sup>49</sup> Imrie, C., Henderson, P. A., Niemeyer, O., *Liq. Cryst.*, (2001), **28**, 463.
- <sup>50</sup> Gao, M., Kim, Y., Zhang, C., Borshch V., Zhou, S., Park, H-S., Jakli, A., Lavrentovich, A. D., Tamba, M-G., Kohlmeier, A., Mehl, G. H., Weissflog, W., Studer, D., Zuber, B., Gnagi, H., Lin, F., *Microsc. Res. Teqhnq.*, (2014), **77**, 754.
- <sup>51</sup> Bouligand, Y. S., Puiseux-Dao, S., *Chromosoma.*, (1968), **24**, 769.
- <sup>52</sup> Pelzl, G., Diele, S., Weissflog, W., *Adv. Mater.* (1999), **11**, 707.
- <sup>53</sup> Achard, M. F., Rouillon, J. C., Macerou, J. P., Laguerre, M., Nguyen, H. T., *J. Mater. Chem.*, (2001), **11**, 2946
- <sup>54</sup> Szydłowska, J., Mieczkowski, J., Matraszek, J., Bruce, D. W., Gorecka, E., Pocięcha, D., Guillon, D., *Phys. Rev. E.*, (2003), **67**, 031703.
- <sup>55</sup> Link, D. R., Natale, G., Shao, R., Maclennan, J. E., Clark, N. A., Korblova, E., Walba, D. M., *Science*, (1997), **278**, 1924.
- <sup>56</sup> Sekine T., Niori T., Watanabe J., Furukawa T., Choi S. W., Takezoe, H., *J. Mater. Chem.*, (1997), **7**, 1307.
- <sup>57</sup> Clark, N. A., Hough, L. E., Jung, T. H., Kruerke, D., Heberling, M. S., Nakata, M., Jones, C. D., Chen, D., Link, D. R., Zasadzinski, J., Heppke, G., Rabe, J. P., Stocker, W., Korblova, E., Walba, D. M., Glaser, M. A., *Science*, (2009), **325**, 456
- <sup>58</sup> Nadası, H., Weissflog, W., Eremin, A., Pelzl, G., Diele, S., Das, B., Grande, S., *J. Mater. Chem.*, (2002), **12**, 1316.
- <sup>59</sup> Rouillon, J. C., Marcerou, J. P., Laguerre, M., Nguyen, H. T., Achard, M. F., *J. Mater.Chem.*, (2001), **11**, 2946.
- <sup>60</sup> Reddy, A. R., Tschierske, C., *J. Mater. Chem.*, (2006), **16**, 907.
- <sup>61</sup> Dierking, I., *Textures of liquid crystals*. 1st ed. Weinheim: Wiley-VCH:2003.
- <sup>62</sup> Olympusmicro.com, (2014). *Olympus Microscopy Resource Center | Polarized Light Microscopy - Microscope Alignment*. [online] Available at: <http://www.olympusmicro.com/primer/techniques/polarized/polmicroalignment.html> [Accessed 26 Aug. 2014].
- <sup>63</sup> Microscopyu.com, (2014). *Nikon MicroscopyU | Polarized Light Microscopy*. [online] Available at: <http://www.microscopyu.com/articles/polarized/polarizedintro.html> [Accessed 26 Aug. 2014].
- <sup>64</sup> Steinmann, W., Seide G., Beckers, M., Walter, S., Gries, T., *Thermal Analysis of Phase Transitions and Crystallization in Polymeric Fibers*. 1st ed. INTECH Open Access Publisher:2013.
- <sup>65</sup> Bragg, W.L. *The Crystalline State: Volume I*. New York: The Macmillan Company: 1934.
- <sup>66</sup> Cnx.org, (2014). *OpenStax CNX*. [online] Available at: <http://cnx.org/contents/517f8f37-f619-4408-a8b4-2ef8a53e8c29@2#eip-170> [Accessed 28 Aug. 2014].
- <sup>67</sup> Seddon, J. M., Demus, D., Goodby, J., Gray, G. W., Spiess, W., Vill, V., *Physical properties of liquid crystals by X-ray diffraction*, Wiley-VCH:1998.
- <sup>68</sup> Ober, C. K., Jin, J-I., Lenz, R. W., *Adv. Polym. Sci.*, (1984), **59**, 103.
- <sup>69</sup> Volander, D., *Z. Phys. Chem.*, (1927), **126**, 449.
- <sup>70</sup> Griffin, A. C., Britt, T. R., *J. Am. Chem. Soc.*, (1981), **103**, 4957.
- <sup>71</sup> Emsley, J. W., Luckhurst, G. R., Shilstone, G. N., Sage, I., *Mol. Cryst. Liq. Cryst.*, (1984), **102**, 223.
- <sup>72</sup> Weissflog, W., Demus, D., Diele, S., Nitschke, P., Wedler, W., *Liq. Cryst.*, (1989), **5**, 111.
- <sup>73</sup> Andersch, J., Tschierske, C., *Liq. Cryst.*, (1996), **21**, 51.
- <sup>74</sup> Jacobi, A., Weissflog, W., *Liq. Cryst.*, (1997), **22**, 107.
- <sup>75</sup> Andersch, J., Tschierske, C., Diele, S., Lose, D., *J. Mater. Chem.*, (1996), **6**, 1297.
- <sup>76</sup> Steglich, W., Neises, B., *Angew. Chemie. Int. Ed.*, (1978), **7**, 522.
- <sup>77</sup> Suzuki, A., Miyaura, N., Yamada, J., *Tetrahedron. Lett.*, (1979), **20**, 3437.
- <sup>78</sup> Williamson, A., *Philos. Mag.*, (1850), **37**, 350.
- <sup>79</sup> Kishner, N., *J. Russ. Phys. Chem. Soc.*, (1911), **43**, 582.
- <sup>80</sup> Wolff, L., *Liebigs Ann.*, (1912), **394**, 86.
- <sup>81</sup> Perrin, D. M., Liu, Z., Lozada, J., *J. Org. Chem.*, (2014), **79**, 5365.
- <sup>82</sup> Miyaura, N., Suzuki, A., *Chem. Rev.*, (1995), **95**, 2457.
- <sup>83</sup> Suzuki, A., *J. Organomet. Chem.*, (1999), **576**, 147.
- <sup>84</sup> Minlon, H., *J. Am. Chem. Soc.*, (1946), **68**, 2487.
- <sup>85</sup> Sonogashira, K., Tohda, Y., Haghira N., *Tetrahedron. Lett.*, (1975), **50**, 4467.
- <sup>86</sup> Hay, A. S., *J. Org. Chem.*, (1962), **27**, 3320.

- 
- <sup>87</sup> Glaser, C., *Ber. Dtsch. Chem. Ges.*, (1869), **2**, 422.
- <sup>88</sup> Mayor, M., Jenny, N. M., Eaton, T. R., *Eur. J. Org. Chem.*, (2011), **26**, 4965.
- <sup>89</sup> Sonogashira, K., *J. Organomet. Chem.*, (2002), **653**, 46.
- <sup>90</sup> Ferrarini, A., Luckhurst, G. R., Nordio, P. L., Roskilly, S. J., *J. Chem. Phys.*, (1994), **100**, 1460.
- <sup>91</sup> Scherrer, P., *Mathematisch-Physikalische Klasse*, (1918), **2**, 98.
- <sup>92</sup> Francescangelli, O., Samulski, E. T., *Soft Matter*, (2010), **6**, 2413.
- <sup>93</sup> Kang, S., Lee, S. K., Tokita, M., Watanabe, J., *Phys. Rev. E.*, (2009), **80**, 042703.
- <sup>94</sup> Sadashiva, B. K., Reddy, R. A., Raghunathan V. A., *Chem. Mater.*, (2004), **16**, 4061.
- <sup>95</sup> Hsieh, C. J., Hsiue G. H., *Liq. Cryst.*, (1994), **16**, 469.
- <sup>96</sup> Meng, H. N. B., Dalton, L. R., Wu, S. T., *Mol. Cryst. Liq. Cryst. Sci. Technol., Sect. A*, (1994), **250**, 303.
- <sup>97</sup> Tamba M-G., Salil, S. M., Zhang, C., Jakli, A., Mehl, G. H., Stannarius, R., Eremin, A., *In publication* (2014).
- <sup>98</sup> Jaunin, R., Baer, T., *Helv. Chim. Acta.*, (1957), **40**, 2245.
- <sup>99</sup> Blackburn, B. K., Lee, A., Baier, M., Kohl, B., Olivero, A. G., Matamoros, R., Robarge, K. D., McDowell, R. S., *J. Med. Chem.*, (1997), **40**, 717.
- <sup>100</sup> Okumara, K., Shimazaki, T., Aoki, Y., Yamashita, H., Tanaka, E., Banba, S., Yazawa, K., Kibayashi, K., Banno, H., *J. Med. Chem.* (1998), **41**, 4036.